Conception de formes d'onde multi-porteuses dans le contexte de systèmes de communication 5G/6G

Iandra Galdino Andrade

HESAM UNIVERSITÉ

le cnam

ÉCOLE DOCTORALE SCIENCES DES MÉTIERS DE L'INGÉNIEUR

THÈSE

présentée par : **Iandra GALDINO ANDRADE**

soutenue le : **26 mars 2021**

pour obtenir le grade de : **Docteur d'Hésam Université**

préparée au : **Conservatoire national des arts et métiers**

Discipline : **Génie électrique, électronique, photonique et systèmes**

Spécialité : **Radiocommunications**

Multicarrier waveform design in the context of 5G/6G communications systems

THÈSE dirigée par :
M. LE RUYET, Didier, Professeur, Cnam

co-dirigée par :
M. CAMPOS, Marcello, Professeur, UFRJ

et co-encadrée par :
M. ZAKARIA, Rostom, Ph.D., Cnam

Jury

Mme. Catherine DOUILLARD, Professeur, Institut Mines-Telecom (IMT) Atlantique, Présidente
M. Carlos BADER, Professeur, Institut Supérieur d'Electronique de Paris (ISEP), Rapporteur
M. Charles CAVALCANTE, Professeur, Université Fédérale du Ceará (UFC), Rapporteur
M. João Cesar MOTA, Professeur, Université Fédérale du Ceará (UFC), Examinateur
M. Paulo DINIZ, Professeur, Université Fédérale du Rio de Janeiro (UFRJ), Examinateur

T H È S E

Para ser grande, sê inteiro:
nada Teu exagera ou exclui.
Sê todo em cada coisa.
Põe quanto és No mínimo que
fazes. Assim em cada lago a lua
toda Brilha, porque alta vive.
Ricardo Reis (Fernando Pessoa)

Resumo da Tese apresentada à COPPE/UFRJ como parte dos requisitos necessários para a obtenção do grau de Doutor em Ciências (D.Sc.)

PROJETO DE FORMA DE ONDA MULTIPORTADORA NO CONTEXTO DE SISTEMAS DE COMUNICAÇÃO 5G/6G

Iandra Galdino Andrade

Março/2021

Orientadores: Marcello Luiz Rodrigues de Campos
Didier Le Ruyet

Programa: Engenharia Elétrica

A utilização de Sistemas com múltiplas portadoras baseados em banco de filtros (FBMC) em futuros sistemas de comunicação *e.g.*, 5G/6G, é promissora. Quando comparado ao OFDM, sistemas FBMC apresentam melhor localização no domínio da frequência, e consequentemente causam menos interferência em sistemas vizinhos.

Sistemas FBMC podem ser associados a diferentes modulações como por exemplo em amplitude e em quadratura, a qual nos leva ao sistema QAM-FBMC, ou offset QAM-FBMC. Em ambos casos o projeto de filtro protótipo é essencial para garantir o bom desempenho, uma vez que ele será usado para construir todos os filtros do banco de filtros.

Nesta tese, nós abordamos o projeto de filtros para sistemas QAM-FBMC e OQAM-FBMC como um problema de otimização. Nós procedemos uma escolha cuidadosa da função objetivo a ser minimizada para reduzir a interferência intrínseca do sistema, porém, mantendo o confinamento espectral.

Nós também investigamos o desempenho destes sistemas através da probabilidade de erro de bit (BEP). Expressões de forma fechada da BEP podem ser encontradas na literatura para sistemas OFDM e OQAM-FBMC. Nós propomos neste trabalho uma expressão matemática para a BEP de sistemas QAM-FBMC. Nós investigamos ainda, como a escolha do filtro protótipo afeta a interferência do sistema e consequentemente a BEP.

Apesar da otimização de filtros, observamos ainda uma interferência residual em sistemas QAM-FBMC. Desta forma, receptores avançados são necessários. Neste trabalho analisamos e propomos um novo receptor para reduzir a interferência em sistemas QAM-FBMC.

Abstract of Thesis presented to COPPE/UFRJ as a partial fulfillment of the requirements for the degree of Doctor of Science (D.Sc.)

MULTICARRIER WAVEFORM DESIGN IN THE CONTEXT OF 5G/6G COMMUNICATION SYSTEMS

Iandra Galdino Andrade

March/2021

Advisors: Marcello Luiz Rodrigues de Campos
Didier Le Ruyet

Department: Electrical Engineering

Filter-Bank Multi-Carrier (FBMC) system, is a promising technology to enable future wireless communications *e.g.*, 5G/6G. When compared to the Orthogonal Frequency division Multiplexing (OFDM), FBMC systems have better frequency localization, and consequently, cause less interference to neighboring systems.

FBMC systems can be associate to different modulations such as quadrature amplitude modulation, which leads us to the QAM-FBMC system, or offset QAM called (OQAM-FBMC). In both cases, the prototype filter design is a key to guarantee good performance, since it will be used to construct all the filters of the filter-bank.

In this thesis, we address the problem of prototype filter design for OQAM-FBMC and QAM-FBMC systems, under the light of the optimization procedures. We proceed a careful choice of the objective function to be minimized for reducing the intrinsic interference while keeping the spectral confinement.

We also investigate the performance of multicarrier systems through their bit error probability (BEP). To evaluate the performance of QAM-FBMC systems we propose a mathematical expression of its BEP. We investigate how the choice of the prototype filter affects the system interference and consequently the BEP.

Although several prototype filters have been designed for QAM-FBMC systems, a residual interference is still observed and degrades system performance. Therefore, a more elaborated receiver is needed. Thus, we also conduct a research on receivers in order to reduce interference and we propose a receiver specifically designed for QAM-FBMC systems.

Abstract of Thesis presented to COPPE/UFRJ as a partial fulfillment of the requirements for the degree of Doctor of Science (D.Sc.)

CONCEPTION DE FORMES D'ONDE MULTI-PORTEUSES DANS LE CONTEXTE DE SYSTÈMES DE COMMUNICATION 5G/6G

Iandra Galdino Andrade

March/2021

Advisors: Marcello Luiz Rodrigues de Campos
Didier Le Ruyet

Department: Electrical Engineering

Le système Filter-Bank Multi-Carrier (FBMC) est une technologie prometteuse pour permettre de futures communications sans fil, par exemple 5G/6G. Par rapport au multiplexage par répartition orthogonale de la fréquence (OFDM), les systèmes FBMC ont une meilleure localisation de fréquence et, par conséquent, causent moins d'interférences aux systèmes voisins. Les systèmes FBMC peuvent être associés à différentes modulations telles que la modulation d'amplitude en quadrature, qui nous conduit au système QAM-FBMC, ou offset QAM appelé (OQAM-FBMC). Dans les deux cas, la conception du filtre prototype est une clé pour garantir de bonnes performances, car elle sera utilisée pour construire tous les filtres du banc de filtres. Dans cette thèse, nous abordons le problème de la conception de filtres prototypes pour les systèmes OQAM-FBMC et QAM-FBMC, à la lumière des procédures d'optimisation. Nous procédons à un choix judicieux de la fonction objectif à minimiser pour réduire les interférences intrinsèques tout en conservant le confinement spectral. Nous étudions également les performances des systèmes à porteuses multiples grâce à leur probabilité d'erreur sur les bits (BEP). Pour évaluer les performances des systèmes QAM-FBMC, nous proposons une expression mathématique de son BEP. Nous étudions comment le choix du filtre prototype affecte les interférences du système et par conséquent le BEP. Bien que plusieurs filtres prototypes aient été conçus pour les systèmes QAM-FBMC, une interférence résiduelle est toujours observée et dégrade les performances du système. Par conséquent, un récepteur plus élaboré est nécessaire. Ainsi, nous menons également une recherche sur les récepteurs afin de réduire les interférences et nous proposons un récepteur spécifiquement conçu pour les systèmes QAM-FBMC.

Résumé de la thèse en français

Chapitre 1 Introduction

Les demandes des clients sont les principaux moteurs du développement des communications mobiles. L'Union internationale des télécommunications (UIT) prévoit une augmentation du trafic estimées entre 10 et 100 fois au cours des 10 prochaines années. En effet, nous assisterons également à une croissance du nombre de services et d'appareils connectés, au-delà de la demande d'une accessibilité accrue. Sachant cela, des solutions innovantes seront nécessaires pour permettre toutes les connexions des utilisateurs.

La cinquième génération de systèmes de communication mobile, le réseau cellulaire 5G, devrait permettre de satisfaire cet énorme volume de connexions. Il doit permettre de connecter les personnes, les objets, les systèmes de transport et les villes dans des environnements de communication et des réseaux intelligents.

Un certain nombre de nouveaux services devraient être fournis par les réseaux 5G. Les nouvelles technologies devraient prendre en charge des applications telles que les maisons et les bâtiments intelligents, les villes intelligentes, la vidéo 3D en ultra haute définition (UHD), le travail et les loisirs dans le cloud, les services médicaux à distance, la réalité virtuelle et augmentée et l'énorme machine-à-machine (M2M) pour l'automatisation de l'industrie.

Les réseaux sans fil de la génération précédente, 3G et 4G, sont actuellement confrontés à plusieurs défis pour fournir ces services, car divers indicateurs de performance clés et souvent contradictoires doivent être satisfaits comme par exemple la fiabilité, les débits de données élevés, la connectivité, l'ultra-haut débit avec une latence très faible. Ce sont des exigences essentielles pour répondre aux nouvelles demandes de service.

Pour faire face à ces exigences strictes des réseaux 5G, une toute nouvelle interface radio est nécessaire. Une nouvelle interface aérienne, appelée 5G NR, a été développée et s'appuie sur de nouvelles fonctionnalités, services et technologies, par exemple Massive MIMO, mmWave, Radio Full-duplex, communication D2D et réseau ultra dense (UDN).

Pour faire face à ces exigences strictes des réseaux 5G, une toute nouvelle in-

terface radio est nécessaire. Une nouvelle interface aérienne, appelée 5G NR, a été développée et s'appuie sur de nouvelles fonctionnalités, services et technologies, par exemple le Massive MIMO, mmWave, Radio Full-duplex, communication D2D et réseau ultra dense (UDN).

Dans ce contexte, ce travail aborde le défi de concevoir des filtres prototypes bien localisés dans le domaine fréquentiel et respectant également les particularités de chaque système considéré. Nous considérons également la conception de filtres courts (K = 1) appliqués au système QAM-FBMC.

Nous étudions et décrivons les interférences intrinsèques et l'énergie hors bande (OOBE) pour chaque système, et concevons des filtres prototypes qui les minimisent. Nous étudions également les contraintes particulières liées à chaque système afin que les symboles transmis puissent être récupérés au niveau du récepteur.

De plus, nous traitons également les interférences intrinsèques du système en analysant la probabilité d'erreur sur les bits (BEP) et en proposant une nouvelle structure de récepteur pour le cas de QAM-FBMC avec des filtres courts.

Chapitre 2 Un aperçu de la 5G

La cinquième génération de systèmes de communication mobile, le réseau 5G, devrait fournir un énorme volume de connexions. Il doit permettre de connecter les personnes, les objets, les systèmes de transport,...

Un certain nombre de nouveaux services devraient être fournis par les réseaux 5G. Les nouveaux technologies devraient prendre en charge des applications telles que les maisons et les bâtiments intelligents, les villes intelligentes, la vidéo 3D en ultra haute définition (UHD), le travail et les loisirs dans le cloud, les services médicaux à distance, la réalité virtuelle et augmentée et aussi l'énorme machine à machine (M2M) communication pour l'automatisation de l'industrie.

Les réseaux sans fil de les générations précédentes, 3G et 4G, sont actuellement confrontés à plusieurs défis pour fournir ces services, car des indicateurs de performance clés diverse et souvent contradictoire doivent être observés, par exemple la fiabilité, les débits de données élevés, la connectivité, et l'ultra-haut débit avec une latence très faible. Ce sont des exigences essentielles pour répondre aux nouvelles demandes de service.

Il existe diverses caractéristiques clés des systèmes 5G NR que nous ne trouvons pas dans les systèmes précédents. Ces fonctionnalités aident la 5G à fournir les services promis. Pour cette proposition, la 5G compte sur certaines caractéristiques connues des systèmes précédents, par exemple, l'agrégation de porteuses, la modulation multiporteuse et les transmissions MIMO. Au-delà de l'amélioration des fonctionnalités déjà existantes, les systèmes 5G compteront également sur de nouvelles fonctionnalités améliorant la capacité, l'efficacité de l'allocation des ressources radio et permettant une adaptation à la diversité des exigences de service et des conditions de canal.

La technologie d'accès 5G de cinquième génération a été développée dans le but non seulement d'augmenter l'efficacité spectrale ou d'augmenter le débit, mais également de fournir de nouveaux services. Les principaux services de la 5G sont représentés sur la Figure 1. Dans la première phase de la 5G, définie par le 3GPP, l'objectif est d'améliorer le haut débit mobile (eMBB) afin d'améliorer la fiabilité de la connexion. Dans un second temps, la 3GPP définit les indicateurs clés de performance (KPI) nécessaires pour fournir de nouveaux types de services tels que les communications massives de type machine (mMTC) et les communications ultra fiables à faible latence (URLLC).

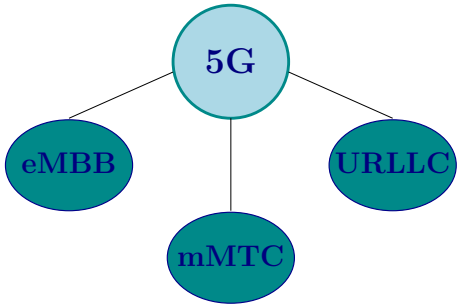

Figure 1: Principaux cas d'utilisation de la 5G.

Chapitre 3 Modulation OQAM-FBMC

Les exigences de la couche physique 5G ont encouragé l'étude d'une interface radio plus flexible basée sur une forme d'onde avec une bonne localisation spectrale. Les formes d'onde multiporteuses ont été étudiées comme solution possible.

Les modulations multiporteuses à base de bancs de filtre (FBMC) sont une forme d'onde prometteuse pour permettre les futures communications sans fil flexibles. Par rapport au multiplexage par répartition orthogonale de la fréquence (OFDM), les systèmes FBMC ont une meilleure localisation fréquentielle et causent par conséquent moins d'interférences aux systèmes voisins.

La modulation d'amplitude Offset en Quadrature associée au système Filter-Bank Multi-Carrier (OQAM-FBMC) est une technologie prometteuse pour permettre de futurs systèmes de communication sans fil flexibles.

Contrairement à l'OFDM, qui nécessite l'orthogonalité de toutes les porteuses pour éviter les interférences, dans un système FBMC, l'orthogonalité est conservée juste entre les sous-porteuses voisines. En fait, dans un FBMC, la bande passante est divisée en plusieurs sous-porteuses, et les données sont transmises via un banc de filtres modulés à bande limitée. Les sous-porteuses n'étant pas orthogonales, pour exploiter toute la bande passante du canal, il est nécessaire d'adapter l'émetteur FBMC.

Un schéma de principe simplifié est représenté sur la figure 2, où la bande passante de transmission est divisée en M sous-bandes espacées de $F = 1/M$.

La conception d'un bon filtre prototype est essentielle pour garantir de bonnes performances en modulation OQAM-FBMC. Le filtre est généralement conçu pour une reconstruction parfaite ou quasi parfaite et une bonne localisation de la réponse en fréquence. Il s'agit d'une exigence contradictoire lorsque la longueur du filtre doit être courte pour minimiser la latence de bout-en-bout (E2E) et la complexité réduite, comme dans le cas des communications à faible latence ultra fiables (URLLC). De plus, les filtres courts sont préférables pour leur meilleure robustesse face aux canaux variant dans le temps.

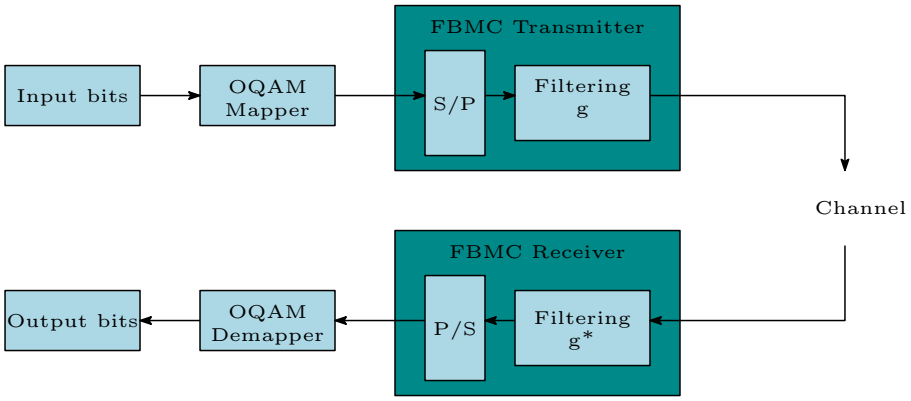

Figure 2: structure du transmultiplexeur OQAM-FBMC

Habituellement, les travaux se concentrent sur le FBMC en utilisant des filtres prototypes avec un facteur de chevauchement $K = 4$ (nombre de symboles FBMC adjacents superposés dans le domaine temporel). Cependant, un filtre prototype court ($K = 1$) peut également être appliqué aux systèmes FBMC. Dans ce chapitre, nous avons abordé le problème de la conception de filtres prototypes courts pour la modulation OQAM-FBMC, basé sur le choix judicieux de la fonction objectif à minimiser pour obtenir une énergie hors bande réduite (OOBE). Le problème est non convexe, ce qui nécessite de mettre en oeuvre des méthodes d'optimisation plus élaborées et personnalisées, pour lesquelles nous proposons une solution par approche heuristique. Pour cela, nous proposons les paramètres qui définissent la fonction à minimiser.

Des expériences numériques ont été menées afin d'évaluer la méthode de conception de filtre proposée. Nous avons utilisé le filtre QMF comme point initial de la procédure d'optimisation, qui appliqué à FBMC conduit à une modulation appelée Lapped-OFDM.

Les filtres prototypes générés ont été analysés sur la base de l'énergie totale de la bande d'arrêt et de la distribution d'énergie le long de la bande d'arrêt. En outre, nous avons analysé la densité spectrale de puissance (PSD) du système lorsque plusieurs sous-porteuses sont activées. Nous supposons qu'une bande passante de 900 kHz (60 sous-porteuses) est allouée là où un bloc de ressources est désactivé au milieu de la bande allouée. Les résultats représentés sur la figure 3 montrent que le filtre optimisé OPF1$(B, 9B)$, pour $B = 9/M$, atteint les meilleures performances en termes d'atténuation de la bande d'arrêt. Il a le niveau de rayonnement le plus bas dans la bande à protéger, autour de -60 dB. En effet, dans les bords extrêmes de la bande, la densité spectrale de puissance diminue rapidement, jusqu'à -90 dB, prouvant sa compétitivité face aux autres filtres testés.

Nous abordons le cas de l'accès asynchrone dans un scénario de coexistence où deux utilisateurs coexistants partagent la même bande de fréquence disponible,

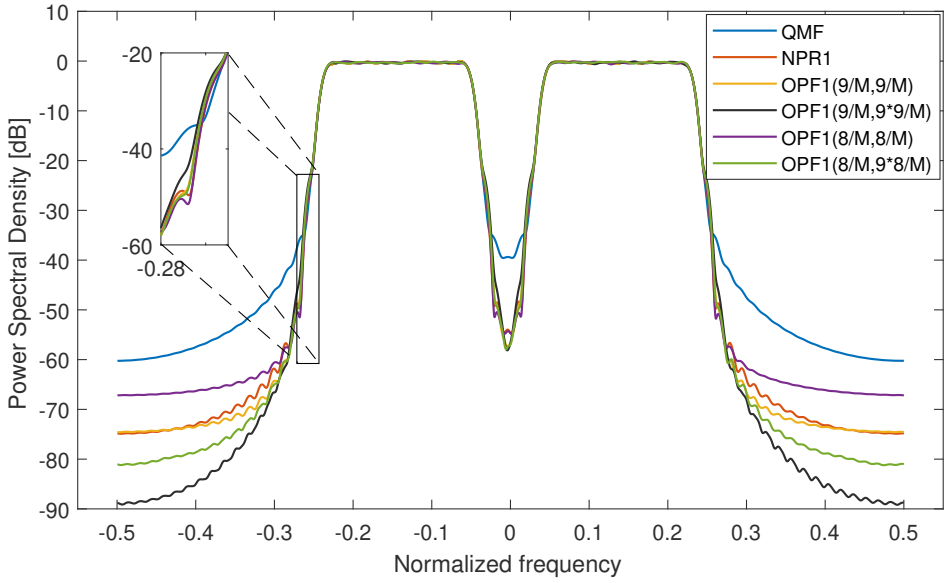

Figure 3: densité spectrale de puissance des différents filtres prototypes.

comme le montre la figure 3.12. Ici, la couleur verte représente les ressources alloués à l'utilisateur un U 1, celle qui l'intéresse, et la couleur rouge représente l'utilisateur interférant deux U 2. Le décalage de fréquence ϵ est représenté par la zone grise entre les utilisateurs U 1 et U 2. Nous représentons également le désalignement temporel de U 1 et U 2 en gris comme τ. En raison de la discordance de synchronisation, le récepteur concerné souffre d'interférences, ce qui entraîne une dégradation des performances.

À des fins de comparaison, nous avons évalué notre filtre conçu par rapport à des concurrents bien connus.

Enfin, nous terminons ce chapitre en résumant les principaux résultats obtenus.

Chapitre 4 Modulation QAM-FBMC

L'OQAM-FBMC offre une flexibilité dans la conception de forme d'onde par rapport à l'OFDM et permet des services hétérogènes, ce qui est également une exigence des systèmes de communication 5G/B5G. Malheureusement, bien que les données soient toujours orthogonales aux interférences, c'est le principal obstacle dans le processus d'estimation de canal et les applications MIMO combiné avec la détection du maximum de vraisemblance (ML) ou le code de bloc spatio-temporel (STBC).

Pour surmonter les inconvénients observés avec la modulation OQAM-FBMC, un schéma FBMC basé sur le QAM (QAM-FBMC) avec un seul prototype de filtre a été proposé. Dans les systèmes QAM-FBMC, la transmission des symboles QAM se produit à chaque période T au lieu de la demi-période $T/2$ comme cela se produit dans OQAM-FBMC. Ce faisant, l'orthogonalité réelle est perdue et par conséquent l'interférence intrinsèque résiduelle, dont les termes deviennent complexes, reste présente dans le récepteur.

Dans la modulation QAM-FBMC, l'interférence intrinsèque peut être considérablement réduite, permettant son application aux technologies MIMO. En outre, en raison de l'utilisation de filtres prototypes bien localisés, des caractéristiques de confinement spectral supérieur sont observées par rapport à l'OFDM.

Nous pouvons examiner les fonctions d'ondes sphéroïdales prolongées proposées par Slepian, comme solution possible pour la conception de filtres prototypes QAM-FBMC. Nous proposons, dans ce chapitre, un filtre prototype long (avec un facteur de chevauchement $K = 4$) conçu spécifiquement pour les systèmes QAM-FBMC qui appliquent un filtre adapté au niveau du récepteur. Nous considérons les séquences sphéroïdales prolate discrètes (DPSS) afin d'obtenir le filtre le plus concentré en énergie pour une limitation de temps/bande passante donnée et de minimiser les interférences intrinsèques du système. Nous comparons les performances des filtres obtenus à certains filtres connus de l'état de la technique.

Nous avons évalué les performances du système QAM-FBMC lors de l'utilisation des filtres prototypes optimisés basés sur DPSS (DPSSb) et comparé les résultats avec ceux obtenus en utilisant des filtres prototypes connus. La performance du filtre prototype a été évaluée par le taux d'erreur sur les bits (BER). Afin d'améliorer les performances globales du système, l'annulation itérative des interférences a été appliquée au récepteur. La figure 4 illustre les comparaisons effectuées.

Dans les systèmes multiporteuses, la durée des symboles et l'espacement des sous-porteuses définissent la structure de réseau temps-fréquence associé au système de communication. La majeure partie des travaux sur la conception des systèmes a porté sur les réseaux rectangulaires. Cependant, une telle approche ne s'avère pas la meilleure pour le cas des canaux à dispersion temps-fréquence.

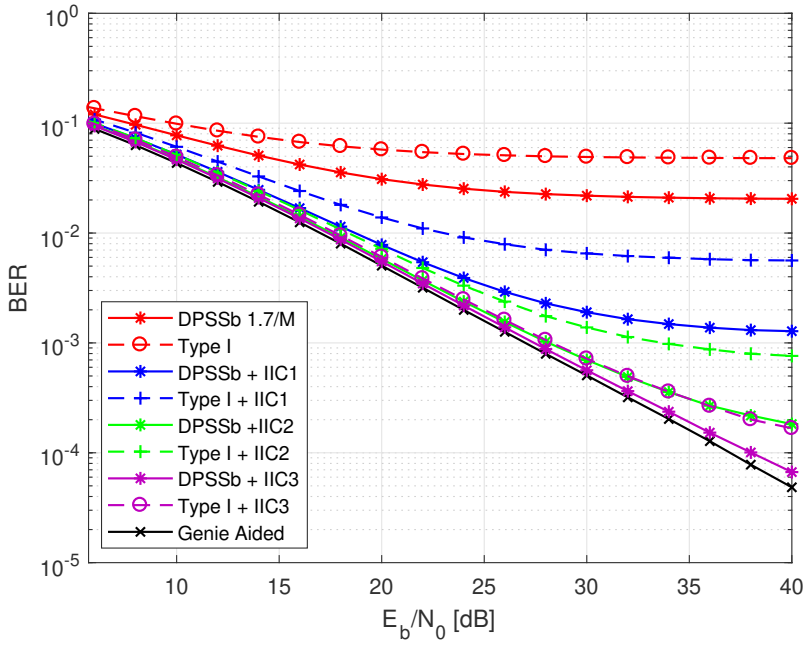

Figure 4: Performance BER du système QAM-FBMC avec modulation 16-QAM, filtre DPSSb $1.7/M$ et filtre de type I sur le canal pedestrian.

Nous proposons dans ce chapitre une structure décalée du QAM-FBMC conventionnel. Nous présentons le système QAM-FBMC implémenté sur la structure en réseau hexagonal (également appelé quinconce), ce que nous appelons HQAM-FBMC, comme illustré dans la figure 5.

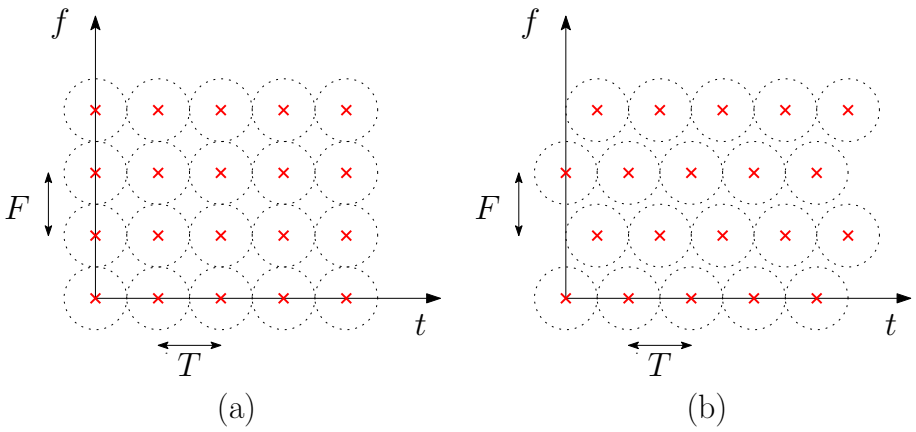

Figure 5: Structure de réseau temps-fréquence, (a) rectangulaire et (b) hexagonale.

Bien que nous trouvions des travaux sur étude des réseaux hexagonal dans divers domaines il n'y a pas à notre connaissance d'étude sur des filtres prototypes spécifiquement conçus pour les systèmes multi-porteuses avec des structures de réseaux hexagonales.

Nous proposons une nouvelle conception de filtre prototype long (avec un facteur de chevauchement $K = 4$) pour cette structure basée sur la conception DPSS.

Ensuite, nous optimisons le filtre proposé afin de surmonter les interférences intrinsèques du système HQAM-FBMC. Nous fournissons également une comparaison des performances du système QAM-FBMC à l'aide de son filtre DPSSb optimisé proposé, et du système HQAM-FBMC proposé également avec son filtre prototype HDPSSb optimisé.

Dans la figure 6, nous comparons les performances des modulations QAM-FBMC et HQAM-FBMC. Comme nous pouvons le voir, les résultats pour QAM-FBMC et HQAM-FBMC sont à peu près les mêmes. Nous avons également utilisé la technique d'annulation des interférences intrinsèques (IIC) afin d'améliorer les performances globales du système. Une fois de plus, pour chaque itération IIC, les deux systèmes obtiennent les mêmes résultats.

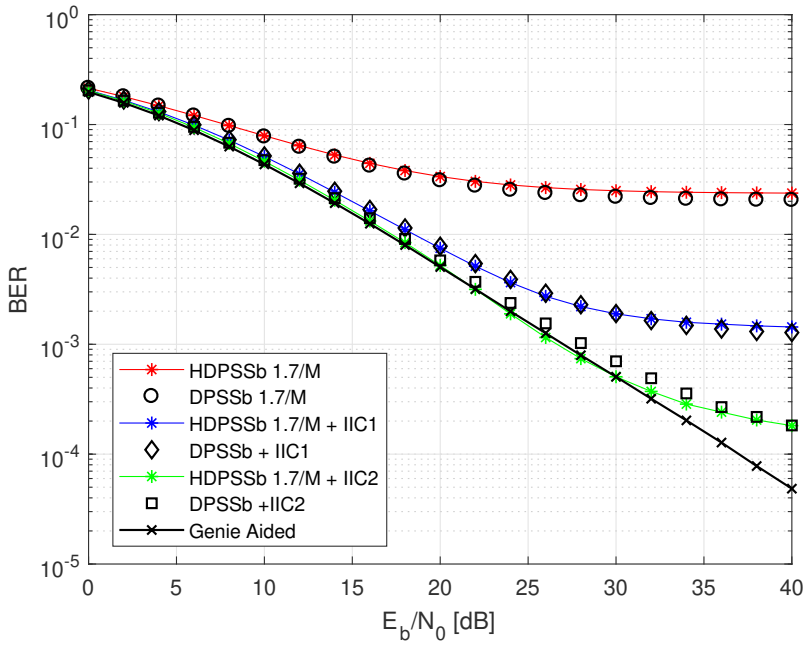

Figure 6: Performance BER du système QAM-FBMC avec modulation 16-QAM avec filtre DPSSb $1.7/M$ et HQAM-FBMC avec filtre HDPSSb $1.7/M$ sur le canal piéton.

Le choix du filtre prototype est fondamental pour la conception du QAM-FBMC, car il est responsable du confinement spectral du système. En outre, cela aura un impact direct sur les interférences intrinsèques et par conséquent sur le taux d'erreur bits (BER). En ce sens, plusieurs travaux ont été réalisés afin d'évaluer les performances des systèmes multiporteuses à travers leur probabilité d'erreur sur les bits (BEP). Des expressions analytiques ont été fournies pour l'OFDM et l'OQAM-FBMC sur un canal de bruit blanc Gaussien additif (AWGN) et sur un canal d'évanouissement de Rayleigh.

Néanmoins, à notre connaissance, l'analyse BEP spécifiquement pour le QAM-FBMC n'a pas encore été étudiée. Pour évaluer les performances des systèmes QAM-

FBMC, nous proposons une expression mathématique de son BEP. Nous étudions comment le choix du filtre prototype impacte sur les interférences intrinsèques et par conséquent sur le BEP du système.

Nous dérivons une expression BEP pour les systèmes QAM-FBMC sur le canal AWGN en tenant compte des interférences intrinsèques générées par la non-orthogonalité du filtre prototype. Nous dérivons également l'expression BEP pour QAM-FBMC sur les canaux d'évanouissement de Rayleigh, en tenant également compte de l'interférence intrinsèque générée par le filtre prototype. De plus, l'expression du BEP a été obtenue en utilisant l'interférence intrinsèque exacte pour un filtre prototype donné.

Nous avons évalué le BEP sur un canal de Rayleigh à évanouissement plat via l'équation proposée en considérant la modulation 4 -QAM et 16 -QAM comme présenté dans la figure 7. Il est possible de vérifier l'efficacité de la méthode proposée puisque les résultats théoriques et simulés sont identiques.

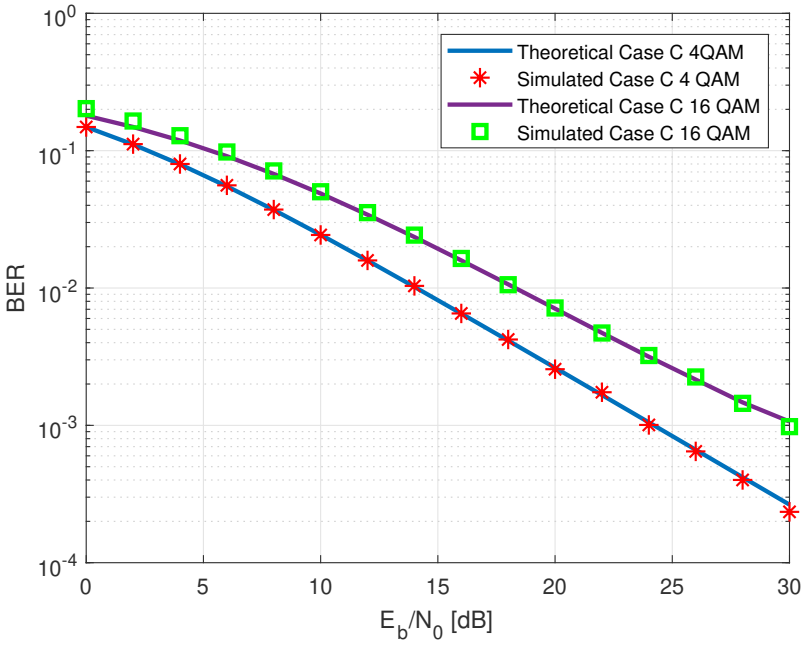

Figure 7: Probabilité d'erreur sur les bits simulés et théorique du système QAM-FBMC avec une modulation de 4-QAM et de 16-QAM sous le canal de Rayleigh.

Chapitre 5 Modulation QAM-FBMC avec filtres courts

Habituellement, la mise en œuvre des systèmes FBMC utilise des filtres prototypes avec une durée supérieure à celle du symbole FBMC, par exemple, un facteur de chevauchement $K = 4$, ce qui conduit à un filtre 4 fois plus élevé que la durée du symbole FBMC. En attendant, il convient de noter que différents facteurs de chevauchement peuvent également être pris en compte. En fait, l'utilisation d'un faible facteur de chevauchement, par ex. $K = 1$, peut être très avantageuse.

En effet, les filtres courts permettent la transmission des trames courtes pour des communications à faible latence, de réduire la consommation d'énergie de l'émetteur et de réduire la complexité de calcul, car la mise en œuvre du réseau polyphasé dépend fortement de la longueur du filtre prototype.

Bien que plusieurs filtres prototypes aient été conçus pour les systèmes QAM-FBMC, dans ce chapitre, nous avons proposé aussi des filtres courts (spécifiquement conçu avec un facteur de chevauchement $K = 1$) afin de réduire la latence du système tout en minimisant les interférences intrinsèques.

Nous avons présenté une conception de forme d'onde pour les systèmes QAM-FBMC qui n'appliquent qu'un seul PF, en prenant en compte de la réduction totale des interférences tout en conservant le confinement spectral, représenté par la limitation de l'énergie hors bande (OOBE). Nous avons formulé deux approches: avec et sans la connaissance du canal et minimisée l'interférence totale, soumise à la contrainte OOBE.

Dans la figure 8 nous présentons l'évaluation des performances BER des filtres optimisés. Comme on le voit, dans toutes les expériences, les filtres optimisés surpassent les filtres NPR1, QMF Gaussian et Hamming.

De plus, à l'instar de ce que nous avons fait pour le cas des filtres longs, nous évaluons également le taux d'erreur bits (BER) de QAM-FBMC en prenant en compte les filtres optimisés et aussi les filtres connus.

Comme la modulation QAM-FBMC ne peut pas satisfaire complètement la condition d'orthogonalité, une interférence résiduelle est toujours observée et dégrade les performances du système. Par conséquent, un récepteur plus élaboré est nécessaire. À notre connaissance, il n'y a pas de travaux spécifiques envisageant la conception de récepteurs QAM-FBMC pour filtres courts. Sachant cela, nous avons également mené une recherche sur les récepteurs QAM-FBMC afin de réduire les interférences.

Nous concevons différents récepteurs pour les systèmes QAM-FBMC qui appliquent des filtres prototypes courts. Nous proposons un récepteur qui effectue une égalisation avant le banc de filtres d'analyse (égaliseur de domaine temporel - TDE) et le comparons au bien connu égaliseur de domaine de la fréquence (FDE),

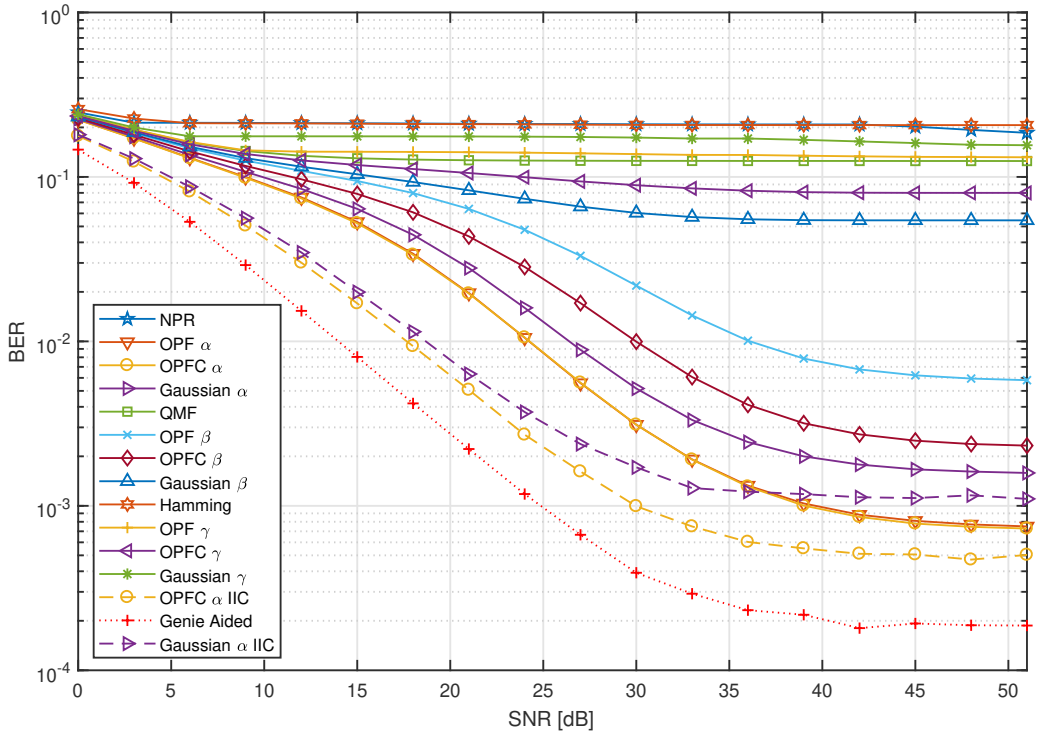

Figure 8: BER moyen évalué à l'aide de filtres OPF, OPFC, NPR, QMF Gaussian et Hamming avec 1000 canaux instantanés.

qui effectue une égalisation de canal après le banc de filtres d'analyse. Nous incluons également le schéma d'annulation d'interférence itérative (IIC) au récepteur et évaluons les performances globales du système.

De plus, nous proposons un nouveau récepteur basé sur l'erreur quadratique moyenne minimale (MMSE) avec annulation d'interférence entre blocs (IBI). Nous comparons les performances des récepteurs proposés avec les récepteurs de l'état de l'art, adapté au cas de filtres courts, en présence de canaux à évanouissements. De même, nous étendons le récepteur MMSE proposé pour le cas de deux utilisateurs.

Chapitre 6 Conclusions

Cette thèse s'est principalement concentrée sur l'analyse et l'optimisation des modulations OQAM-FBMC et QAM-FBMC vues comme une alternative à la modulation OFDM afin de répondre aux exigences des futurs systèmes de communication mobile. La question de la conception et de l'optimisation des filtres est l'essence et la motivation principale de ce travail.

Nous avons présenté les principales caractéristiques des réseaux à 5 G. Nous avons discuté des principaux cas d'utilisateurs et des technologies qui seront nécessaires pour ces services. En raison des nouveaux services, la modulation OFDM n'est pas suffisante pour fournir les conditions nécessaires au réseau à 5 G. Par conséquent, une couche physique complètement nouvelle a été développée. La modulation multiporteuse étant le thème central de cette thèse, des informations sur les modulations OFDM, OQAM-FBMC et QAM-FBMC ont été introduites comme base pour le reste de cette thèse.

Nous avons principalement analysé les interférences intrinsèques du système OQAM-FBMC, l'énergie hors bande passante et la condition de reconstruction parfaite. Ensuite, nous avons introduit une nouvelle conception de filtre prototype court qui minimise l'OOBE avec une fonction objectif soigneusement choisie sans violer la condition d'orthogonalité. Nous avons évalué les performances des filtres obtenus et comparés aux performances des filtres connus. Enfin, nous avons également analysé le comportement du système dans le contexte de l'accès asynchrone en considérant plusieurs utilisateurs. Les filtres obtenus semblent surpasser les filtres connus.

Nous avons décrit l'interférence intrinsèque des systèmes QAM-FBMC à travers les coefficients d'interférence. Nous avons proposé un filtre prototype basé sur DPSS et l'avons optimisé pour réduire les interférences intrinsèques du système. Par rapport aux filtres proposés dans la littérature, il s'est avéré possible d'améliorer les performances du système grâce à l'utilisation des filtres proposés. De plus, nous avons proposé un système hexagonal QAM-FBMC (HQAM-FBMC), et un filtre prototype pour le système HQAM-FBMC basé sur le DPSS, puis nous l'avons optimisé pour réduire les interférences intrinsèques. Étonnamment, nous avons montré qu'il n'y avait aucune différence significative entre les performances en terme de BER des systèmes QAM-FBMC avec les performances du HQAM-FBMC utilisant des filtres optimisése BER. Nous avons ainsi mis en évidence que, dans les conditions présentées dans cette thèse, il n'y a aucun gain à utiliser le réseau hexagonal.

Enfin, nous avons analysé la probabilité d'erreur sur les bits du système. Nous avons proposé l'expression du BEP pour les systèmes QAM-FBMC afin de prédire les performances du système. La précision de l'expression proposée a été validée par divers résultats de simulation, en tenant également compte de différents canaux.

Nous avons également présenté le QAM-FBMC qui utilise des filtres prototypes courts. Nous avons proposé un nouveau prototype de conception de filtre qui minimise les interférences intrinsèques du système soumis à une limitation OOBE. Dans ce cas, nous avons également pris en compte les informations sur le canal et optimisé un filtre pour une distribution de canal donnée. L'efficacité du filtre proposé a été analysée et nous avons montré qu'il surpassait les filtres connus. Nous avons également effectué une analyse de probabilité d'erreur sur les bits en utilisant l'expression proposée. Les expressions proposées concordent avec les résultats simulés, ce qui confirme l'applicabilité de la méthode proposée quel que soit le facteur de chevauchement.

Enfin, différents récepteurs pour un système QAM-FBMC qui applique des filtres courts ont été proposés afin d'améliorer ses performances. Les résultats ont montré que notre récepteur MMSE proposé, suivi de l'annulation IBI, présente les meilleures performances par rapport aux récepteurs conventionnels existants et même au récepteur de pointe. En résumé, notre récepteur proposé s'avère être applicable au QAM-FBMC avec des filtres courts utilisant un seul bloc pour effectuer l'égalisation.

Contents

List of Figures

List of Tables

List of Abbreviations and Acronyms

3GPP	3rd Generation Partnership Project, p. 8
4G-LTE	Fourth Generation Long Term Evolution, p. 9
5G-NSA	Fifth Generation Non-Stand Alone, p. 9
3G	Third generation of mobile communication systems, p. 1
4G	Fourth generation of mobile communication systems, p. 1
5G NR	5G New radio, p. 5
5G	Fifth generation of mobile communication systems, p. 1
AWGN	Additive white Gaussian noise, p. 41
BEP	Bit error probability, p. 2
BW-MMSE	Block-wise MMSE receiver, p. 109
CA	Carrier aggregation, p. 5
CCDF	Complementary Cumulative Distribution Function, p. 95
CFO	Carrier frequency offset, p. 35
CP	Cyclic prefix, p. 2
CR	Cognitive Radio, p. 18
D2D	Device-to-device communication, p. 1
DPSS	Discrete prolate spheroidal sequences, p. 40
DPSSb	Discrete Prolate spheroidal sequences based filter, p. 48
E2E	End-to-End, p. 11
EVA	Extended Vehicular-A, p. 92

F-OFDM Filtered Orthogonal Frequency-Division Multiplexing, p. 13

FBG Fiber bragg grating, p. 40

FDD Frequency Division Duplex, p. 5

FDE Frequency domain equalizer, p. 83

FFT-FBMC Fast Fourier Transform Filterbank Multicarrier, p. 13

FIR Finite impulse response, p. 22

FR Frequency range, p. 6

H2H Human-to-Human, p. 10

HDPSSb Hexagonal DPSS based filter, p. 63

HQAM-FBMC Hexagonal QAM-FBMC, p. 60

ICI Inter-Carrier Interference, p. 19

IDFT Inverse Discrete Fourier Transform, p. 23

IFFT Inverse Fast Fourier Transform, p. 11

IIC Iterative interference cancellation, p. 15

IOTA Isotropic orthogonal transform algorithm, p. 15

IP Interior point, p. 32

ISI Inter-symbol Interference, p. 12

ITU International Telecommunications Union, p. 1

IoT Internet of Things, p. 10

LDPC Low Density Parity Check Codes, p. 5

LOFDM Lattice OFDM, p. 60

LTE Long term evolution, p. 5

M2M Machine-to-machine, p. 1

MCM Multicarrier Modulation, p. 13

MFTN Multicarrier faster than Nyquist, p. 60

MIMO	Multiple-input Multiple-output, p. 1
ML	Maximum likelihood, p. 15
MMB4	Martin-Mirabassi-Bellanger 4, p. 27
MMSE	Minimum mean square error, p. 40
MSE	Mean Square Error, p. 36
NMSE	Normalized Mean Square Error, p. 36
NPR1	Near-to-perfect reconstruction, p. 18
OFDM	Orthogonal Frequency Division Multiplexing, p. 2
OOBE	Out-of-band energy, p. 2
OPF1	Optimized prototype filter, p. 32
OPFC	Optimized prototype filter considering a channel, p. 90
OQAM-FBMC	Offset Quadrature Amplitude Modulation Filter-bank Multi Carrier, p. 2
PAM	Phase amplitude modulation, p. 14
PAPR	Peak-to-average power ratio, p. 95
PDP	Power delay profile, p. 89
PER	Packet Error Rate, p. 11
PF	Prototype filter, p. 25
PHYDYAS	PHYsical layer for DYnamic AccesS and cognitive radio, p. 15
PPN	Polyphase network, p. 22
PSD	Power Spectral Density, p. 34
PSWFs	Prolate spheroidal wave functions, p. 40
QAM-FBMC	Quadrature Amplitude Modulation Filter-bank Multi Carrier, p. 2
QAM	Quadrature Amplitude Modulation, p. 11
QCQP	Quadratically Constrained Quadratic Programming, p. 30

QMF	Quadrature Mirror Filter, p. 18
QoS	Quality of Service, p. 5
RB	Resource block, p. 32
SA	Stand Alone, p. 9
SCS	Subcarrier spacing, p. 7
SNR	Signal-to-noise rate, p. 44
STBC	Spatial time block coding, p. 15
TDD	Time Division Duplex, p. 5
TDE	Time domain equalizer, p. 83
TO	Timing offset, p. 35
TTI	Time Transmission Interval, p. 11
UDN	Ultra Dense Network, p. 1
UF-OFDM	Universal-Filtered Orthogonal Frequency-Division Multiplexing, p. 13
UHD	Ultra high definition, p. 1
ZF	Zero forcing, p. 107
eMBB	Enhanced mobile broadband, p. 6
mMTC	Massive Machine-type Communications, p. 6
mmWave	Millimeter wave, p. 1
uRLLC	Ultra Reliable Low Latency Communications, p. 6

Chapter 1

Introduction

CUSTOMER demands are the principal drivers of mobile communications development. The International Telecommunications Union (ITU) predicts increases in traffic estimated between 10 and 100 times in the next 10 years. Indeed, we will also witness a growth in the number of services and connected devices, beyond the demand for enhanced affordability. Knowing that, innovative solutions will be required in order to enable all user's connections.

The fifth generation of mobile communication systems, 5G network, is expected to provide this enormous volume of connections. It has promised to connect people, things, transport systems, and cities in smart network communication environments.

An amount of new services should be delivered by 5G networks. New technologies are expected to support applications such as smart homes and buildings, smart cities, 3D video in ultra high definition (UHD), work and play in the cloud, remote medical services, virtual and augmented reality, and massive machine-to-machine (M2M) communications for industry automation.

Previous generation wireless networks, 3G and 4G, currently face several challenges in providing these services since diverse, and often contradicting key performance indicators need to be observed, *e.g.*, reliability, high data rates, connectivity, ultra-high speed with very low latency. These are essential requirements to meet the new service demands.

For dealing with these strict requirements of 5G networks a completely new radio air interface is necessary. A new air interface, called 5G NR, has been developed, and it counts on new features, services, and technologies, *e.g.*, Massive MIMO, mmWave, Full-duplex Radio, D2D communication and ultra dense network (UDN).

Objectives of this work

Multicarrier modulation is an auspicious technology to achieve the high required data rates of 5G. Several works have been carried out in the context of comparing different multicarrier modulations [3–7], with the aim of finding the best one for the physical layer of future mobile communications systems. However, in this work, we have focused on the study and optimization of the existing multicarrier modulations through their pulse shape filters.

The functions used to filter each subcarrier will directly impact the multicarrier system performance. Besides it will determine the flexibility of the system, the spectral occupation, and the implementation complexity. It will also limit the degrees of freedom for the system design.

In the literature, several proposals for prototype filter design have been presented for different multicarrier systems, respecting the particular characteristics of each one. Such study is of great interest, since it is possible to choose the best filter for the system, it represents a degree of freedom in the system project. Indeed, the prototype filter can be designed to satisfy some specific characteristics, *e.g.*, time and frequency localization.

Usually we can classify the multicarrier modulation schemes according to the length of the applied prototype filter as memoryless block transmission, when the filter has the duration of one symbol and its overlapping factor is defined as $K = 1$. Furthermore, we classify as overlapped block transmission systems when the filter is longer than the symbol period, what also means that the blocks overlap in time domain. Thus the overlapping factor is higher than one.

The main objective of this thesis is to analyze, study, and optimize the most prominent multicarrier systems in the context of 5G/B5G communication networks: the Offset Quadrature Amplitude Modulation Filter-bank Multi Carrier (OQAM-FBMC) and the Quadrature Amplitude Modulation Filter-bank Multi Carrier (QAM-FBMC).

In this context, this work deals with the challenge of designing prototype filters well shaped in frequency domain and also respecting the particularities of each considered system. We consider also the design of short filters ($K = 1$) applied to QAM-FBMC system.

We investigate and describe the intrinsic interference and the out-of-band energy (OOBE) for each system, and design prototype filters that minimize them. We also investigate the particular constraints related to each system so that the transmitted symbols can be recovered at the receiver.

In addition, we also deal with the intrinsic interference of the system by analyzing the bit error probability (BEP) and proposing a new receiver structure for the case

of QAM-FBMC with short filters.

Thesis outline

Chapter 1 - An overview on 5G

In this chapter, we present an overview and the state of the art of some 5G communication system concepts to be used in this thesis. First, we present some basic features of 5G and user cases. Then, the challenges of physical layer design are discussed. The general concept of multicarrier communication is provided, and we give a brief description of OFDM based systems and FBMC based systems.

Chapter 2 - OQAM-FBMC modulation

In this chapter, the OQAM-FBMC system is considered. After introducing the system model and its polyphase implementation, we propose a prototype filter design based on the minimization of the OOBE subject to the perfect reconstruction condition. Furthermore, we evaluate the OQAM-FBMC system performance through its spectrum and bit error rate when using the proposed optimized filters. We also analyze the robustness of the system to the asynchronous access.

Chapter 3 - QAM-FBMC modulation

In this chapter, we analyze the QAM-FBMC system. We present a system model and propose a novel prototype filter design based on Discrete Prolate Spheroidal Sequences (DPSS). Furthermore, we propose a new QAM-FBMC system based on the hexagonal lattice (HQAM-FBMC) structure together with an appropriate prototype filter design. We compare the performance of the standard QAM-FBMC with the one of our proposed HQAM-FBMC. Finally, we propose a bit error probability expression for QAM-FBMC systems.

Chapter 4 - QAM-FBMC modulation with short filters

In this chapter, we discuss the QAM-FBMC system when using short prototype filters. We present the known short filters found in the literature. We show that the prototype filter construction can be seen as an optimization problem, and propose a novel short prototype filter design based on the minimization of the observed interference. We also provide a bit error probability analysis for this system. In addition, advanced receivers are proposed specifically for QAM-FBMC systems with short filters.

Chapter 5 - Conclusions

Finally, in this chapter, we draw the final conclusions and we emphasize the main contributions of this thesis. Furthermore, we present possible future works.

List of publications

The results of this thesis work have been disseminated in renowned journals such as IEEE Transaction on Vehicular technology, IEEE Communication Letters, and IEEE Access. A part of the work have also been disseminate through the conference papers in *Simpósio Brasileiro de Telecomunicações-SBrT*.

Journal papers

J1. Andrade, I.G., Zakaria, R., Le Ruyet, D., Campos, M.L.R. de, "Intrinsic interference reduction in QAM-FBMC modulation using short filter design".in *IEEE Communications Letters*, Vol. 24, pp.1487-1491,2020.

J2. Galdino, I., Zakaria, R., Le Ruyet, D., Campos, M.L.R. de, "Short prototype filter design for OQAM-FBMC modulation", in *IEEE Transactions on Vehicular Technology*, Vol. 69, pp. 9163-9167, 2020.

Conference papers

C1. Galdino, I., Zakaria, R., Le Ruyet, D., Campos, M.L.R. de, "Avaliação da performance do sistema QAM-FBMC utilizando filtros Gaussianos curtos", in *proceeedings of XXXVII Simpósio Brasileiro de Telecomunicações - SBrT2019*; Petrópolis, Brazil.

C2. Galdino, I., Zakaria, R., Le Ruyet, D., Campos, M.L.R. de, "Probabilidade de erro de bit em sistemas QAM-FBMC", in *proceeedings of XXXVIII Simpósio Brasileiro de Telecomunicações - SBrT2020*. Online.

Chapter 2

An overview on 5G

It is expected that 5G brings a leap to the existing communication technologies. An ubiquitous coverage, massive connection, and strict Quality of Service (QoS), which are essential 5G characteristics, call for power consumption optimization as a matter of prime importance [8]. The use of small cells and relays can be a prominent solution for reducing the energy consumption, which leads to what we call green communications.

Frequency Division Duplex (FDD) and Time Division Duplex (TDD) techniques, for low frequency band an high frequency band respectively, will also be implemented in 5G. For providing high data rate transmission, forward error correction will be performed through Low Density Parity Check Codes (LDPC), instead of turbo codes, which was used in the previous 4G system.

In addition, carrier aggregation (CA) will be flexible and enhanced to enable dual simultaneous connectivity of LTE and 5G. This technique will lead to an improvement of data rates and throughput [9].

5G arises with a quite superior air interface compared to the existing ones. It comes with the necessity of supporting new services, and, for ensuring these demands, the 5G NR architecture is made to be flexible so that numerous applications can be enabled.

2.1 Features of 5G NR

There are various key features of 5G NR systems that we do not find in previous systems. These features help 5G deliver the promised services. For this propose, 5G counts on some known features from previous systems *e.g.*, carrier aggregation, multicarrier modulation, and MIMO transmissions. Beyond the enhancement of the already existing features, 5G systems will also count on new features improving the capacity, efficiency of the radio resource allocation, and enabling adaptation to the

diversity of service requirements and channel conditions. Some of them are listed in the following.

2.1.1 Massive MIMO

Massive Multiple-input Multiple-output (MIMO) is an extension of the traditional MIMO already used in 4G networks, it is helpful in providing a massive connection in 5G networks.

Nowadays, MIMO systems are using two or four antennas, but, the idea of 5G is to deploy an array of antennas geographically dispersed which have tens or hundreds of antenna units. The main objective of massive MIMO is to enjoy the benefits of MIMO, however in a large scale.

Massive MIMO is an evolving technology of next generation networks, which brings huge capacity gain to the system, it is energy efficient, robust, secure, and spectrum efficient [10], however, at the expense of increased infrastructure cost.

Together with the increase in the number of base station antennas, the number of channel estimations will significantly increase for each terminal. It will cause an increase in the number of transmissions to feedback the channel responses to the base station. A possible solution for this problem is to operate in Time Division Duplexing (TDD) mode [11].

2.1.2 High frequency operation

For addressing the requirements and usage scenarios, 5G systems will operate in two different frequency ranges, FR1 and FR2. FR1 includes frequencies from 0.45GHz up to 6GHz, it will basically provide broad and deep indoor coverage and improve system capacity. FR2 ranges from 24GHz to 52.6GHz [12], and it will generally be used for sustaining applications and cases that require extremely high data rates as presented in Table 2.1, [9]. When the system operates in frequency band FR2, more specifically in frequencies higher than 52.2GHz, it will use millimeter waves (mmWave). The operation through mmWave offers the possibility of using a large amount of spectrum and very wide transmission bandwidths, enabling the higher data rate services and providing high traffic capacity. 5G NR system design is made to be flexible so that the three different use cases (Enhanced Mobile Broadband - eMBB, massive Machine-type Communications - mMTC and Ultra Reliable Low Latency Communications - uRLLC) can be supported in different deployment scenarios.

Despite the improvement brought by the advent of mmWave, transmissions over high frequencies come at a cost of high radio channel attenuation, which limits the network coverage. However, this disadvantage can be overcome by the use of

Table 2.1: Frequency bands and supporting services.

	Frequency Rage	Maximum Bandwidth	Application
FR1	Below 2GHz	50/100 MHz	Broad and deep indoor coverage
	2GHz to 6GHz	50/100/200MHz	Capacity and coverage
FR2	Above 6GHz	20/400MHz	Extremely high data rates

advanced multi-antenna at the transmitter and at the receiver. For this, the antenna size should be smaller and with substantialy improved coverage property.

2.1.3 Flexible spectrum

5G is being developed to be flexible in time and frequency domains. A flexible frame structure has been designed to efficiently multiplex diverse 5G services and provide forward compatibility for future ones. The flexibility of spectrum access includes the usage of different frequency bands for different types of communications, each one with its own particular requirements. Therefore, the 5G NR framework will be able to support the diverse services, features, and deployment scenarios envisioned for 5G.

2.1.4 Flexible Numerology

5G networks will count on scalable subcarrier spacing (SCS) and different symbol duration. This feature will allow flexibility to the requirements necessary for the variety of desired services. Different subcarrier spacing will allow, for example to deal with different channel conditions. Another reason for different SCS is the different performance requirement for each application. For example, high subcarrier spacing allows low latency transmissions whereas low subcarrier spacing increases the efficient usage of the transmission band and makes the system more robust to delays.

Numerology is defined as the frame organization and in 5G it can vary depending on the application used. This variation will lead in different frame organizations. It is identified as a parameter μ and range from 0 to 4, as presented in Table (2.2) [12].

Table 2.2: 5G numerology and frame organization

μ	Δf	symbols/slot	slot/subframe	subframe/frame
0	15 KHz	14	1	10
1	30 KHz	14	2	10
2	60 KHz	14	4	10
3	120 KHz	14	8	10
4	240 KHz	14	16	10

The first group of numerologies $\mu = \{0, 1, 2\}$, is dedicated to the frequency range FR1, for sub 6 GHz transmissions. The second group $\mu = \{2, 3, 4\}$, corresponding to FR2 is dedicated to the mmWave transmissions, for frequencies above 6 GHz. The numerology $\mu = 5$ is not supported yet [13]. The subcarrier spacing will be defined through the numerology index $\Delta f = 2^{\mu} \times 15$ KHz. It is worth mentioning that all numerologies must provide the same symbol density as in LTE. As the duration of a slot depends on the numerology, the number of slots per-subframe also vary according to the numerology. It makes the 5G resource grids flexible in terms of resource allocation while ensuring high efficiency.

Each slot is composed of a fixed number of OFDM symbols. Furthermore, the concept of a fractional sized mini-slot can address the efficiency and latency of 5G requirements by transmitting short blocks of data.

The frame duration in 5G is defined as 10 ms, as it happens in 4G [12]. The frame is then divided into 10 subframes of duration 1ms each one. The subframes are independent, they can be separately decoded. Differently from what happens in 4G, in this case, each subframe can be divided into a flexible number of slots according to the chosen numerology. Hence, the slot duration will vary for each numerology ($1\text{ms}/2^{\mu}$). However, the number of symbols in one slot is fixed to 14, consequently, the symbol duration will also vary ($1\text{ms}/2^{\mu} \times 14$).

2.1.5 Carrier aggregation

Carrier aggregation is a technique already used in 4G systems to increase the data rate per user. It consists of assigning multiple contiguous subcarriers to the same user. By doing this, the overall data rate of a cell is increased, thanks to the better resource allocation.

In 5G systems, carrier aggregation, including different carriers having same or different numerologies, is supported. The maximum number of carriers for carrier aggregation is 16 [14].

2.2 Use cases

The fifth generation, 5G, access technology has been developed not only aiming to increase the spectral efficiency or increase the throughput, but also to provide new services [15]. The main services of 5G are represented in Figure 2.1. The first phase of 5G, defined by 3GPP, was focused on Non-Stand Alone (5G-NSA) procedure, in which 5G is supported by the 4G-LTE structure. In this case, the target is to enhance the mobile broadband (eMBB) in order to improve connection reliability. In a second moment, Stand Alone (SA) operation defines 5G as the next generation architecture

completely independent of 4G-LTE [14]. In SA phase, 3GPP Release 15 [16] defines critical Key Performance Indicators (KPIs) necessary to provide new service types such as massive Machine-type Communications (mMTC), and Ultra Reliable Low Latency Communications (URLLC). The eMBB provides better coverage, high data rate, and high capacity, the mMTC will allow a huge amount of simultaneously connected devices, and URLLC will offer very high reliability and very low latency.

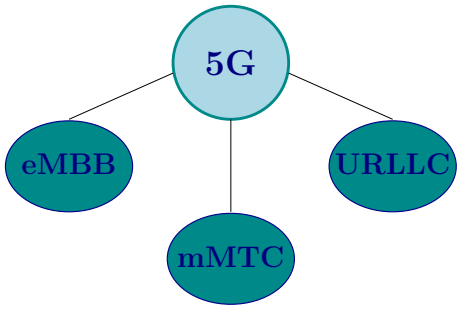

Figure 2.1: Principal uses cases of 5G.

2.2.1 Enhanced Mobile Broadband (eMBB)

The eMBB extends the support of conventional MBB, already provided by LTE systems, which is now refereed as eMBB. It attempts to improve data rates, capacity, and coverage of previous systems. Among typical use cases we can cite file downloads, internet browsing, videoconferencing, voice over IP, and multimedia streaming. The eMBB transmission requires low latency communications (1ms), reliable broadband access (99.9999%) and extremely high data rate. Consequently, modulations with guard intervals, in frequency or time domain, that are responsible for decreasing the system spectral efficiency does not fit the 5G needs.

These types of requirements are contradictory due to the simultaneous coexistence of eMBB and URLLC. Indeed, researchers have been working on possible solutions to meet both URLLC and eMBB requirements concomitantly, such as the research presented in [17], in which the authors proposed a solution based on a preemptive spatial scheduler based on a null-space-based spatial preemptive scheduler.

Through the improvements brought by the eMBB, 5G networks will be capable to offering enhanced broadband access in highly dense areas, including not only smartphones but also connected Internet-of-Things devices. It will also be capable of providing consistent access everywhere at any time, even in vehicular connections, including high speed trains. Besides, virtual interactions will be held in real time.

2.2.2 Massive Machine-type Communications (mMTC)

Also known as the Internet of Things (IoT) [18], mMTC employs a massive amount of sensors that need to be connected to the network. Due to its typical applications, *e.g.*, natural ecosystem monitoring, remote diagnostics, autonomous driving, and factory automation, the transmission is commonly assumed to be mostly unidirectional [19]. In this case, it is mandatory to provide connectivity for an increasing number of devices. In addition, wide area coverage and deep indoor penetration area are key properties. Moreover, this type of transmission is sporadic and usually requires relatively small packets per connections, consequently, the data rate is low. However, the desired user density is very high, up to 300000 users connected into a cell [20], which makes the total data rate high.

Previous systems were designed for Human-to-Human Communications (H2H) and this technology is not able to support Machine-to-Machine Communications (M2M) since it requires high reliability and security. Besides, there are several MTC applications and each one demanding its own Quality of Service (QoS), which is a challenge for 4G networks.

Another important aspect of the mMTC is the limited hardware resources. Thus, the implemented modulation must be designed to keep the energy consumption as low as possible. Also, in order to reduce energy consumption, the signaling related to the synchronization procedure must be reduced. To achieve this reduction, it is necessary to support asynchronous communications.

2.2.3 Ultra-reliable Machine-Type Communications (uMTC)

Defined by 3GPP as Ultra Reliable Low Latency Communications (URLLC) [21], it can enhance the quality of the network and makes it potentially sufficient for supporting several applications.

URLLC consists in the transmission characterized by the very low latency and very high reliability, which are contradicted if provided simultaneously. However, latency and reliability play an important role in real-time applications and services. Typical URLLC applications include management and synchronization of traffic, vehicle to anything communications (including autonomous vehicle), vital signal monitoring and remote surgery beyond industrial control applications through robots. [22]

The expectancy for 5G is to achieve latency lower than 1ms and very small packet error rate (PER), 10^{-5} [23]. As we may know, the latency is directly related to the Time Transmission Interval (TTI), which in 4G-LTE is defined as 1ms, corresponding to the transmission of 2 Resource Blocks (RB) [16]. Consequently, in 4G-LTE systems, even disregarding the propagation delay, hardware latency and

transmission delay, the overall end-to-end (E2E) communication delay is 1ms. One should notice that the 5G latency requirement is not fulfilled by the 4G-LTE technology. Therefore, different solutions have been investigated to deal with 5G latency requirements.

Providing low latency and high reliability simultaneously is a challenging task. Several works have been conducted in order to provide good solutions [23, 24].

A proposal to deal with this problem has been studied in [25]. The basic idea is to reduce the OFDM symbol duration, but keeping the same number of OFDM symbols in a resource block (RB). It can be done by reducing the FFT size. As a consequence, the subcarrier frequency spacing will be increased. OFDM modulation requires the same frequency spacing to be used for all users, in order to keep the orthogonality, which makes its use in 5G systems questionable.

Another approach consists in reducing the number of OFDM symbols transmitted in a RB. Nonetheless, the major drawback of this solution is that it compromises the channel estimation, and consequently the equalization process. Therefore, alternative modulation techniques may be required for supporting URLLC.

2.3 Challenges on 5G physical layer

To meet the demands of the user and to overcome the challenges that has been put forward in the 5G system a drastic change in the strategy of designing the 5G wireless cellular architecture is needed. The requirements of 5G physical layer have encouraged the study of a more flexible air interface based on a waveform with good spectral localization. Multicarrier waveforms have been studied as a possible solution.

Multicarrier modulation has been the most widespread communication technique due to its capacity to overcome multi-path fading channel obstacles. This technique consists of dividing the available bandwidth into several orthogonal sub-channels centered at different subcarrier frequencies f_k, $k = [0, \ldots, M-1]$ (also called sub-band) spaced by $\Delta f = \frac{1}{M}$. In this case, each sub-band is independently filtered. In Figure 2.2 we have a simplified multicarrier modulation structure.

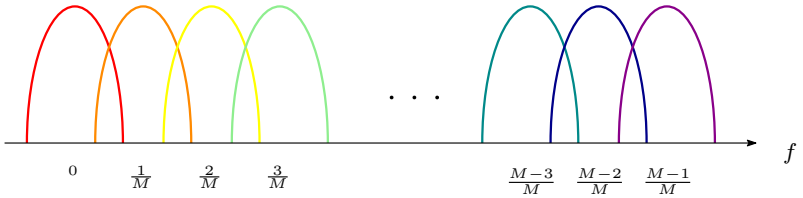

Figure 2.2: Example of MCM spectrum.

The number of used subcarriers must be carefully chosen in such a way that the

space between them will be less than the coherence time of the channel, T_L. As a consequence, each sub-channel will experiment a flat channel, and the equalization process can be simplified.

In this Section we will present some of the most known multicarrier techniques in the literature and point out their possible applicability to the 5G.

2.3.1 OFDM

Several multicarrier techniques have been studied, among them the most widespread is called Orthogonal Frequency Division Multiplexing (OFDM). Firstly introduced in 1971 by Weinstein and Ebert [26], OFDM broadly applies to cellular, local area and vehicular communications by several reasons: due to its efficient implementation through the inverse fast Fourier transform (IFFT), robustness against multipath channels thanks to the cyclic prefix (CP), and also due to its applicability to multiple-input multiple-output (MIMO) communications.

The main idea of OFDM is to divide the transmission bandwidth into M subbands and send a complex symbol in each one. In this scheme, each quadrature amplitude modulated (QAM) symbol, $d_{k',n'}$, $n' \in \mathbb{Z}$, sent to the subcarrier k' at a time instant n', is shaped by a rectangular window. Then, the base-band transmitted signal can be written as:

$$s[m] = \frac{1}{\sqrt{M}} \sum_{k'=0}^{M-1} \sum_{n'} d_{k',n'} g\left[m - n'(M + L_{CP})\right] e^{j2\pi \frac{k'm}{M}}, \tag{2.1}$$

where M represents the number of subcarriers, L_{CP} the cyclic prefix length, and the transmitter filter, g, is defined by:

$$g\left[m\right] = \begin{cases} 1, & \text{if} \quad -L_{CP} \leq m \leq M \\ 0, & \text{otherwise} \end{cases} \tag{2.2}$$

Considering the ideal channel, it is possible to achieve perfect reconstruction of complex symbols by respecting the complex orthogonality condition:

$$\sum_{n} g\left[m - nM\right] e^{j2\pi \frac{km}{M}} g\left[m - n'M\right] e^{j2\pi \frac{k'm}{M}} = \Delta_{k,k'} \Delta_{n,n'}, \tag{2.3}$$

where k is the observed subcarrier at the receiver, and $\Delta_{k,k'} = 1$ when $k = k'$, and $\Delta_{k,k'} = 0$ when $k \neq k'$.

To avoid inter-symbol interference (ISI), the addition of a sufficiently large guard interval is used in order to separate sequential symbols [27]. Considering the transmitted signal as contiguous signal blocks, in a multipath channel, it is possible to notice a block overlapping. As long as we consider the length of the channel impulse

response smaller than the symbol length, $L_C \leq M$, this overlapping affects only two consecutive blocks.

Also, considering the IFFT based implementation, each IFFT index is directly related to each subcarrier. At the output of the IFFT, a time-domain signal of M samples is obtained. Finally, a cyclic prefix of legth T_{CP} is inserted by duplicating the last T_{CP} samples at the beginning of the signal. Therefore, the time duration of the OFDM symbols is $T = (T_o + T_{CP})/F_s$, admitting that the OFDM signal is transmitted with a frequency sample of F_s.

The multipath channel can introduce inter-symbol interference, however, if the CP length is larger than the delay spread of the channel, it will act as a guard-interval and ISI can be avoided. Besides, it is also possible to have a per-subcarrier equalization at the receiver.

Despite OFDM has been defined as the most appropriate multicarrier modulation for 3G and 4G networks, it is not indicated to support many emerging 5G applications. Its drawbacks come essentially from the rectangular-shaped filter that is used, which presents a high level of out-of-band energy (OOBE) and poor spectral efficiency due to the usage of CP. From the physical layer perspective for 5G, it is essential to have well localized filters in frequency/time to avoid the need for stringent synchronized transmissions among heterogeneous networks. Indeed, the rectangular receiver filter brings a significant amount of interference from asynchronous users [28].

Knowing the inability of OFDM to meet the requirements of 5G, recent researches address the challenges of the 5G physical layer. Thus, several waveforms have been proposed. Among them we can cite: Filtered Orthogonal Frequency-Division Multiplexing (F-OFDM), Filter-Bank Multicarrier offset-Quadrature Amplitude Modulation (OQAM-FBMC), Filter-Bank Multicarrier Quadrature Amplitude Modulation (QAM-FBMC), and most recently Fast Fourier Transform Filter-Bank Multicarrier (FFT-FBMC). The main difference among them lies on the orthogonality (real, imaginary or non-orthogonal), and in the type of filtering (per subcarrier or per group of subcarriers).

2.3.2 F-OFDM

Filtered-OFDM has been presented as a potential 5G waveform candidate in [29]. This scheme is based on the conventional OFDM followed by a spectrum shaping filter. The main purpose of this filtering is to avoid interference leakage to the neighboring subbands and thus overcome the asynchronous communications interference. The proposed approach consists of improves the out-of-band radiation of the traditionl OFDM signal by using a filter. At the reception, the interference that comes

from asynchronous adjacent users is attenuated by the use of a similar filter at the input of the OFDM receiver.

The filtering process applied by the F-OFDM generates inter-block interference, however, if the chosen filter is appropriately designed, its impact on the communication performance can be neglected [29]. F-OFDM has lower sidelobes. This allows a higher utilization of the allocated spectrum, leading to increased spectral efficiency.

2.3.3 OQAM-FBMC

In order to overcome the drawbacks of OFDM, a FBMC based system that offers better spectral localization and flexible access to the resources has been proposed.

Differently from the OFDM, that uses rectangular filter, in FBMC systems the use of well frequency localised filter leads to better adjacent channel leakage performance compared to OFDM. Furthermore, by respecting Nyquist constraints in the prototype filter design, combined with the transmission of OQAM symbols, it is possible to ensure the orthogonality between adjacent symbols and adjacent subcarriers while keeping maximum spectral efficiency.

In OQAM-FBMC systems, the transmitted symbols $a_{k',n'}$ are QAM modulated. According to the OQAM transmission, $d_{k',n'} = a_{k',n'} e^{j\phi_{k',n'}}$ where $a_{k',n'}$ are real symbols whose mean energy σ_a^2 is half of that of the QAM symbols energy σ_d^2. Besides, the in-phase and quadrature components of the QAM symbols are staggered by half a symbol period, *i.e.*, $T/2$.

Let $g[m]$ be a causal prototype filter with length $L_g = KM$, where K is the overlapping factor [30] and M is the number of subcarriers. The discrete-time transmitted signal in OQAM-FBMC can be written as [31–33]

$$s[m] = \sum_{k'=0}^{M-1} \sum_{n'} a_{k',n'} e^{j\phi_{k',n'}} g\left[m - n'M/2\right] e^{j\frac{2\pi}{M}k'm}, \tag{2.4}$$

where $\phi_{k',n'}$ is a phase term commonly defined in the literature as [33, 34]

$$\phi_{k',n'} = \frac{\pi}{2}(k' + n') - \pi k' n'. \tag{2.5}$$

The phase offset inserted by $\phi_{k',n'}$ ensures that the frequency-time neighbor PAM symbols are in quadrature with each other.

By defining $g_{k',n'}$ as

$$g_{k',n'} = g\left[m - n'M/2\right] e^{j\frac{2\pi}{M}k'm} e^{j\phi_{k',n'}}, \tag{2.6}$$

we can summarise the real orthogonality condition, restricted to the real field, that we should obey during the prototype filter design in order to guarantee perfect

reconstruction of the transmitted signal at the receiver. Thus, by relaxing the orthogonality condition presented for OFDM systems in Equation (2.3) which is kept just in real domain, the prototype filter must be designed such that it satisfies:

$$\Re\left\{\sum_{m} g_{k',n'}\left[m\right] g_{k,n}^{*}\left[m\right]\right\} = \Delta_{k,k'}\Delta_{n,n'}, \tag{2.7}$$

where $g_{k,n}^{*}$ represents the receiver filter.

Despite the benefits of OQAM-FBMC systems, they usually employs long prototype filters, *e.g.*, PHYDYAS filter [35] and IOTA filter [36], both with $K = 4$. This feature calls into question its applicability to low latency communication systems [37]. Besides, as it relaxes the orthogonality condition, which is kept only in the real domain, the transmitted data, which are real valuated, are contaminated by purely imaginary interference. Although the data are always orthogonal to the interference, this is a major problem in, *e.g.*, channel estimation, in multiple-input multiple-output (MIMO) systems with spatial time block coding (STBC) [38], or maximum likelihood (ML) detection [39].

In this sense, some solutions have been proposed to reduce the interference such as the iterative interference estimation and cancellation (IIC) at the receiver. However, the error propagation during the estimation process limits the obtained results [40]. It has also been demonstrated that to overcome this problem, the intrinsic interference level should be kept smaller than a certain threshold [41].

2.3.4 QAM-FBMC

In order to overcome the intrinsic interference in FBMC, the authors in [40] proposed to use QAM modulated symbols, which leads to a system called QAM-FBMC. By sending QAM symbols at each symbol duration T, it becomes possible to overcome a significant part of the intrinsic interference that was observed in OAQM-FBMC. It is important to point out that as the orthogonality is no longer kept, the observed interference becomes two dimensional.

The main idea of QAM-FBMC [39] is to modify the already presented OQAM-FBMC system to transmit QAM data symbols at each period nT, $n \in \mathbb{Z}$, instead of OQAM symbols at each half period $T/2$, in order to reduce the intrinsic interference. Thus, the expression of the discrete-time transmitted QAM-FBMC signal $s[m]$ can be given by:

$$s[m] = \sum_{k=0}^{M-1} \sum_{n'} d_{k',n'} g\left[m - n'M\right] e^{j\frac{2\pi}{M}k'm}, \tag{2.8}$$

where $d_{k',n'}$ are complex symbols allocated on the k'-th subcarrier and sent in the n'-th QAM-FBMC symbol. $g[m]$ is the prototype filter with length $L_g = KM$,

where M is the number of subcarriers and K is the overlapping factor.

Since there is no orthogonality to be kept, we will have more freedom in the prototype filter design. Hence, it is possible to optimize simultaneously spectrum localization, self-interference level, and overall spectral efficiency. In this sense, several proposals can be found in the literature [1, 42, 43].

In order to improve the performance of QAM-FBMC a more complex structure, composed of two prototype filters, has been proposed and studied in [2] and [44]. An even more complex structure, based on several prototype filters, was proposed in [45]. Despite reducing the interference, elaborated receivers are needed in order to mitigate the residual intrinsic interference.

2.3.5 FFT-FBMC

More recently, a precoded FBMC has been proposed in [46] and [33] to solve the intrinsic interference issue. This proposed scheme, called FFT-FBMC, precodes the data in a subcarrier level through the IFFT. In doing this, the interference that comes from the same subcarrier can be overcome by a simple equalization. This procedure is possible thanks to the subcarrier wise precoding process through the IFFT, FFT decoding, and also the cyclic prefix insertion.

The interference that comes from adjacent subcarriers (ISI) can be avoided through the use of well frequency-shaped prototype filters. In addition, an special data arrangement strategy is used to overcome the interference.

The main IFFT-FBMC proposal consist of selecting $N/2$ data symbols for each subcarrier k, and proceed an N point IFFT. The arrangement strategy consist of alternatively fill the first and the last $N/2$ IFFT bins of each subcarrier. After that, the N-IFFT outputs are optionally extended with a cyclic prefix CP of size L and fed to the k-th subcarrier of an FBMC with M subcarriers.

Let us denote $a_{k',p}[l]$ the l-th data symbol sent at the p-th data block that will be transmitted in the k'-th FBMC subcarrier. Hence, according to [33], the input information at the k'-th FBMC subcarrier $d_{k',n'}$ is given by:

$$d_{k',n'} = \frac{e^{j\pi n(k'+1)}}{\sqrt{N}} \sum_{l=0}^{\frac{N}{2}+1} a_{k',p}[l] e^{\frac{j2\pi nl}{N}}, \tag{2.9}$$

where $p = \lceil \frac{n}{N+L} \rceil + 1$ and the exponential term $e^{\frac{j2\pi nl}{N}}$ is responsible for the strategically alternate data.

At the receiver, after the FBMC, the serial symbols in a given subcarrier k are converted to parallel blocks and the CP is discarded. Afterwards, only N symbols are kept in each block, which fed the N-FFT, whose only $N/2$ output symbols go

to the equalization and detection.

In this system, the intercarrier interference is avoided due to the use of half of the IFFT bins. By doing this it is possible to isolate the adjacent subbands [47]. We might point out that the complex orthogonality is restored in FFT-FBMC.

Chapter 3

OQAM-FBMC modulation

OFFSET Quadrature amplitude modulation associated to Filter-Bank Multi-Carrier (OQAM-FBMC) system, is a promising technology to enable future flexible wireless communication systems. When compared to OFDM, OQAM-FBMC systems have better frequency localization, and consequently, cause less interference to neighbouring systems [3].

In this chapter, we describe the OQAM-FBMC principle, its implementation through the polyphase network (PPN). Moreover, we address the problem of short prototype filter ($K = 1$) design for OQAM-FBMC, based on the careful choice of the objective function to be minimized for reducing out-of-band energy. The problem is non-convex, which calls for more elaborate and customized optimization methods, for which we propose a solution via heuristic method. For this propose we provide the parameters that define the function to be minimized.

We also analyze the system behavior in an asynchronous scenario, by considering timing offset and frequency offset. For the sake of comparison, we evaluated our designed filter against well known competitors, such as the Quadrature Mirror Filter (QMF) and the near-to-perfect reconstruction (NPR1) filter proposed in [48], using parameters corresponding to 4G/LTE wireless communication systems, which are also applicable to 5G.

Finally, we finish this chapter by summarizing the main obtained results.

3.1 OQAM-FBMC Principle

Unlike OFDM, which requires the orthogonality of all carriers to avoid interference, in an FBMC system the orthogonality is kept just between neighbor subcarriers. Actually, in an FBMC the bandwidth is divided into several subcarriers, and the data are transmitted over a bank of modulated band-limited filters. As the subcarriers are not orthogonal, in order to exploit all the channel bandwidth, it is necessary to

adapt the FBMC transmitter.

The conditions required to perform a transmission over these systems was first derived by Chang and Saltzberg in [49, 50], where an offset-QAM modulation was proposed, yielding the system called OQAM-FBMC. A simplified block diagram is depicted in Figure 3.1, where the transmission bandwidth is split into M subbands that are spaced by $F = 1/M$.

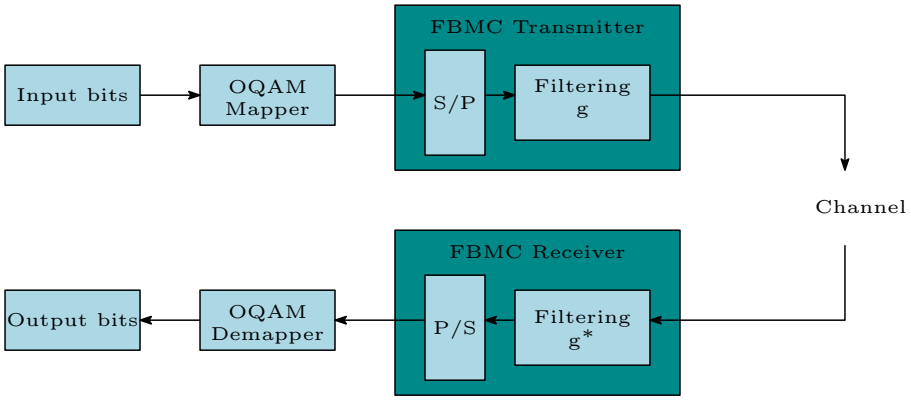

Figure 3.1: OQAM-FBMC transceiver structure

If each subband interferes only with the neighbor subbands, there is no need of a guard interval, which means that there is no spectral efficiency loss (*i.e.* symbol density $\eta = 1$) as in a CP-less OFDM. However, it is not possible to have a filter well localized in time domain and in the frequency domain. By relaxing the orthogonality condition, kept just in real domain, if the transmitted data are real, it is possible to recover the information on the receiver side free of ISI and inter-carrier interference (ICI) in distortion-free channels. Based on that, the real transmitted data can be phased amplitude modulated (PAM) instead of QAM. Besides, in order to maintain the same data rate, the in-phase and quadrature data must be shifted by half symbol duration [28]. With this, we can guarantee that all phase-rotated adjacent PAM symbols and adjacent FBMC symbols are in quadrature. This arrangement is schematically represented in Figure 3.2.

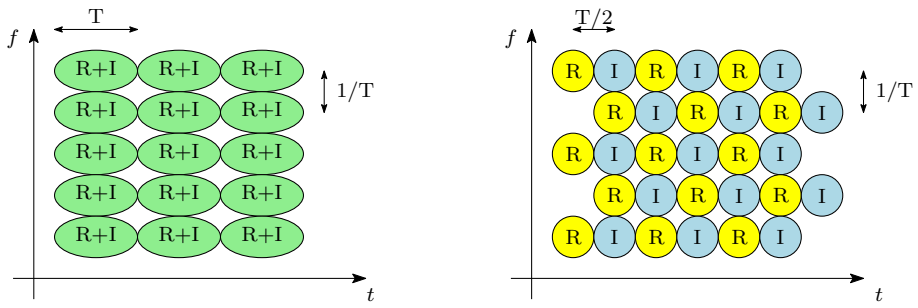

Figure 3.2: Comparison between CP-less OFDM and Offset QAM modulation.

The main advantages of OQAM-FBMC are the orthogonality in the real domain, thanks to the OQAM scheme, the time-frequency-localization, which is better

shaped than OFDM due to its per subcarrier filtering, and finally, its higher spectral efficiency due to absence cyclic prefix.

3.2 OQAM-FBMC system model

The main idea of the OQAM-FBMC is to send offset-QAM symbols. Considering a system with M subcarriers, the complex transmitted symbols $s_{k',n}$ are split into its in-phase and quadrature parts $s^R_{k',n}$ and $s^I_{k',n}$. These may be seen as a pair of symbols coming from the PAM constellation, where the in-phase and quadrature components are delayed by half symbol period $T/2$ during the transmission. Besides, consecutive PAM symbols of neighbor subcarriers are also delayed in time by $T/2$. Therefore, the transmitted PAM symbols are both shifted in time and frequency by $\pm\pi/2$.

The transmitted symbols $a_{k',n}$ are real-valued, which are either the real or the imaginary parts of the QAM symbols. According to the OQAM transmission, $x_{k',n} = a_{k',n}e^{j\phi_{k',n}}$ where $a_{k',n}$ are real symbols whose mean energy σ_a^2 is half of that of the QAM symbols energy σ_x^2.

Let $g[m]$ be a causal prototype filter with length $L_g = KM$, where K is the overlapping factor. By considering the overlapping factor $K = 1$, the discrete-time baseband transmitted signal can be written as [32, 33]

$$s[m] = \sum_{k'=0}^{M-1} \sum_{n'=-\infty}^{+\infty} a_{k',n} e^{j\phi_{k',n'}} g\left[m - n'M/2\right] e^{j\frac{2\pi}{M}k'm}, \tag{3.1}$$

where $\phi_{k',n'}$ is a phase term commonly defined in the literature as [33, 34]

$$\phi_{k',n'} = \frac{\pi}{2}(k' + n') - \pi k'n'. \tag{3.2}$$

The phase offset inserted by $\phi_{k',n'}$ ensure that the frequency-time neighbor PAM symbols are in quadrature with each other.

For the sake of simplicity, we can also define

$$g_{k',n'}[m] = g[m - n'M/2]e^{j\phi_{k',n'}}e^{j\frac{2\pi}{M}k'm}, \tag{3.3}$$

and rewrite Equation (3.1) as

$$s[m] = \sum_{k'=0}^{M-1} \sum_{n'=-\infty}^{+\infty} a_{k',n'} g_{k',n'}[m]. \tag{3.4}$$

Assuming a distortion-free and noiseless channel, the subband separation is

achieved by applying the matched receiver filter described as

$$\boldsymbol{g}_{RX}[m] = \boldsymbol{g}^{*}_{TX}[-m]. \tag{3.5}$$

In practice, the transmitter and receiver filters are real valued and symmetric.

At the demodulation stage, after the analysis filter-bank, the recovered symbol at the k-th subcarrier can be represented by:

$$\begin{aligned} y_{k,n} =& \sum_{m} s[m] g^{*}_{k,n}[m] \\ =& \sum_{m} \sum_{k'=0}^{M-1} \sum_{n'=-\infty}^{+\infty} a_{k',n'} g_{k',n'}\left[m\right] g^{*}_{k,n}[m]. \end{aligned} \tag{3.6}$$

Let us now consider just a pulse, with unitary amplitude, sent in subcarrier k_0 and time instant n_0, then, at the receiver side, the demodulated signal at the subcarrier k and at time instant n can be expressed as:

$$\begin{aligned} y_{k,n} &= \sum_{m} g_{k_0,n_0}\left[m\right] g^{*}_{k,n}[m] \\ &= \sum_{m} g\left[m\right] e^{j\frac{2\pi}{M}k_0 m} e^{j\left(\frac{\pi}{2}(n_0+k_0)-k_0 n_0 \pi\right)} g[m - n_0 M/2 - nM/2] e^{-j\frac{2\pi}{m}km} e^{-j\left(\frac{\pi}{2}(n+k)-kn\pi\right)} \\ &= \sum_{m} g\left[m\right] g[m - (n-n_0)\, M/2] e^{j\frac{2\pi}{M}(k_0-k)m} e^{j\left(\frac{\pi}{2}(n_0+k_0)-\frac{\pi}{2}(n+k)\right)} e^{j(kn\pi - k_0 n_0 \pi)}. \end{aligned} \tag{3.7}$$

By considering $\Delta k = k - k_0$ and $\Delta n = n - n_0$ we can also have

$$y_{k,n} = \sum_{m} g\left[m\right] g[m - \Delta n M/2] e^{-j\frac{2\pi}{M}\Delta k m} e^{-j\frac{\pi}{2}(\Delta n + \Delta k)} e^{-j\pi(kn - k_0 n_0)}. \tag{3.8}$$

The impulse response of a transmultiplexer is strongly dependent on the prototype filter, which must be designed in such way that the orthogonality is kept in the real domain. So we have

$$\Re\left\{ \sum_{m} g_{k',n'}[m] * g_{k,n}[m] \right\} = \Delta_{k,k'} \Delta_{n,n'}, \tag{3.9}$$

Hence, thanks to orthogonality condition, we can write Equation (3.6) as

$$y_{k,n} = a_{k,n} + \underbrace{\sum_{(k',n') \neq (k,n)} a_{k',n'} \sum_{m} g_{k',n'}\left[m\right], g^{*}_{k,n}[m]}_{I},$$

where I represents the intrinsic interference of OQAM-FBMC systems.

As we can notice, the transmission of real valued symbols, PAM modulated, associated with the orthogonality condition, generate purely imaginary interference terms. Therefore the transmitted symbols can be recovered by catching just the real part of the received demodulated signal

$$\hat{a}_{k,n} = \Re\left\{y_{k,n}\right\}. \tag{3.10}$$

Due to this procedure, the intrinsic interference is entirely canceled.

3.3 Polyphase Network Implementation

In order to obtain a compact representation of this system, Bellanger proposed in [51] a polyphase network (PPN) structure, enabling a low complexity implementation of the OQAM-FBMC transceiver. In this approach, the transmitter is composed by an inverse fast Fourier transform (IFFT) and one PPN to implement the filtering process, and at the receiver this process is undone.

Let us consider a finite impulse response (FIR) filter $g[l]$ of size $L_g = KM$, where K is the overlapping factor (set as $K = 1$ in this work), and M is the number of subcarriers used in the system. Its Z-domain representation can be defined as

$$G(z) = \sum_{l=0}^{L_g-1} g[l]z^{-l}. \tag{3.11}$$

The main idea of the polyphase representation of a filter-bank structure is the decomposition of this filter into M elementary filters, $E_m[z^M]$, the first one composed by every sample of $g[l]$ whose indexes are multiples of M, the next one with every sample of $g[l]$, whose index are multiples of $1 + M$ and so on. Assuming that the filter length is a product of two factors, the M elementary sequences of K coefficients can be expressed as follows:

$$\begin{aligned} G(z) &= \sum_{m=0}^{M-1}\sum_{i=0}^{K-1} g[iM+m]z^{-(iM+m)} \\ &= \sum_{m=0}^{M-1} \underbrace{\left(\sum_{i=0}^{K-1} g[iM+m]z^{-iM}\right)}_{E_m[z^M]} z^{-m} \end{aligned} \tag{3.12}$$

As we may know, usually a filterbank is constructed by shifting the prototype

filter frequency response, so that, its Z-transform can also be derived as

$$G_k(z) = \sum_{l=0}^{L_g-1} g[l] e^{j\frac{2\pi}{M}kl} z^{-l}. \tag{3.13}$$

Using the polyphase decomposition, $G_k(z)$ can be represented by

$$\begin{aligned} G_k(z) &= \sum_{m=0}^{M-1}\sum_{i=0}^{K-1} g[iM+m] e^{j\frac{2\pi}{M}k(iM+m)} z^{-(iM+m)} \\ &= \sum_{m=0}^{M-1} e^{j\frac{2\pi}{M}km} \underbrace{\left(\sum_{i=0}^{K-1} g[iM+m] z^{-iM}\right)}_{E_m[z^M]} z^{-m} \\ &= \sum_{m=0}^{M-1} e^{j\frac{2\pi}{M}km} E_m[z^M] z^{-m}. \end{aligned} \tag{3.14}$$

Considering that in a filterbank we have several modulated filters, originated from the prototype one, we can also denote $W = e^{-j\frac{2\pi}{M}}$ and write in matrix form

$$\begin{bmatrix} G_0(z) \\ G_1(z) \\ \vdots \\ G_{M-1}(z) \end{bmatrix} = \underbrace{\begin{bmatrix} 1 & 1 & \dots & 1 & 1 \\ 1 & W^{-1} & \dots & W^{-(M-2)} & W^{-(M-1)} \\ \vdots & \vdots & \ddots & \vdots & \vdots \\ 1 & W^{-(M-1)} & \dots & W^{-(M-1)(M-2)} & W^{-(M-1)^2} \end{bmatrix}}_{\text{IDFT}} \underbrace{\begin{bmatrix} E_0[z^M] \\ z^{-1}E_1[z^M] \\ \vdots \\ z^{-(M-1)}E_{M-1}[z^M] \end{bmatrix}}_{\text{PPN}}. \tag{3.15}$$

As we can notice, it is possible to use the M-point inverse discrete Fourier transform (IDFT) and PPN to implement synthesis filterbanks. In Figure 3.3 we have a block representation of a synthesis filterbank.

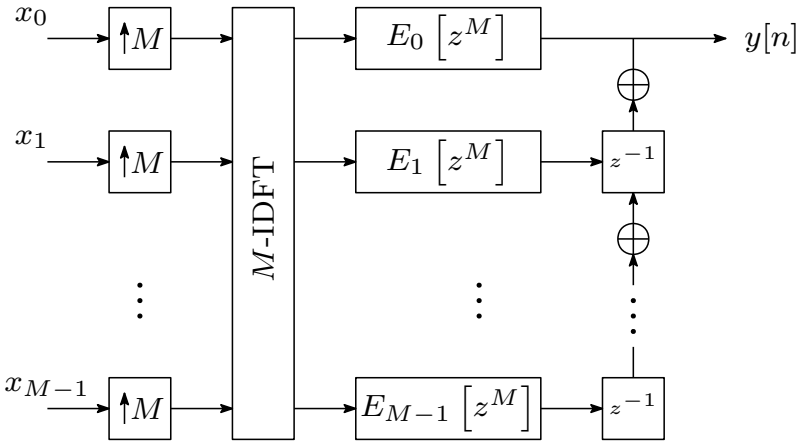

Figure 3.3: Synthesis filterbank structure

The analysis filterbank is the dual of the previous structure presented. Consid-

ering $F_{-k}(z)$ the demodulated version of $G_k(z)$, we can write the polyphase components of $F_{-k}(z)$ as

$$\begin{aligned} F_{-k}(z) &= \sum_{l=0}^{L_g-1} f[l] e^{-j\frac{2\pi}{M}kl} z^{-l} \\ &= \sum_{m=0}^{M-1} e^{-j\frac{2\pi}{M}km} R_m[z^M] z^{-m}. \end{aligned} \tag{3.16}$$

We can also have a matrix representation:

$$\begin{bmatrix} F_0(z) \\ F_{-1}(z) \\ \vdots \\ F_{-(M-1)}(z) \end{bmatrix} = \underbrace{\begin{bmatrix} 1 & 1 & \dots & 1 & 1 \\ 1 & W & \dots & W^{(M-2)} & W^{(M-1)} \\ \vdots & \vdots & \ddots & \vdots & \vdots \\ 1 & W^{(M-1)} & \dots & W^{(M-1)(M-2)} & W^{(M-1)^2} \end{bmatrix}}_{DFT} \underbrace{\begin{bmatrix} R_0[z^M] \\ z^{-1}R_1[z^M] \\ \vdots \\ z^{-(M-1)}R_{M-1}[z^M] \end{bmatrix}}_{PPN}. \tag{3.17}$$

A block representation of the analysis filterbank is also presented in Figure 3.4.

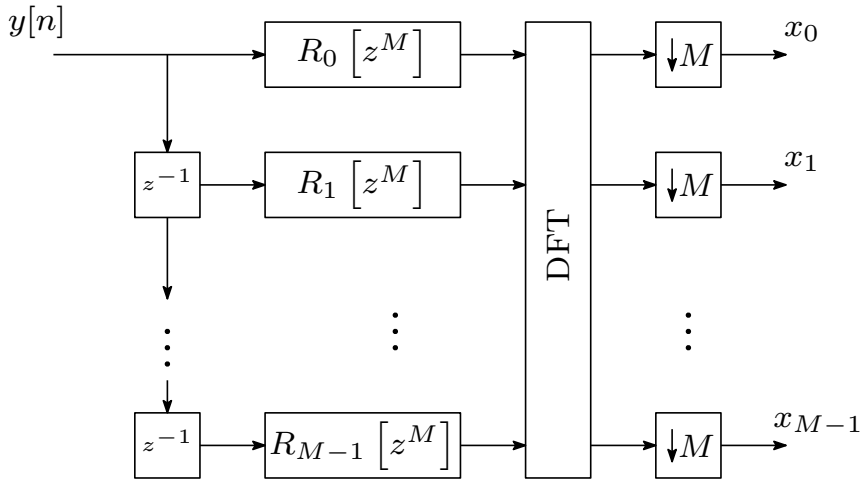

Figure 3.4: Analysis filterbank structure

3.3.1 OQAM-FBMC implementation through PPN

The structure of the OQAM-FBMC can be implemented by using the polyphase decomposition of the filterbank. Considering the transmission of PAM symbols $a_{k,n}$, the structure of the OQAM-FBMC can be split into two sub-systems. It follows that each sample of the first subsystem can be obtained by convolving each IDFT output with each polyphase component of $g_k[m]$. In the second one, each IDFT output is convolved with each polyphase component of $g_k[m - M/2]$. The direct implementation of the OQAM-FBMC transmitter is presented in Figure 3.5

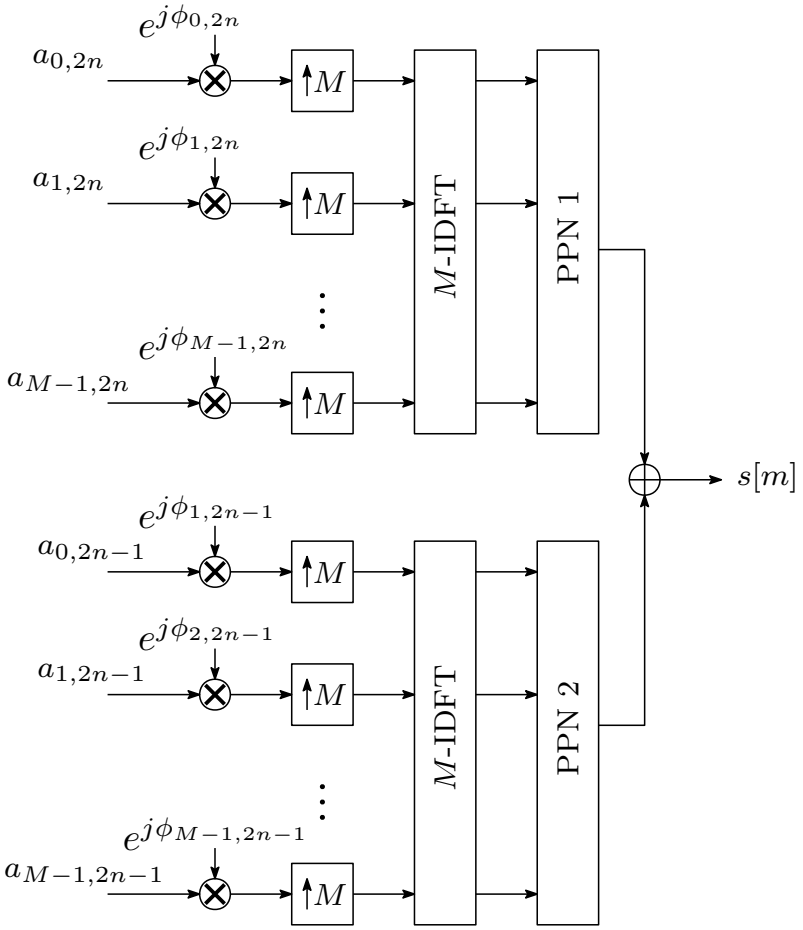

Figure 3.5: Block diagram of the OQAM-FBMC transmitter implemented through FFT and PPN.

It is also possible to avoid the use of two IDFT at the transmitter side having a single IDFT working at a rate $2/M$. We can also move the delay of $M/2$ for outside of the second sub-system. Due to this we will have a structure with two identical PPN.

When using short prototype filter (PF), in our case $K = 1$, the polyphase network approach can be seen as a windowing process, which means that each IDFT output is simply multiplied by the filter impulse response. As a consequence, there is a significant reduction in the implementation cost.

At the receiver side, the dual operations with respect to those performed by the transmitter can be also rearranged into two sub-systems. By doing this and using the polyphase implementation, we can have the receiver structure as presented in Figure 3.6.

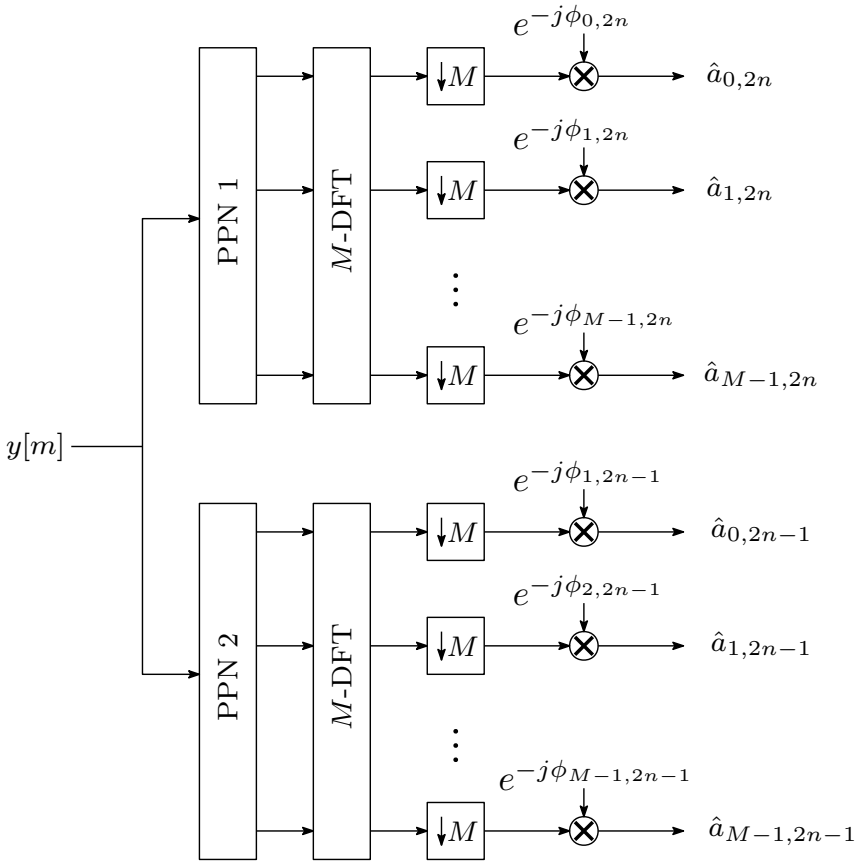

Figure 3.6: Block diagram of the OQAM-FBMC receiver implemented through FFT and PPN.

3.4 Prototype filter

The conventional OFDM system is constructed based on a rectangular PF. As a consequence, the resulting sub-channel filters are not well shaped in frequency. The main advantage of OQAM-FBMC consists in its ability to provide improved frequency selectivity due to the use of well shaped prototype filters when compared to the rectangular one.

The design of a good prototype filter is the key to ensuring good performance in OQAM-FBMC communication systems. The filter is usually designed for perfect, or quasi-perfect, reconstruction and good frequency response localization [52]. This is a conflicting requirement when filter length must be kept short to minimize end-to-end (E2E) latency and transceiver complexity, as in, e.g., URLLC. Furthermore, short filters are preferable for their improved robustness against time varying channels.

Usually, works are focused on FBMC using prototype filters with overlapping factor $K = 4$ (number of adjacent FBMC symbols overlapped in time domain). However, a short prototype filter ($K = 1$) can also be applied to FBMC, as demonstrated in [48]. Also in this reference, a short filter was proposed by the authors. The proposed filter has the same length as the FBMC symbol, and it is designed by in-

terchanging the time and frequency axes of the MMB4 (Martin-Mirabassi-Bellanger with $K = 4$) prototype filter [53].

The study of prototype filters is particularly interesting since the design of a transceiver mainly concentrates on its choice. Therefore, we are interested in designing short prototype filters that have the same size as one OFDM symbol ($L_g = KM$), which leads to the overlapping factor $K = 1$, for OQAM-FBMC systems.

After briefly presenting the existing short filters found in the literature, we present a novel short prototype filter design using optimization method, that shows relevant performance improvements.

3.4.1 Quadrature mirror filter - QMF

QMF has been of great interest for filterbanks since their introduction due to its good characteristics that can avoid aliasing on the received signal. Regarding its association with FBMC, presented in [54], it leads to a modulation denoted Lapped-OFDM.

The greatest advantage of QMF is the possibility to avoid aliasing. The prototype filter can be designed so that the filterbank is very close to perfect reconstruction.

In its basic form, the QMF prototype filter in time domain, constructed for an M band system, can be analytically expressed as follows [55]:

$$g[m] = \sin\left(\frac{m\pi}{M}\right). \tag{3.18}$$

3.4.2 Near to perfect reconstruction filter - NPR1

A specific procedure to design prototype filters directly in the frequency domain for FBMC was initially developed by Martin in [56] and improved by Bellanger in [30] and Mirabbasi in [57]. The remarkable characteristic of this method is that the frequency domain coefficients are adjustable to achieve high stop-band attenuation. Besides, its coefficient values have been derived for different overlapping factors, $K = 3$, $K = 4$. The PF obtained by $K = 4$ was exhaustively studied at the scope of PHYDYAS European research [53]. In this dissertation, the PF obtained for $K = 4$ will be called MMB-4.

In [48], Nadal proposed a short prototype filter with overlapping factor $K = 1$. Its main design procedure is based on inverting the time and frequency axes of the filter bank impulse response when applying MMB-4 prototype filter. The filter bank impulse response of MMB-4 is well localized in frequency domain, consequently it is possible to identify interference only in one adjacent subcarrier.

Inverting the time and frequency axes of the obtained filter bank impulse response when applying the MMB-4 filter, we can generated the filter coefficients that will

cause interference only to the adjacent FBMC symbols. As a consequence, the coefficients can be deduced from a given FBMC impulse response.

By definition the FBMC impulse response is composed of the values obtained at the output of the receiver when just one information is sent. Thus, a prototype filter $\boldsymbol{g}[m]$ can be designed by taking advantages of the real valued and symmetry of the MMB-4 to obtain a simpler analytical expression [48]

$$g[m] = \sqrt{1 - 2\sum_{l=0}^{2} P_g(l) \cos\left(\frac{2\pi(2l+1)m}{M}\right)} \tag{3.19}$$

where:

$$\begin{aligned} P_g(0) &= 0.564447 \\ P_g(1) &= -0.066754 \\ P_g(2) &= 0.002300 \end{aligned}$$

The designed prototype filter was called NPR1 due to its near to perfect reconstruction characteristic and overlapping factor $K = 1$.

3.4.3 A novel short prototype filter design

In this section we describe a novel short prototype filter design, which is specifically developed for OQAM-FBMC systems, and represents the major contribution of this chapter. The main idea of the proposed procedure to develop the design short prototype filters starts by looking to this problem as an optimization problem. Furthermore, we propose to design short PF satisfying perfect reconstruction conditions [58], which means that a delayed copy of the original signal can be perfectly recovered in the critically sampled system in the absence of noise. In this context, we will minimize the out-of-band energy.

Perfect reconstruction condition

A basic constraint of data transmission is the Nyquist criterion, that must be attended to avoid interference. In the time domain, the Nyquist criterion says that the impulse response of the prototype filter must be zero at each multiple of the symbol period. In frequency domain, it can be seen as a symmetry condition, related to the cutoff frequency. Thus, in digital transmissions, the prototype filter at the transmitter and at the receiver are, usually, half-Nyquist. Thus, the symmetry condition is met by the square of the frequency coefficients.

By respecting exactly the Nyquist criterion, the perfect reconstruction can be

achieved, and we can also avoid any crosstalk between neighbor subchannels in the back-to-back connection of transmitter and receiver.

It is worth emphasizing that, the prototype filter can be designed to provide perfect reconstruction, nevertheless, the perfect reconstruction is achieved just in the case of ideal channel.

Considering the M polyphase components of the prototype filter $E_m[z]$, as defined in Equation (3.12), we can summarize the set of necessary and sufficient orthogonality condition as [59, 60]

$$E_m^*[-z]E_m[z] + E_{m+M/2}^*[-z]E_{m+M/2}[z] = \frac{2}{M}, \qquad (3.20)$$
$$m = 0, ..., \frac{M}{2} - 1.$$

In the case of short prototype filters ($K = 1$), all the polyphase components are reduced to 1-tap filters, i.e., $E_m[z] = g[m]$, $m = 0, \ldots, M-1$.

Consequently, we can simplify the perfect reconstruction condition (3.20), for $K = 1$, as

$$g^2[m] + g^2[M/2 + m] = \frac{2}{M}, \quad m = 0, \ldots, \frac{M}{2} - 1. \qquad (3.21)$$

Since we have chosen the prototype filter, the transceiver can be constructed by design the filter-bank. For doing this, the prototype filter must be modulated to generate all the filters for each subcarrier k. The filter for a subcarrier k is obtained by multiplying the prototype filter by $e^{j\frac{2\pi}{M}km}$.

In this section we propose to design short prototype filters satisfying perfect reconstruction conditions [58], which means that a delayed copy of the original signal can be perfectly recovered in the critically sampled system in the absence of noise. In this context, we will design short prototype filters that minimize the out-of-band energy OOBE. This problem is formulated as an optimization problem subject to the perfect reconstruction conditions presented in Equation (3.21).

Optimization problem

The design procedure of the prototype filter requires the definition of an appropriate objective function. The starting point is to define a function related to the magnitude of the frequency response of the desired filter. Since the FBMC system requires the design of a low pass filter, we can address this problem in a well-known

traditional form [61]

$$\min_{\boldsymbol{g}}\{E(\Omega_p)\} = \min_{\boldsymbol{g}}\left\{\int_{\Omega_p}^{0.5}|G(f)|^2\mathrm{d}f\right\} \quad \text{s.t.} \quad \int_{-0.5}^{0.5}|G(f)|^2\mathrm{d}f = 1 \tag{3.22}$$

where $G(f)$ is the frequency response of the prototype filter, Ω_p is the passband frequency edge and the frequency sampling is defined as $F_s = 1$. Defining $\boldsymbol{g} \in \mathbb{R}^{L_g \times 1}$ as the prototype filter coefficient vector, we can also rewrite Equation (3.22)

$$\begin{aligned} \min_{\boldsymbol{g}} \quad & \boldsymbol{g}^{\mathrm{H}}\boldsymbol{Q}\boldsymbol{g} \\ \text{s.t.} \quad & \boldsymbol{g}^{\mathrm{H}}\boldsymbol{g} = 1 \end{aligned} \tag{3.23}$$

Here, $\boldsymbol{Q} \in \mathbb{R}^{(L_g \times L_g)}$ is a symmetric and positive-definite matrix with (l, c)-th component given by

$$q_{lc} = \frac{\sin(\pi(l-c)(1-B_W))}{\pi(l-c)} e^{j\pi(l-c)}, \tag{3.24}$$

and $B_W = 2\Omega_p$ is the passband width.

Finally, from (3.23) and under the constraints given in (3.21) we can establish the classical optimization problem for the design of prototype filter as follows:

$$\begin{aligned} \min_{\boldsymbol{g}} \quad & \boldsymbol{g}^{\mathrm{H}}\boldsymbol{Q}\boldsymbol{g} \\ \text{s.t.} \quad & g^2[m] + g^2[M/2+m] = 2/M \quad m = 0, ..., M/2-1 \end{aligned} \tag{3.25}$$

The optimization problem (3.25) is a quadratically constrained quadratic programming (QCQP) problem. Since we have quadratic equality constraints, then (3.25) is a non-convex and NP-hard problem. Consequently, there is no guarantee to find its global optimal minimum.

Simulations show that optimizing the problem in Equation (3.25) results in unsatisfactory out-of-band energy decay, which can be significantly improved with the modified cost function proposed in the next section.

New optimization problem formulation

This section describes the proposed objective function to be minimized in order to obtain a prototype filter with improved spectrum. We provide a filter design by minimizing a weighted objective function as is shown in Figure 3.7(b). We propose a function with smooth transition between the passband and the stopband, rather than the strict sharp transition used in the previous subsection.

For comparison, we show in Figure 3.7(a) the rectangular function corresponding to the classical objective function, and the proposed weighted objective function in Figure 3.7(b). Here Ω_p is the frequency from which we start the minimization with weights. For the frequencies higher than Ω_r, the weights are equal to 1. $B = 2\Omega_p$ is the region where there is no minimization and $A = 2\Omega_r$ is the sum of B and the transition region.

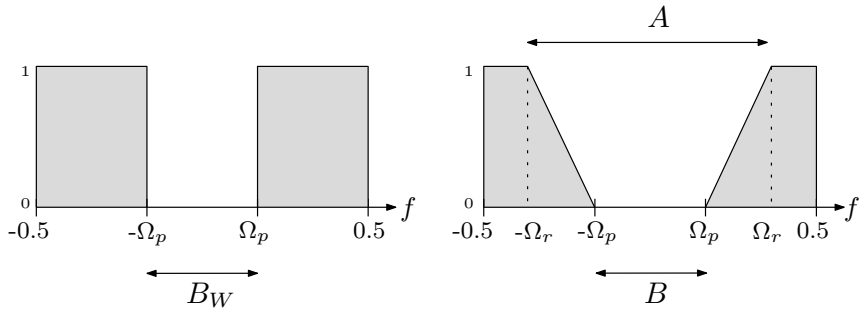

(a) (b)

Figure 3.7: Frequency weighted function corresponding to: (a) classical objective function and (b) proposed objective function with soft transition between the pass region and stop region.

According to Figure 3.7(b), the proposed frequency domain weighted function can be obtained from the convolution product of a rectangular function of width $X = (A - B)/2$ and a 1/2-circularly shifted rectangular function of width $Y = 1 - (A + B)/2$.

In the time domain, this results in a simple multiplication of two sinc functions which can be given by

$$s_1[n] = \frac{1}{X}\frac{\sin(\pi X n)}{\pi n}, \tag{3.26}$$

and

$$s_2[n] = \frac{\sin(\pi Y n)}{\pi n} e^{j\pi n}. \tag{3.27}$$

Hence, we can write the proposed objective function as

$$\boldsymbol{g}^{\mathrm{H}} \boldsymbol{P} \boldsymbol{g}, \tag{3.28}$$

where $\boldsymbol{P} \in \mathbb{R}^{(L \times L)}$ is a symmetric and positive-definite matrix whose (l, c)-th element is defined by

$$p_{l,c} = s_1[l - c] \times s_2[l - c]. \tag{3.29}$$

In terms of constraints, there are no modifications. By using the constraints previously presented in (3.21), we can set up the alternative optimization problem

as

$$\begin{aligned} \min_{\boldsymbol{g}} \quad & \boldsymbol{g}^{\mathrm{H}}\boldsymbol{P}\boldsymbol{g} \\ \text{s.t.} \quad & g^2[m] + g^2\left[\frac{M}{2}+m\right] = \frac{2}{M} \quad m = 0, ..., \frac{M}{2}-1 \end{aligned} \tag{3.30}$$

Obviously, the optimization problem above is also a non-convex QCQP. We use, in this thesis, the interior point (IP) method [62] for solving (3.30). Our obtained optimized prototype filter, with $K = 1$, is denoted OPF1(B, A). The choice of $A = B$ leads us to the first optimization problem (3.25), which corresponds to the classical function depicted in Figure 3.7(a).

3.4.4 Numerical evaluation

Numerical experiments were conducted in order to evaluate the proposed filter design method. We used the QMF filter as the initial point of the optimization procedure, which applied to FBMC leads to a modulation known as Lapped-OFDM, as presented in [55].

The generated prototype filters were analyzed based on the total stopband energy and the energy distribution along the stopband. Moreover, parameters corresponding to the 4G/LTE (also applicable to 5G) were set and a notch of 12 subcarriers, equivalent to one Resource Block (RB), was inserted in the spectrum between two blocks, with 2 RB each one, to evaluate the capacity of supporting secondary systems. If the attenuation in this region is high enough, then this frequency band can be used by a secondary system without interfering with the primary system.

The optimization procedure was applied to the initial problem (3.25), and to the proposed problem (3.30). We considered an OQAM-FBMC system with $M = 128$ subcarriers, overlapping factor $K = 1$, and filter length $L_g = KM$.

Figures 3.8 and 3.9 show the magnitude response of the optimized filters when we set $B = 8/M$ and $B = 9/M$, respectively and also for $A = 4B$, $6B$, and $9B$. In addition, the optimized filters are compared with QMF and NPR filters.

For all the conducted experiments, QMF presents the highest energy level in the stopband, and although the NPR1 filter shows greater attenuation, its stopband energy level is still high when compared to OPF1. As we have mentioned in Section 3.4.3, the observed OOB energy of the filter obtained by optimizing problem (3.25), named OPF1(B, B), is lower than the ones with $B = 8/M$ or even when $B = 9/M$.

The proposed method provides a filter OPF1(B, A) whose attenuation in the stopband increases progressively and more aggressively than the competitors considered herein. With a judicious choice of parameters A and B, we can design a prototype filter which is short and presents better compromise of OOB energy

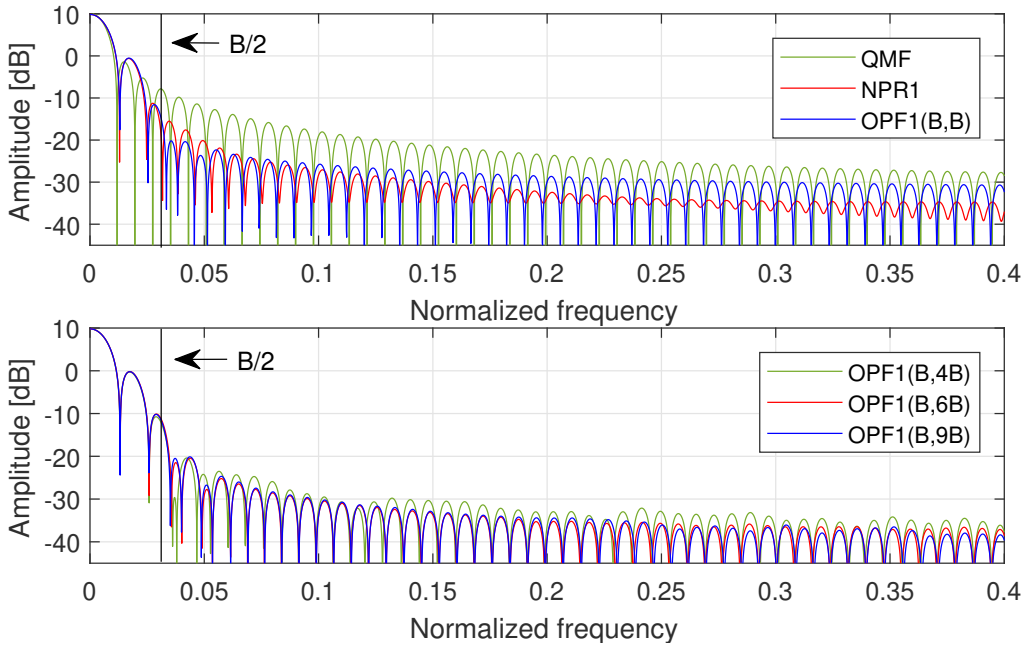

Figure 3.8: Magnitude responses of prototype filters in the case of $M = 128$, $B = 8/M$ and $K = 1$.

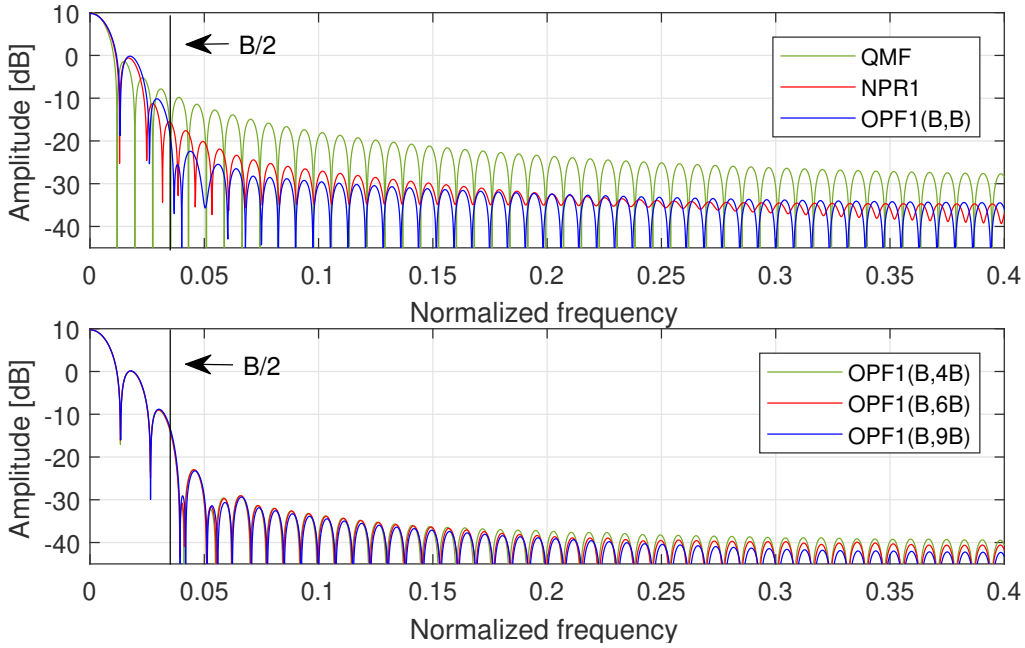

Figure 3.9: Magnitude responses of prototype filters in the case of $M = 128$, $B = 9/M$ and $K = 1$.

and transition-band attenuation, with better performance when compared to QMF, NPR1 and OPF(B,B).

In Figures 3.8 and 3.9, one can further evaluate the impact of variable A for two different choices of parameter B. Best results are obtained for $B = 9/M$ and $A = 9B$.

In addition, we depict in Figure 3.10 the evolution of the measured OOBEs

of different filters for a bandwidth b, ranging from $b = 0$ up to $b = 30/M$. In the case $b = 0$, all the energy is outside of the considered bandwidth (OOBE = 1). Analogously, in the case of $b = 1$, all the energy is inside of the considered bandwidth (OOBE = 0).

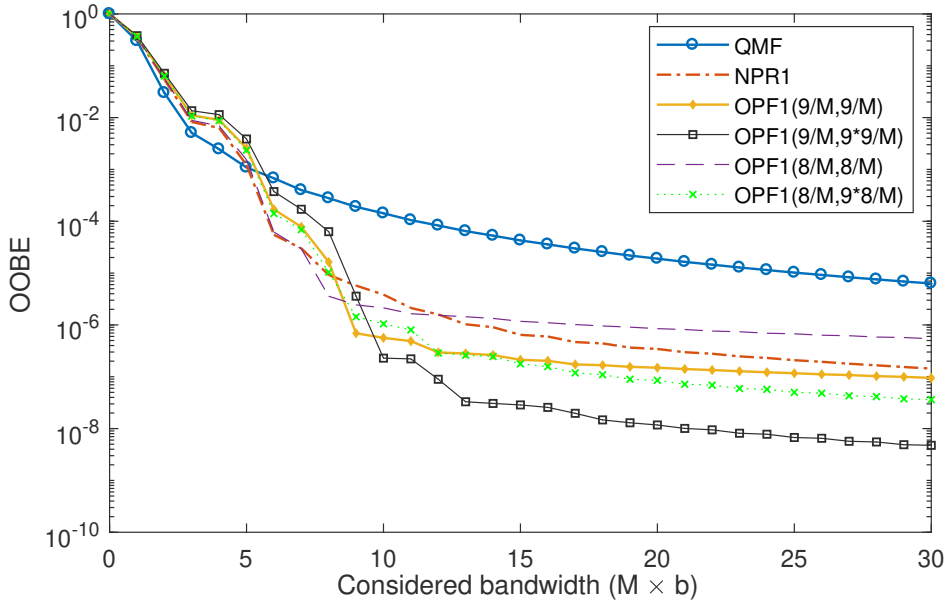

Figure 3.10: Out-of-band energy achieved by each filter for different transmission bandwidth sizes.

It is possible to verify that the energy outside of the considered bandwidth for QMF is the smallest one until $b = 5/M$, whereas OPF1$(B, 9B)$, for $B = 9/M$, has the lowest OOBE when the considered bandwidth is greater than $9/M$. Indeed, we can observe that the OOBE of OPF1$(B, 9B)$ is 28 times smaller than NPR1 when the bandwidth is greater than $13/M$. As a consequence, for $b \leq 5/M$, QMF has the smallest OOBE, whereas OPF1$(B, 9B)$ has the smallest OOBE for $b \geq 9/M$.

We also analyzed the Power Spectral Density (PSD) when several subcarriers are activated. We assume that a bandwidth of 900kHz (60 subcarriers) is allocated where one RB is switched off in the middle of the allocated band. The results depicted in Figure 3.11 show that the optimized filter OPF1$(B, 9B)$, for $B = 9/M$, achieves the best performance in terms of stopband attenuation. It has the lowest radiation level in the notch region, around -60dB. Indeed, in the extreme edges of the band, the power spectral density quickly decreases, up to -90dB, proving its competitiveness against the other tested filters.

We can also notice that for the proposed objective function, the shape of the spectrum at the edge of the transmission band (between -0.26 and -0.28) is almost unchanged.

The designed prototype filters presented in this work and other examples of different sizes and different parameters are available online at the homepage [63].

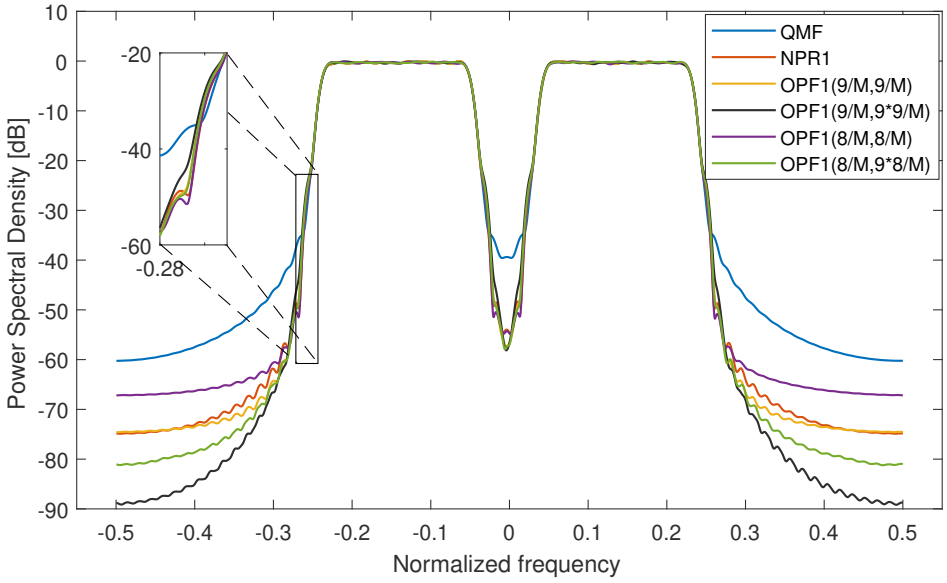

Figure 3.11: PSD evaluation for different prototype filters.

3.5 Asynchronous access

The main causes of desynchronization in multicarrier communication systems are timing offset (TO) and carrier frequency offset (CFO). The timing offset occurs when, at the receiver, the received signal is not sampled at the ideal instant. The carrier frequency offset occurs when the oscillators at the transmitter and receiver are not perfectly tuned in the same frequency or it can also be observed when the transmitter or receiver are on the move, that is what we call Doppler shift.

It is well known that OQAM-FBMC systems are more resilient than OFDM to carrier frequency offset and also timing misalignment [34, 64]. In this section we analyze the sensitivity of OQAM-FBMC systems using different prototype filters to the asynchronous scenario.

We now tackle the case of asynchronous access in a coexistence scenario where two coexisting users share the same available frequency band, as depicted in Figure 3.12. Here the green color represents the resources allocated to the user one U1, the one of interest, and the red color represents the interfering user two U2. The frequency offset ϵ is represented by the gray area between users U1 and U2. We also represent the timing misalignment of U1 and U2 in gray as τ. Due to the synchronization mismatch the receiver of interest suffers from interference, which causes performance degradation.

3.5.1 Numerical evaluation

To evaluate the robustness of the QAM-FBMC system to the asynchronous access 2 RB are allocated to the user one, denominated useful signal, and the interfering

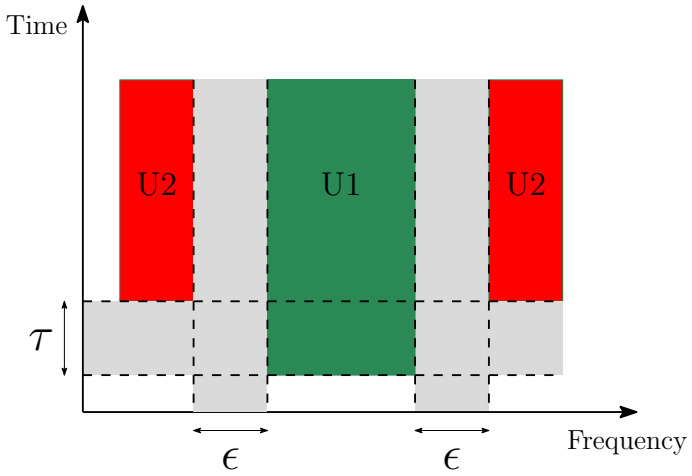

Figure 3.12: Coexistence of two asynchronous users with timing offset τ and frequency offset ϵ

signal is composed of two blocks of 2 RB corresponding to the user two, each one allocated on each side of the useful signal.

The transmitter was considered to be perfectly synchronized in both time and frequency domains. However, a time and/or frequency misalignment can occur between the user of interest and the other user. First, as in [4], we evaluate the system robustness to Timing Offset from $-\tau/2$ until $\tau/2$, where $\tau = 66.66\mu s$ corresponding to one OFDM symbol duration assuming no Carrier Frequency Offset. Also, in order to highlight the interference we consider free distortion channel between the transmitter and receiver.

We evaluate the Normalized Mean Square Error (NMSE), in other words, we divided the MSE at the receiver by the average power of the signal constellation. Due to this, the NMSE is independent of the used constellation scheme. The per carrier NMSE, as presented in Figure 3.13, can provide a meaningful information about the interference over the useful subcarriers. Besides, we use a color map indicates the NMSE levels from -40 dB until -5 dB.

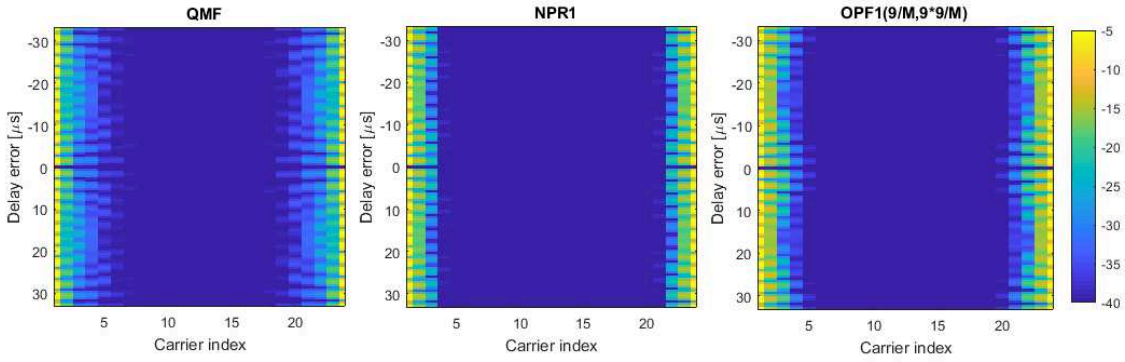

Figure 3.13: NMSE evaluation for each subcarrier and time delay for different prototype filters.

The per subcarrier NMSE of OQAM-FBMC using QMF, NPR1, and OPF1($9/M, 9 \times 9/M$) in the presence of TO are depicted in Figure 3.13. As we can notice, a very small number of edge subcarriers are affected by the interfering user thanks to the application of NPR1 and OPF1($9/M, 9 \times 9/M$) filters. Such behavior is directly related to the spectral confinement of the prototype filter. It is worth mentioning that, although the OPF1 was not specifically designed to support asynchronous communication, its performance is so good as the NPR1 in the presence of timing offset.

Finally, we evaluated the impact of CFO in OQAM-FBMC systems performance assuming that both users were perfectly synchronized in time domain ($\delta = 0$). However, there was an offset ϵ between their subcarriers that we consider here varying from 0 to 1.5KHz. By doing this, it is possible to evaluate the degradation of the useful signal caused by the inter-user interference. It is worth notice that the CFO shift both interfering spectrum in the same direction.

The per subcarrier NMSE generated by the CFO for QMF, NPR1 and OPF1($9/M, 9 \times 9/M$) are presented in Figure 3.14. Here one can see the effect of changing the prototype filter applied to the OQAM-FBMC system. As we can notice, the interference reaches only a small amount of subcarriers at the edge of the transmission band in the case of using QMF NPR1 and OPF1($9/M, 9 \times 9/M$).

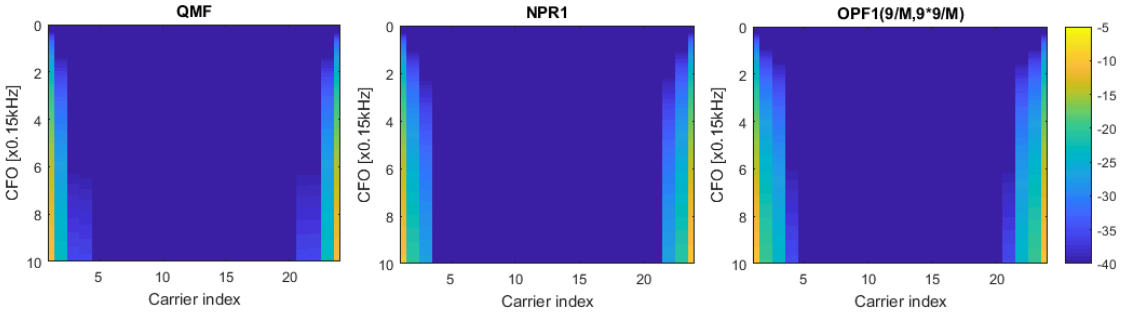

Figure 3.14: NMSE evaluation for each subcarrier and carrier frequency offset for different prototype filters.

Once again we can confirm that although the OPF1 was not specifically designed to support asynchronous communication, its performance is so good as the NPR1 in the presence of CFO.

3.6 Chapter Conclusion

In this chapter a novel short prototype filter design suitable for QAM-FBMC was proposed. The main idea of the proposal is to keep the orthogonality which leads to perfect reconstruction of the transmitted signal. We have demonstrated that a short

filter can be designed based on the optimization of the out-of-band energy with a carefully chosen objective function without violating the orthogonality condition.

Different prototype filters have been compared not only in terms of stopband energy, but also in terms of spectrum decaying in the stopband since the frequency selectivity is a desired property in FBMC applications.

We have also studied and analysed system behavior in the asynchronous scenario. Carrier frequency offset and timing offset was applied to the system in the context of multiple users to numerically evaluate the degradation.

Numerical results validated the effectiveness of the proposed method. It provides a filter whose attenuation in the stopband increases progressively and faster than the competing alternatives found in the literature. As a consequence, the resulting filter bank offers improved performance in terms of latency and out-of-band energy, which are important characteristics of candidates in future mobile communications systems. Besides, it is still competitive in terms of performance in the presence of CFO and TO.

3.6.1 Contributions

- The proposed short prototype filter design that is described in Section 3.4.3 and the asynchronous access analysis presented in Sec 3.5 has been published in [65]: I. Galdino, R. Zakaria, D. Le Ruyet, and M. L. R. de Campos, "Short Prototype Filter Design for OQAM-FBMC Modulation, "*IEEE Transactions on Vehicular Technology*, vol. 69, no. 8, pp. 9163–9167, 2020

Chapter 4

QAM-FBMC modulation

In conventional wireless communications, the cyclic-prefix orthogonal frequency division multiplexing (CP-OFDM) has been adopted as the baseline multicarrier scheme. Despite its corroborated merits, they are observed only in a synchronous and strictly orthogonal scenario. To overcome the limitations observed in CP-OFDM, to improve robustness against channel impairments, and to support the constraints imposed by different 5G scenarios [14, 15, 66], several waveforms have been proposed.

The waveform design for post OFDM systems, *e.g.* the fifth generation (5G) and beyond (B5G), is a challenge due to the amount and the nature of the services that might be provided [14, 66, 67]. Among the recent candidates we can cite the OQAM-FBMC [3, 68]. Its major characteristic lies in using a per-subcarrier pulse-shaping to reduce out-of-band emissions. Consequently, it provides flexibility in waveform design when compared to OFDM and allows heterogeneous services, which is also a 5G/B5G communications systems requirement. Unfortunately, although the data are always orthogonal to interference, this is the main obstacle in the channel estimation process and MIMO applications combined with maximum likelihood (ML) [69] detection or space time block code (STBC) [70].

To overcome the drawbacks observed in OQAM-FBMC, a QAM-based FBMC scheme (QAM-FBMC) with a single prototype filter has been proposed in [39], which makes intrinsic interference of the system bidimensional both in time and in frequency [46]. In QAM-FBMC, the intrinsic interference can be significantly reduced, allowing its application to MIMO technologies. Also, due to the use of well localized prototype filters, superior spectral confinement characteristics are observed when compared to OFDM.

In QAM-FBMC systems, the transmission of QAM symbols occurs each period T instead of half period $T/2$ as it happens in OQAM-FBMC. By doing this real orthogonality is lost and consequently the residual intrinsic interference, whose terms become complex, remains present in the receiver. In order to reduce interference in

QAM-FBMC systems, several solutions have been proposed in the literature, *e.g.*, decision feedback equalizer [71], precoding scheme [72], waveform design [1, 2] and also prototype filters.

Several researchers have been working on different techniques for enhancing QAM-FBMC performance. A basic iterative interference estimation and cancellation has been proposed in [73]. The authors in [71] proposed an interference mitigation scheme based on precoding and decision feedback equalization. In [74] researchers proposed an iterative interference cancelation (IIC) receiver to minimize the interference. Also, the authors of [75] proposed a nonlinear receiver, that uses IIC and parallel interference cancellation (PIC) concepts in multiple-input multiple-output (MIMO) systems with minimum mean square error (MMSE) receiver.

A more complex structure of QAM-FBMC, composed of two prototype filters, has been proposed and studied in [2] and [44]. However, the bandwidth of the second applied filter is significantly higher that of the first filter. This change makes the comparison to the case of using one prototype filter unfair. Besides, an increase in the complexity of the system can also be observed. Moreover, an even more complex structure based on several prototype filters was proposed in [45]. Despite reducing the interference, more elaborated receivers are needed in order to mitigate the residual interference.

We can look at prolate spheroidal wave functions proposed by Slepian [76, 77], as a possible solution for QAM-FBMC prototype filter design. David Slepian proposed a solution for the time/frequency localization through a set of functions denominated prolate spheroidal wave functions (PSWFs), which are maximally energy concentrated in a given time/bandwidth limitation. It is known that the Slepian solution for the discrete-time problem, called discrete prolate spheroidal sequences (DPSS), is the equivalent version of PSWFs in discrete-time domain [78], consequently they have the same properties. Both of them, the DPSS and PSWFs, have been widely studied together with their applications [79–82].

The DPSS has a wide range of classical as well as recent signal processing applications [83–89], including many in signal processing. Compressive sensing [84], parametric waveform and detection of extended targets [85], wall clutter mitigation and target detection [86], design of baseband receivers [87], fiber bragg grating (FBG) sensors for optical sensing systems [88], and multipath suppression for continuous wave [89] are just a few examples.

We propose, in this chapter, a prototype filter designed specifically for QAM-FBMC systems that apply matched filter at the receiver. We consider the discrete prolate spheroidal sequences (DPSS) in order to achieve the most energy concentrated filter for a given time/bandwidth limitation and minimize the intrinsic interference of the system. We compare the performances of the obtained filters to some

known filters from the state of the art.

As we may know, the prototype filter choice is essential for good performance of QAM-FBMC, since it is responsible for the spectral confinement of the system. Further, its choice will directly impact the intrinsic interference and consequently the bit error rate of the system. In this sense, several works have been done in order to evaluate the performance of multicarrier systems through their bit error probability (BEP). Closed form expressions have been provided for OFDM and OQAM-FBMC over additive white Gaussian noise (AWGN) [90] and Rayleigh fading channels [91, 92].

Nonetheless, to the best of our knowledge, the BEP analysis specifically for the QAM-FBMC has not yet been investigated. To evaluate the performance of the QAM-FBMC systems we propose in this Chapter a mathematical expression of its BEP. We derive a BEP expression for QAM-FBMC systems over AWGN channel taking into account the intrinsic interference generated by the non-orthogonality of the prototype filter. We also derive the BEP expression for QAM-FBMC over Rayleigh fading channels, by also considering the intrinsic interference generated by the prototype filter. Additionally, the expression of the BEP has been obtained using the exact intrinsic interference for a given prototype filter.

4.1 QAM-FBMC System Model

In a conventional FBMC system the transmitted data symbols are offset QAM modulated. At the receiver, the data symbols are contaminated by imaginary interference terms, called intrinsic interference. The main idea of QAM-FBMC [39] is to modify the OQAM-FBMC system to transmit QAM data symbols each period T in order to reduce the intrinsic interference. In this approach, the expression of the discrete-time transmitted signal $s[m]$ can be given by

$$s[m] = \sum_{k'=0}^{M-1} \sum_{n'} d_{k',n'} g\left[m - n'M\right] e^{j\frac{2\pi}{M}k'm}, \tag{4.1}$$

where $d_{k',n'}$ are complex symbols from a QAM constellation, allocated on the k'-th subcarrier and sent in the n'-th QAM-FBMC symbol. $g[m]$ is the prototype filter with length $L_g = KM$, where M is the number of subcarriers and K is the overlapping factor.

In practice, the transmitted signal signal is analog and it is obtained from the discrete time samples $s[m] = s(mT_s)$ by using the Nyquist sampling theorem [93], where $T_s = \frac{T}{M}$ is the sampling period. Hence, the transmitted signal of the QAM-FBMC with M subchannels, also known as the Weyl–Heisenberg system of functions

[94] can be given by

$$s(t) = \sum_{k'=0}^{M-1} \sum_{n'} d_{k',n'} g(t - n'T) e^{j2\pi F k' t}, \tag{4.2}$$

where $g(t)$ is the unit-energy prototype filter, and F is the subcarrier frequency separation.

Considering additive white Gaussian noise channel, the continuous time received signal can be described as

$$r(t) = s(t) + v(t), \tag{4.3}$$

where $v(t)$ represents the white noise.

At the receiver, the output of the n-th symbol of the k-th filter after the signal sampling with time and frequency intervals T and F, respectively, can be expressed as

$$\begin{aligned}
\tilde{d}_{k,n} &= \int_{-\infty}^{\infty} r(t) g^*(t - nT) e^{-j2\pi F k t} \mathrm{d}t \\
&= \int_{-\infty}^{\infty} \left(\sum_{k'=0}^{M-1} \sum_{n'} d_{k',n'} g(t - n'T) e^{j2\pi F k' t} + v(t) \right) g^*(t - nT) e^{-j2\pi F k t} \mathrm{d}t \\
&= \sum_{k'=0}^{M-1} \sum_{n'} d_{k',n'} \int_{-\infty}^{\infty} g(t - n'T) g^*(t - nT) e^{-j2\pi F (k-k') t} \mathrm{d}t + v_{k,n} \\
&= d_{k,n} + \underbrace{\sum_{(k',n') \neq (k,n)} d_{k',n'} \int_{-\infty}^{\infty} g(t - n'T) g^*(t - nT) e^{-j2\pi F (k-k') t} \mathrm{d}t}_{\text{interference}} + v_{k,n},
\end{aligned} \tag{4.4}$$

where $v_{k,n} = \int_{-\infty}^{\infty} v(t) g^*(t - nT) e^{-j2\pi F k t} \mathrm{d}t$.

Let us recall the ambiguity function definition [95]

$$A_g(T, F) = \int_{-\infty}^{+\infty} g(t) g^*(t - T) e^{-j2\pi F t} \mathrm{d}t, \tag{4.5}$$

where * denotes the complex conjugate. By setting $\Delta_n = (n - n')$ and $\Delta_k = (k - k')$ we can derive the function $A_g((\Delta_n)T, (\Delta_k)F)$ as

$$A_g(\Delta_n T, \Delta_k F) = \int_{-\infty}^{+\infty} g(t - n'T) g^*(t - nT) e^{-j2\pi \Delta_k F t} \mathrm{d}t. \tag{4.6}$$

Thus, by using (4.6) we can rewrite (4.4) as

$$\tilde{d}_{k,n} = d_{k,n} + \underbrace{\sum_{(k',n') \neq (k,n)} d_{k',n'} A_g(\Delta_n T, \Delta_k F)}_{\text{interference}} + v_{k,n}. \tag{4.7}$$

As an example, we show in Fig. 4.1 the ambiguity function of the prototype filter case C proposed in [1] for the QAM-FBMC system with a single filter. The red marks represent the rectangular lattice structure of the QAM-FBMC system. These points, except for the central one ($(\Delta_k, \Delta_n) = (0, 0)$), indicate where we should sample the ambiguity function in order to obtain the intrinsic interference coefficients which will be used compute the interference of the system.

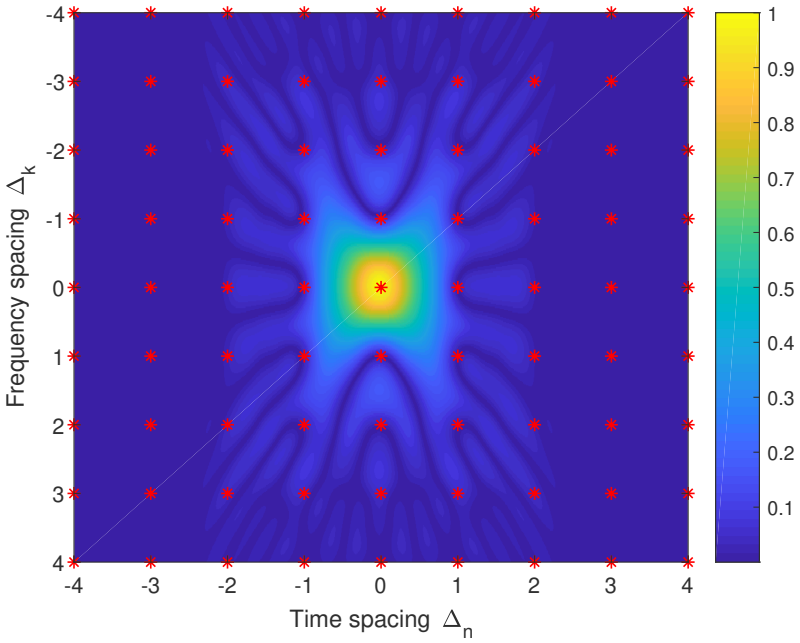

Figure 4.1: Ambiguity surfaces for Case C prototype filter [1], ($|A_g(T, F)|$).

Let us define the intrinsic interference coefficients as $\Gamma_{\Delta_n,\Delta_k} = A_g(\Delta_n T, \Delta_k F)$, represented by the red points in Fig. 4.1. Therefore, the total interference over k-th subcarrier at the n-th time instant can be calculated using the interference coefficients to weight the neighbor symbols as follows

$$I_{k,n} = \sum_{(k',n')\neq(k,n)} d_{k',n'} \Gamma_{\Delta_k \Delta_n}. \tag{4.8}$$

As we can see, these coefficients are essential to calculate the intrinsic interference, since the quantity of $\Gamma_{\Delta_k,\Delta_n}$, when $(k', n') \neq (k, n)$, is dedicated to the interference that comes from the surrounding symbols (k', n').

4.2 Prototype filter

QAM-FBMC has been considered a prominent waveform candidate to cope with the new 5G air interface requirements. It exhibits better spectral confinement thanks to the use of a time and frequency well localized prototype filter. Actually, the choice of

this filter can significantly impact the performance of the system. Furthermore, the length of the prototype filter impacts considerably the transceiver, since increasing it, (by increasing the overlapping factor, *e.g.*, $K = 4$), better spectral confinement can be achieved. Therefore, the careful design of prototype filters is of high interest to improve the QAM-FBMC performance.

We can also find in the literature several works on prototype filter design for QAM-FBMC systems in an attempt to enhance its performance. In [2] the authors proposed the so called Type I prototype filter designed based on the minimization of the self inter-symbol interference (ISI) subject to the fall-of rate limitation. As the obtained filter in [2] was poor in time domain, another waveform design considering time domain localization based on single prototype filter was suggested in [1] at a cost of a slight increase in interference. In that work the real coefficients were obtained from the minimization of self signal-to-interference ratio (self-SIR), under the constraints of fall-off rate and time dispersion. By using a global optimization algorithm, they proposed three different filters. The number of frequency domain coefficients of their filters was set as 7, 11, and 15, which lead to the filters named Case A, Case B, and Case C, respectively. Beyond that, we can also cite filter design proposals considering carrier frequency offset (CFO) [42]; filter design proposals specifically for minimum mean square error (MMSE) based receiver for given signal-to-noise rate (SNR) value [43]; and, more recently, a design based on the ISI minimization subject to OOBE limitation [96]. However, the performance evaluation of the proposed prototype filters remains unsatisfactory, since each proposal considers different parameters for the optimisation, such as a specific SNR, bandwidth, or class of receiver. Consequently, a direct comparison of their performance is questionable.

In this context, a novel prototype filter design method is presented in this section, moreover we optimize the proposed filter. For doing this, we consider the discrete prolate spheroidal sequences in order to achieve the most energy concentrate filter and minimize the intrinsic interference of the system. We compare the performances of the obtained filters to the known filters in the literature.

4.2.1 Discrete prolate spheroidal sequence (DPSS)

The problem of confining a signal in time and frequency domains simultaneously have been discussed in digital signal communication systems for a long time [97]. The energy time-concentration level of a signal can be measured as the fraction of the signal's energy lying in a time interval of length $2T_0$. This measure can be

mathematically written as

$$\mathrm{P} = \frac{\int_{-T_0}^{T_0} |g(t)|^2 \mathrm{d}t}{\int_{-\infty}^{+\infty} |g(t)|^2 \mathrm{d}t}. \tag{4.9}$$

If $g(t)$ is strictly time-limited to the interval $[-T_0, T_0]$ the energy concentration level P will achieve its maximum value of one. As time and frequency are inversely related, the Fourier transform of a time limited function is equal to an infinitely wide band function in frequency domain, indeed it is not possible to band-limit a time-limited signal.

The time/frequency concentration issue, which consists in maximizing P while keeping $g(t)$ band-limited, was first studied by Slepian, Pollac, and Lindau [76, 77]. They developed a set of band limited functions $\psi_p(t, b)$ that are maximally energy concentrated in a given time interval [76]. These functions are called Prolate Spheroidal Wave Functions (PSWFs) also known as Slepian functions.

The approach used by Slepian is based on angular and radial solutions in spheroidal coordinates of the first kind to the Helmholtz wave equation $S_{0_p}(b, t)$ and $R_{0_p}(b, 1)$ respectively. Hence, the PSWFs can be expressed as [76, 98]:

$$\psi_p(t, b) = \frac{\sqrt{\lambda_p(b)/T_0}}{\sqrt{\int_{-1}^{1} \left(S_{0_p}(b, t)\right)^2 \mathrm{d}t}} S_{0_p}\left(b, \frac{t}{T_0}\right), \tag{4.10}$$

where $\lambda_p(b)$ is given by

$$\lambda_p(b) = \frac{2b}{\pi} \left[R_{0_p}(b, 1)^2\right]. \tag{4.11}$$

The PSWFs are dependent on the continuous time parameter t, on the order p of the function, on the time parameter T_0, and also on the parameter b which is defined as

$$b = \frac{T_0 B}{2}, \tag{4.12}$$

where B, is the bandwidth of $\psi_p(t, b)$ of a given order p.

The PSWFs, $\psi_p(t, b)$, concentrated in the interval $[-T_0, T_0]$, can be defined as the normalized eigenfunctions of the following integral equation [78, 79]:

$$\int_{-T_0}^{T_0} \frac{\sin\left(\pi(x - t)B\right)}{\pi(x - t)} \psi_p(t, b)\mathrm{d}t = \lambda_p(b)\psi_p(x, b). \tag{4.13}$$

The sinc function in (4.13) can be regarded as a symmetric Toeplitz operator kernel, and the integral of $\psi_p(t, b)$ multiplied by this kernel can be called a symmetric Toeplitz operator [78]. Also, $\lambda_p(b)$ are the eigenvalues of the sinc function kernel, which can also be seen as the index of energy concentration on the interval $[-T_0, T_0]$ [99]. If $\lambda_0(b)$ denotes the largest eigenvalue of (4.13), then its corresponding eigenfunction, $\psi_0(t, b)$, is commonly called Slepian window, or prolate spheroidal window

in the continuous-time domain.

In addition, we can also think in time/frequency concentration problem in discrete-time. In [100], Slepian defined for a given time interval $2T_0$ with L samples, and for each $p = 0, 1, 2, \ldots, L-1$, the discrete Prolate Spheroidal Sequences (DPSS), $\phi_c^{(p)}(L, B)$, as the real solution to the system of equations

$$\sum_{l=0}^{L-1} \frac{\sin(\pi(c-l)B)}{\pi(c-l)} \phi_l^{(p)}(L, B) = \lambda_p(L, B)\phi_c^{(p)}(L, B) \tag{4.14}$$

for $c \in \mathbb{Z}$, and $\lambda_p(L, B)$ are the eigenvalues of the sinc function kernel. This is the discrete time representation of the system described in (4.13).

In our application we are interested in the sequences $\phi_c^{(p)}(L, B)$ limited to $c \in \{0, L-1\}$. It is obtained by index-limiting the DPSS. In this case, the sequence $\boldsymbol{\phi}^{(0)}(L, B)$ is the unique sequence that is time limited and the most frequency concentrated, $\boldsymbol{\phi}^{(1)}(L, B)$ is the second sequence having maximum energy concentration among the DPSS, and orthogonal to $\boldsymbol{\phi}^{(0)}(L, B)$, and so on. Therefore, we can rewrite (4.14) in a matrix approach as

$$\mathbf{Q}(L, B)\boldsymbol{\phi}^{(p)}(L, B) = \lambda(L, B)\boldsymbol{\phi}^{(p)}(L, B). \tag{4.15}$$

These sequences are thus seen to be the eigenvectors of the $L \times L$ matrix $\mathbf{Q}(L, B)$ with elements [100, 101]:

$$\mathbf{Q}(L, B)_{l,c} = \frac{\sin(\pi(l-c)B)}{\pi(l-c)} \quad l, c = 0, 1, 2, \ldots, L-1 \tag{4.16}$$

In Fig. 4.2 we illustrate some of these sequences.

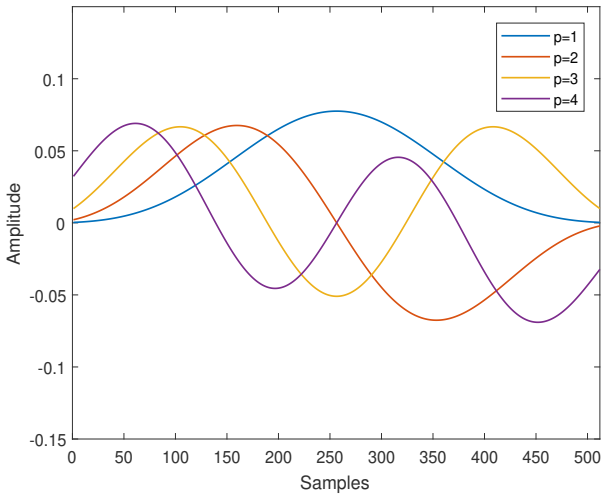

Figure 4.2: Example of Discrete prolate spheroidal sequences (DPSS) of length $L = 512$.

PSWFs should not be confused with the solution of the discrete-time energy concentration problem, the DPSS. DPSS are much simpler to calculate, and they are known only in a finite interval [79].

4.2.2 A novel prototype filter design

The features presented here suggest the potential utility of DPSS for filter-bank multicarrier systems. The first prolate sequence, $\boldsymbol{\phi}^{(0)}(L, B)$, is also known as the classical prolate window. It provides the optimally-concentrate pulse in frequency for a given filter length and bandwidth. It is defined as the eigenvector corresponding to the highest eigenvalue of the matrix $\mathbf{Q}(L, B)$, usually called Slepian window, or prolate spheroidal window in the discrete-time domain.

Another possible solution that we can think for filter design is the Kaiser window [52, 102], which employs Bessel functions in order to obtain an approximation of the prolate window. Although it has the advantage of its formulation through a closed form expression, it is sub-optimal in terms of out-of-band leakage when compared to the prolate window.

Knowing favorable characteristics of discrete prolate spheroidal sequences, we propose a prototype filter design technique based on DPSS, and we optimize the obtained filter. For this, we consider the spectral confinement, through the band-time parameter of DPSS, and minimize the intrinsic interference of the QAM-FBMC system by using its ambiguity function. We start by designing a function that represents the desired prototype filter using the DPSS.

As the eigenvalues can be regarded as the index of energy concentration of the DPSS [76], our proposal consists in selecting the eigenvectors $\boldsymbol{\phi}^{(p)}(L_g, B)$ of matrix $\mathbf{Q}(L_g, B)$ whose eigenvalues $\lambda_p(L_g, B)$ are higher than a certain threshold ξ. The first eigenvalues have strong energy concentration behavior, they are very close to 1, and the remaining eigenvalues are close to 0 [76]. By doing this process, we will select the N_e most energy concentrate sequences $\boldsymbol{\phi}^{(p)}(L_g, B)$ for a given band limitation B.

Finally, the proposed prototype filter can be described as a weighted sum of the N_e sequences as follows:

$$\boldsymbol{g} = \sum_{p=0}^{N_e-1} w_p \boldsymbol{\phi}^{(p)}(L_g, B), \tag{4.17}$$

where $\boldsymbol{g} = [g[0], g[1], \ldots, g[L_g - 1]]$ is the discrete response of $g(t)$ with $g[m] = g\left(m\frac{T}{M}\right)$, and w_p is the weight coefficient.

From the definition of the desired prototype filter given in (4.17), and taking into account the interference of the system described in (4.8), we propose an optimization problem to find the best prototype filter for QAM-FBMC systems. In this sense,

we want to find the optimal weights w_p of the prototype filter that minimize the energy of the interference coefficients $\Gamma_{\Delta_k \Delta_n}$ subject to the filter energy constraint. So that, we formulate our optimization problem as

$$\begin{aligned} \min_{\boldsymbol{\omega}} \quad & \sum_{\substack{(k',n') \\ \neq \\ (k,n)}} \left| \sum_m g[m - n'M] g^*[m - nM] e^{-j \frac{2\pi \Delta_k m}{M}} \right|^2 \\ \text{s.t.} \quad & \boldsymbol{g}^{\mathrm{H}} \boldsymbol{g} = 1 \end{aligned} \tag{4.18}$$

where the cost function is the discrete version of the ambiguity function given in (4.6).

In order to solve the above optimization problem, we use in this work the interior point method [62]. However, this problem is non-convex, so we can have several local minima. To deal with this, we have done the optimization several times, each time with different random initial weights $\boldsymbol{w}$, and we select the best obtained result, *i.e.* the one with the lower interference. Our obtained prototype filters are denoted as DPSS based filers (DPSSb).

Algorithm (1) describes the procedure adopted to solve problem (4.18).

Algorithm 1 Prototype Filter Design

procedure FILTER DESIGN(L_g, B, i_{max})
  interf$_{min} \leftarrow \infty$
  compute $\mathbf{Q}(L_g, B)$ as in (4.16)
  select the eigenvalues greater than ξ
  select the corresponding eigenvectors $\boldsymbol{\phi}^{(p)}(L_g, B)$
  for $i = 1$ to i_{max} **do**
    $\boldsymbol{w} \sim \mathcal{CN}(\mathbf{0}_{N_e \times 1}, \boldsymbol{I}_{N_e})$
    $\boldsymbol{w} \leftarrow \boldsymbol{w} / \|\boldsymbol{w}\|$
    compute $\mathbf{g}$ according to (4.17)
    $\boldsymbol{w} \leftarrow$ solution of problem (4.18) through IP
    compute $\boldsymbol{g}$ according to (4.17)
    interf $= \sum_{(k',n') \neq (k,n)} |\Gamma_{\Delta_k \Delta_n}|^2$
    if interf $<$ interf$_{min}$ **then**
      interf$_{min} \leftarrow$ interf
      $\boldsymbol{g}_{opt} \leftarrow \boldsymbol{g}$
    end if
  end for
  return $\boldsymbol{g}_{opt}$
end procedure

Optimization results

We set the overlapping factor of the desired filter as $K = 4$, and the number of subcarriers $M = 128$, which results in a filter length $L_g = 512$.

We established a threshold of $\xi = 0.99$ for the eigenvalues, it means that we select all eigenvalues greater than 0.99. For a fair comparison to the state-of-the-art filters known in the literature, we determined the bandwidth limitation of $B = 7/M$ for the optimization of the filter that was compared to the Case C filter proposed in [1]. For the comparison to the Type I filter proposed in [2] we set the bandwidth $B = 1.7/M$. The compared filters have approximately the same bandwidth. These filters have been chosen due to their characteristics, they were not optimized for a specific SNR or CFO. Although, to the best of our knowledge, there is no prototype filter in the literature for QAM-FBMC with passband $B = 3/M$, we optimized a prototype filter with this bandwidth in order to demonstrate the proposed procedure flexibility.

In the case of $B = 1.7/M$, by setting $\xi = 0.99$, we have $N_e = 3$ eigenvectors, therefore we have to optimize 3 weights w_i. In Fig. 4.3 we present the ambiguity surface of the DPSS-based optimized filter. As we can notice, the interference spreads differently in time and frequency domains. It spreads more in time than in the frequency domain.

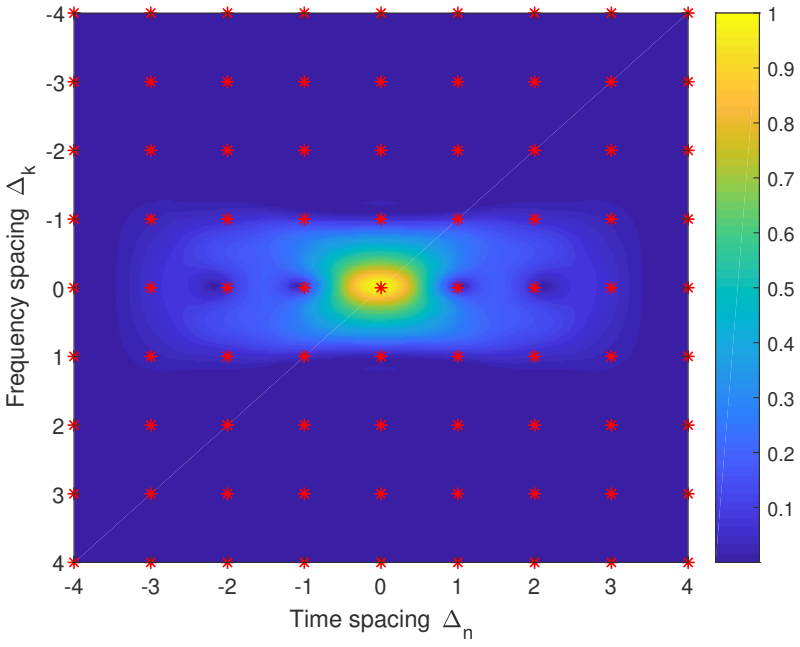

Figure 4.3: Ambiguity surface of the proposed DPSSb $1.7/M$ filter, ($|A_g(T, F)|$).

We have also compared the frequency response of the optimized DPSSb $B = 1.7/M$ filter with the frequency response of Type I filter [2] in Fig. 4.4. As expected, due to the choice of B, they have approximately the same bandwidth, however, as

we can notice their energy distribution is not the same.

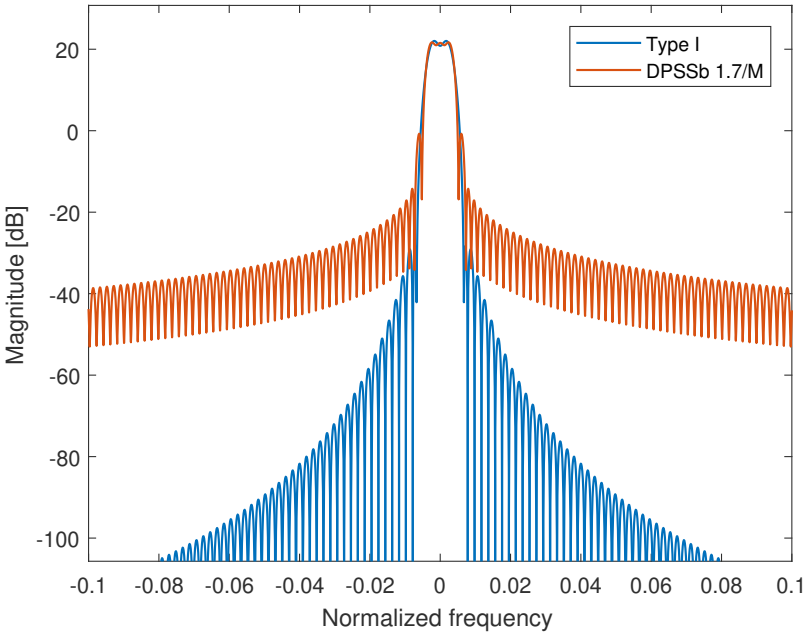

Figure 4.4: Magnitude frequency response of the proposed DPSSb $1.7/M$ filter and Type I filter [2].

The optimization procedure was also applied for the comparison with the Case C filter [1]. We present in Fig. 4.5 the ambiguity surface of the optimized DPSSb $B = 7/M$ filter, which is also non symmetric due to the complex nature of the weights. For this optimization, considering $\xi = 0.99$, the number of selected eigenvectors was $N_e = 25$.

As we can see, the ambiguity surface of the DPSS-based $7/M$ optimized filter is not symmetric. This fact comes from the complex nature of the optimized weights. As expected, comparing this ambiguity surface to the case of $B = 1.7/M$, we can notice an increasing in the spread of interference in the frequency domain. This comes from the fact that, in this case, we are optimizing a filter with bandwidth far greater than the subcarrier spacing $1/M$.

The comparison between the frequency response of the DPSSb $7/M$ filter and the Case C [1] filter is also presented in Fig. 4.6. Once again, the optimized filter and the known filter have approximately the same bandwidth, however their energy distribution is not the same.

Despite to achieving higher attenuation at the extremities of the transmission band, the passband of the DPSSb $7/M$ seem worse than that of DPSSb $1.7/M$. This result comes from the fact that the bandwidth of DPSSb $7/M$ comprises more than one subcarrier spacing $(1/M)$. As we minimize the interference coefficients $\Gamma_{\Delta_k \Delta_n}$, which are spaced by one subcarrier spacing, some of them are inside of the considered passband of the optimized filter.

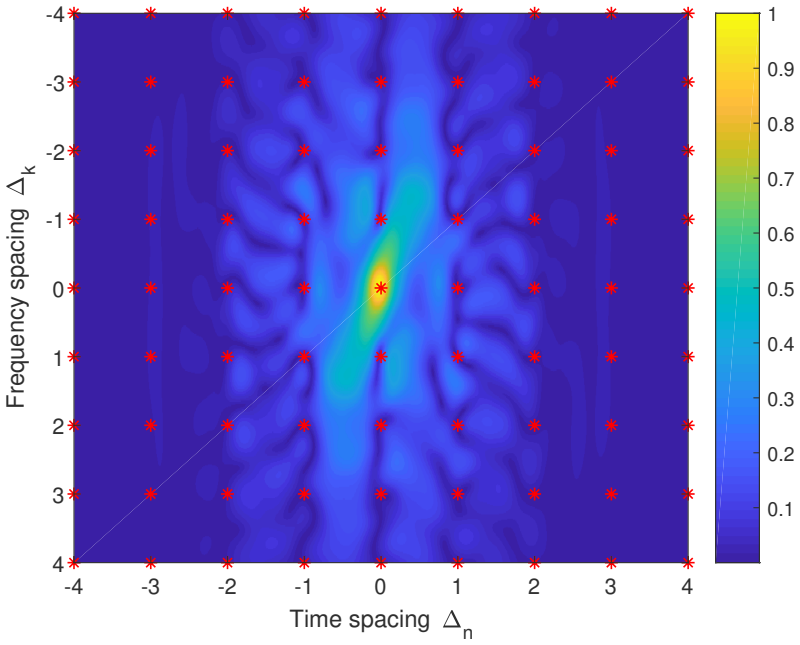

Figure 4.5: Ambiguity surface of the proposed DPSSb filter $7/M$, ($|A_g(T, F)|$).

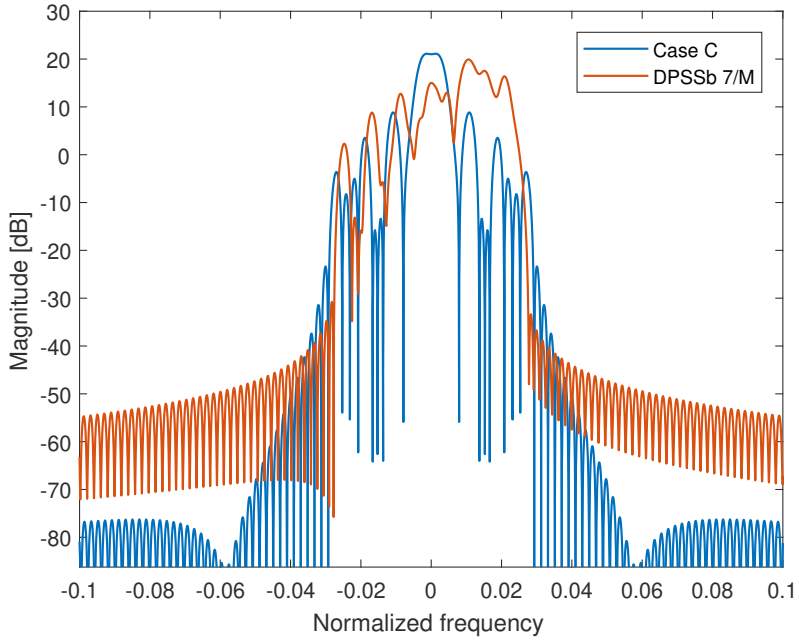

Figure 4.6: Magnitude frequency response of the proposed DPSSb $7/M$ filter and Case C [1]

In order to make a comparison of the prototype filters, we present in Table 4.1 some characteristics of the known filters and the proposed ones. We compare the inter-symbol interference (ISI) observed in a QAM-FBMC system when using all of these prototype filters. Besides, we evaluate the OOBE of them considering their transmission bandwidth and we also classify them by the nature of their coefficients.

Table 4.1: ISI and OOBE of different filters.

Filter	ISI	Coefficient	OOBE
Case C [1]	-17.4256 dB	Real	5.2782e-04
DPSSb (proposed) 7/M	-18.9553 dB	Complex	4.8993e-05
DPSSb (proposed) 3/M	-14.4736 dB	Complex	3.3082e-05
Type I [2]	-10.6314 dB	Complex	4.6839e-06
DPSSb (proposed) 1.7/M	-12.6009 dB	Complex	3.5464e-04

By increasing the desired transmission band it is possible to decrease the ISI of the optimized prototype filter. However, it happens at a cost of the OOBE increase. Despite having approximately the same transmission bandwidth, the DPSSb $1.7/M$ filter presents smaller ISI than Type I filter, also at a cost of slightly increasing the OOBE. Unlike what happens with the DPSSb $1.7/M$ filter, the optimized DPSSb $7/M$ has approximately the same transmission bandwidth of the Case C filter and its ISI is smaller, however its OOBE does not increase. This fact can be explained by the complex nature of the optimized filter coefficients, whereas Case C filter coefficients are real. It is important to point out that the proposed DPSSb $7/M$ filter achieves the highest interference attenuation among the optimized filters.

Although we do not find in the literature a prototype filter with passband $B = 3/M$, we present in Table 4.1 the characteristics of the optimized filter DPSSb $3/M$ in order to exemplify the flexibility of the proposed method.

4.2.3 Performance evaluation

In this section we evaluate the performance of QAM-FBMC system when using the optimized prototype filters DPSS based (DPSSb) and compare the results with those obtained when using the prototype filter Case C proposed in [1] and Type I proposed in [2].

The prototype filter performance was evaluated through the bit error rate (BER) over AWGN channel and also over pedestrian channel. The presented results are obtained by averaging over different channel instantaneous realizations. Besides, the evaluation performance was performed over different modulation levels: 4-QAM, 16-QAM and, 64-QAM.

In order to enhance the overall system performance, the iterative interference cancellation was applied at the receiver. For the sake of clarity, we also present the Genie Aided performance, when the interference is supposed to be completely known at the receiver.

In Fig. 4.7 and Fig. 4.8 we present the BER performance of QAM-FBMC system over AWGN channel with 4-QAM and 16-QAM modulations respectively.

We compare the results using DPSSb $1.7/M$ optimized filter with Type I filter.

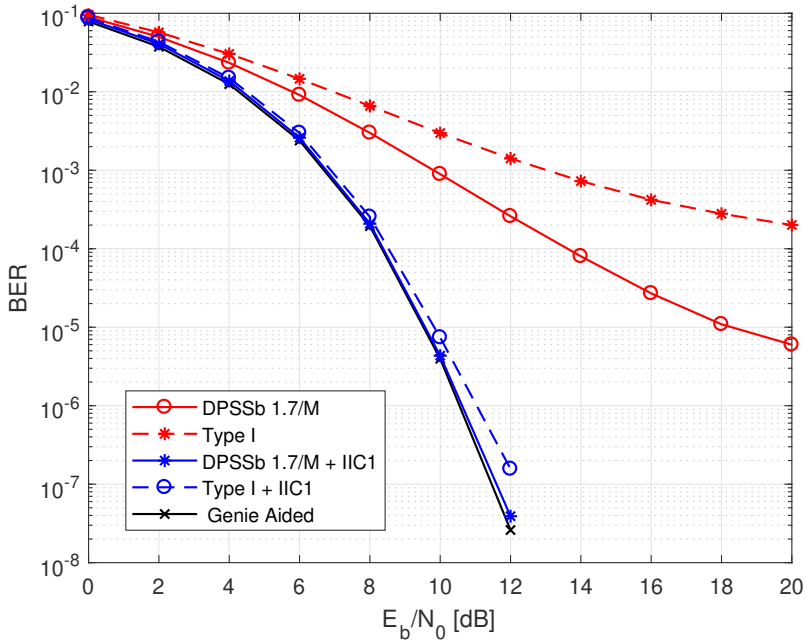

Figure 4.7: BER performance of QAM-FBMC system with 4QAM modulation, DPSSb 1.7/M filter and Type I [2] filter over AWGN channel.

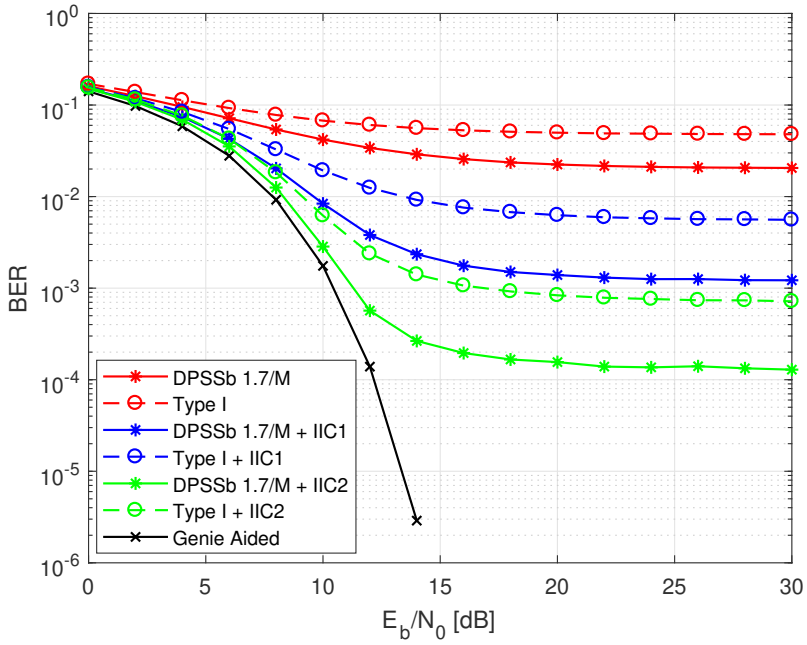

Figure 4.8: BER performance of QAM-FBMC system with 16QAM modulation, DPSSb 1.7/M filter and Type I [2] filter over AWGN channel.

When using 4-QAM modulation, the system performance can be significantly improved by the use of the optimized filter. However, with just one IIC iteration it is possible to achieve the same performance for both filters, which is the same of the Genie Aided, when the interference is supposed to be completely known. Even

observing a significant degradation in the performance for 16-QAM modulation, compared to the 4-QAM modulation, the proposed filter outperforms the Type I filter. Besides, applying the IIC technique, even with two IIC iterations DPSSb $1.7/M$ outperforms Type I filter .

The QAM-FBMC system was also evaluated over pedestrian channel. Fig. 4.9, Fig. 4.10, and Fig. 4.11 compare the performance of DPSSb $1.7/M$ and Type I filters when using 4, 16, and 64-QAM modulation respectively. In the case of 4-QAM modulation, even without using IIC technique, the DPSSb $1.7/M$ performance is very close to that of Genie aided, whereas for Type I one IIC iteration is necessary to achieve the same performance.

Passing to the 16-QAM and 64QAM modulation we can observe an overall system degradation as expected. Once again the optimized filter outperforms Type I filter and achieve the Genie Aided performance with 16-QAM modulation by performing 3 IIC iterations. Although for 64-QAM modulation the system suffer of high degradation, we can still confirm the superiority of the DPSSb $1.7/M$ filter, since it outperforms Type I even after 5 IIC iterations

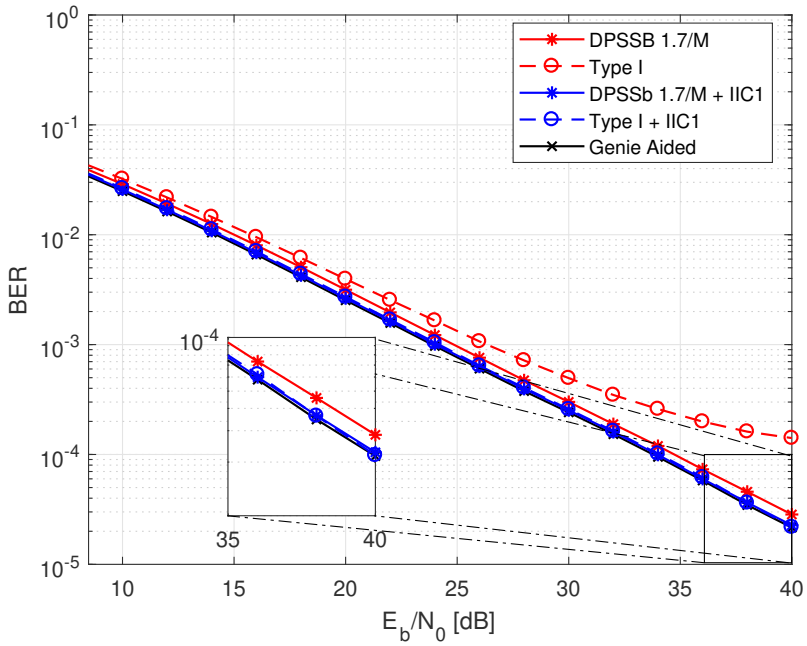

Figure 4.9: BER performance of QAM-FBMC system with 4QAM modulation, DPSSb $1.7/M$ filter and Type I [2] filter over pedestrian channel.

As we did not find in the literature a prototype filter with approximately the same bandwidth to make a fair comparison to the DPSSb $3/M$, we present its performance alone in Fig. 4.12, Fig. 4.13, and Fig. 4.14 in the cases of 4-QAM, 16-QAM, and 64-QAM modulation respectively.

As we can see, for 4-QAM modulation we achieve the same performance as

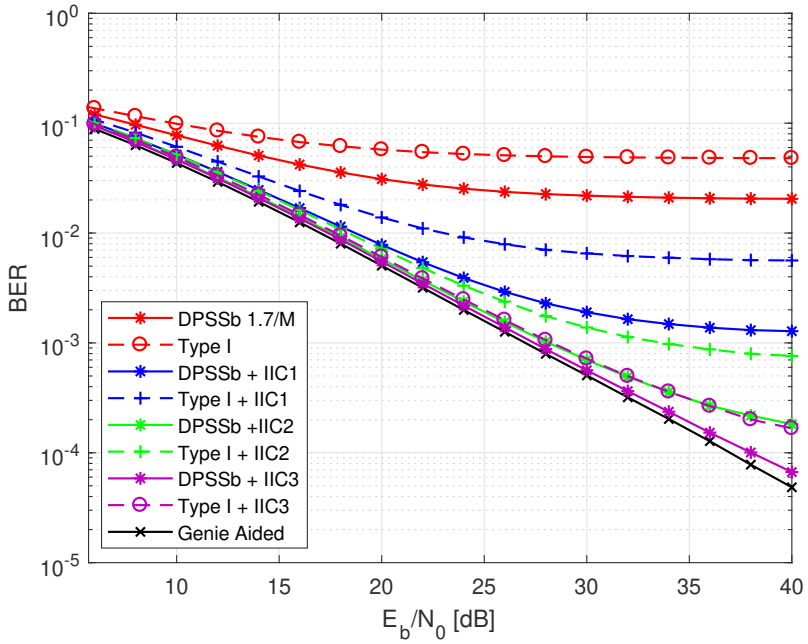

Figure 4.10: BER performance of QAM-FBMC system with 16QAM modulation, DPSSb 1.7/M filter and Type I [2] filter over pedestrian channel.

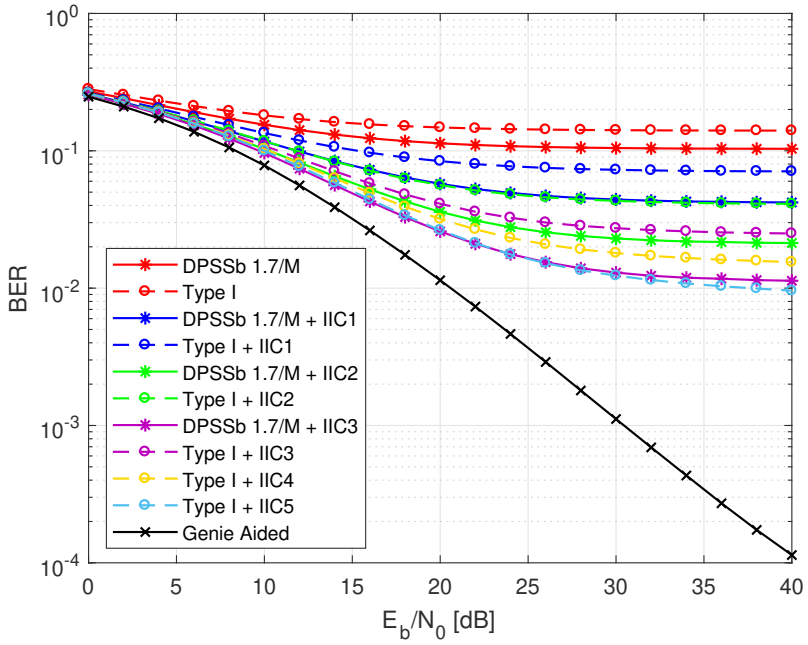

Figure 4.11: BER performance of QAM-FBMC system with 64QAM modulation, DPSSb 1.7/M filter and Type I [2] filter over pedestrian channel.

the Genie Aided, even without IIC. Whereas the Genie Aided is achieved with 3 IIC iterations when the 16-QAM modulation is applied, for the case of 64-QAM modulation the overall system performance worsens, but it still can be significantly improved through the IIC application.

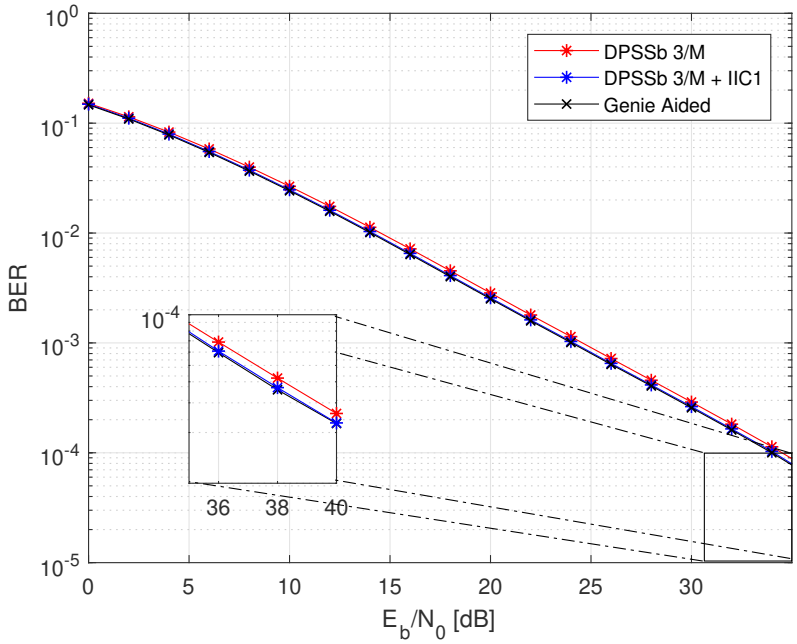

Figure 4.12: BER performance of QAM-FBMC system with 4QAM modulation, DPSSb 3/M filter over pedestrian channel.

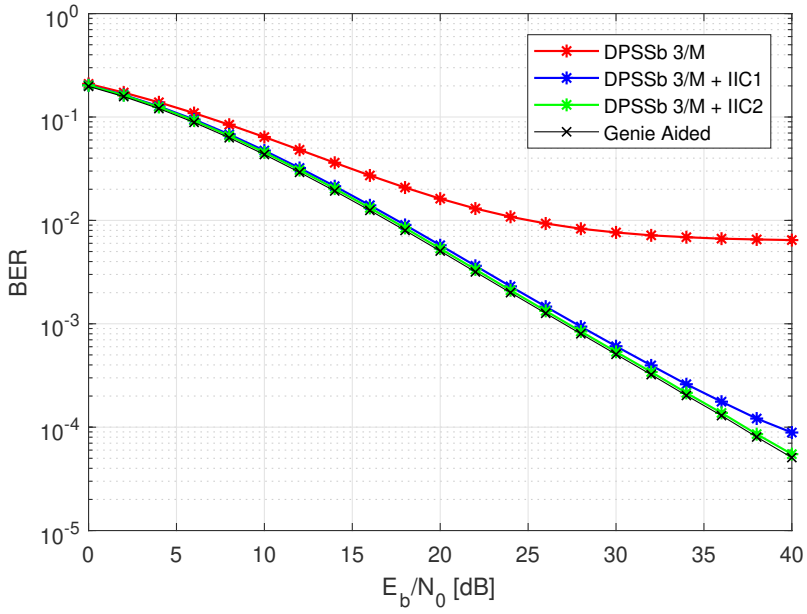

Figure 4.13: BER performance of QAM-FBMC system with 16QAM modulation, DPSSb 3/M filter over pedestrian channel.

For the comparison to the Case C filter, we have optimized a prototype filter DPSSb with passband $B = 7/M$. We present in Fig. 4.15, Fig. 4.16, and Fig. 4.17 the system performance when applying 4-QAM, 16-QAM, and 64-QAM modulation respectively.

As we can see, for the case of 4-QAM modulation, the Genie Aided performance is achieved even without IIC. Besides, both filters have the same performance until

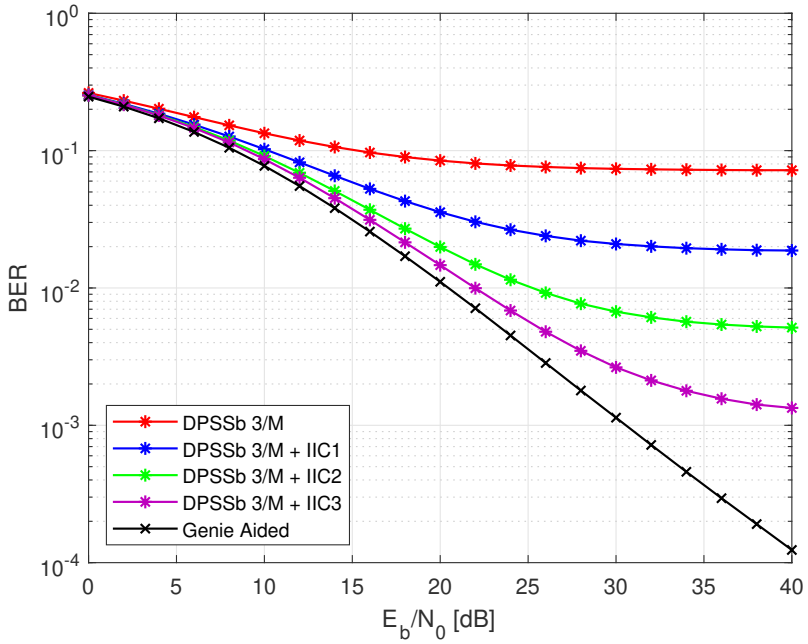

Figure 4.14: BER performance of QAM-FBMC system with 64QAM modulation, DPSSb 3/M filter over pedestrian channel.

approximately 34dB of E_b/N_0. After that, the performances are slightly different. One IIC iteration is needed for achieving the same performance of Genie Aided in the case of 16-QAM modulation for both filters. However, without IIC the optimized filter outperforms the Case C filter. Once again we can notice a slight difference between the performances for E_b/N_0 greater than 34dB. As foreseen, for the case of 64-QAM modulation the overall system performance deteriorates. Despite that, DPSSb 7/M filter achieves better results when compare with Case C filter, even if we apply three IIC iterations.

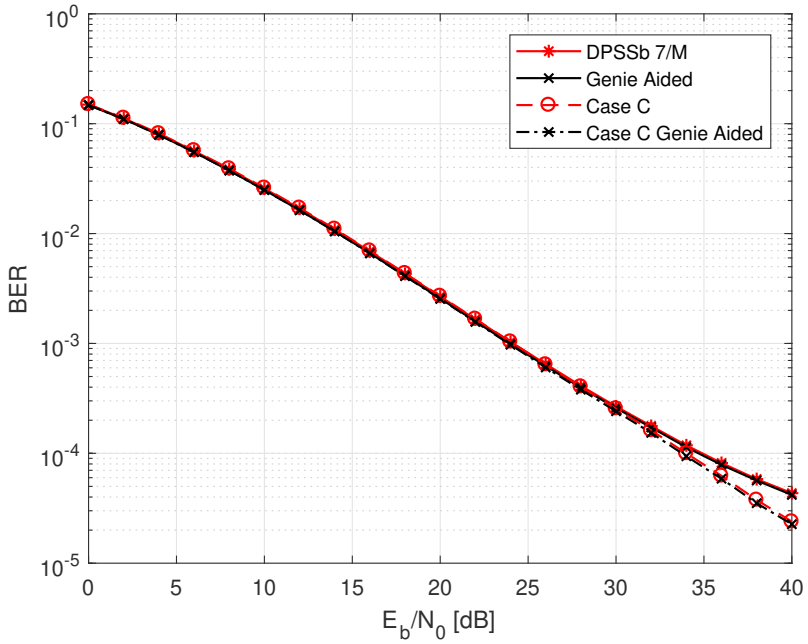

Figure 4.15: BER performance of QAM-FBMC system with 4QAM modulation, DPSSb $7/M$ filter and Case C [1] filter over pedestrian channel.

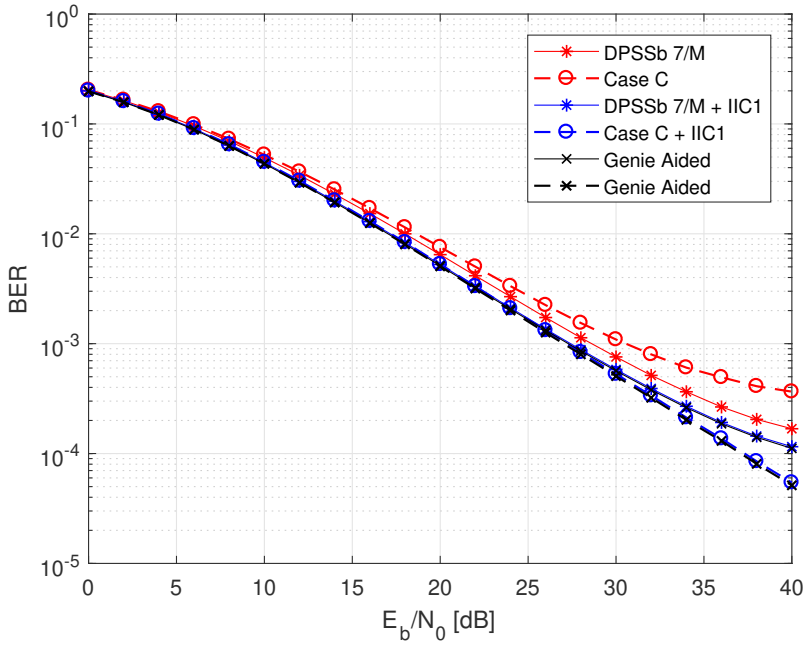

Figure 4.16: BER performance of QAM-FBMC system with 16QAM modulation, DPSSb $7/M$ filter and Case C [1] filter over pedestrian channel.

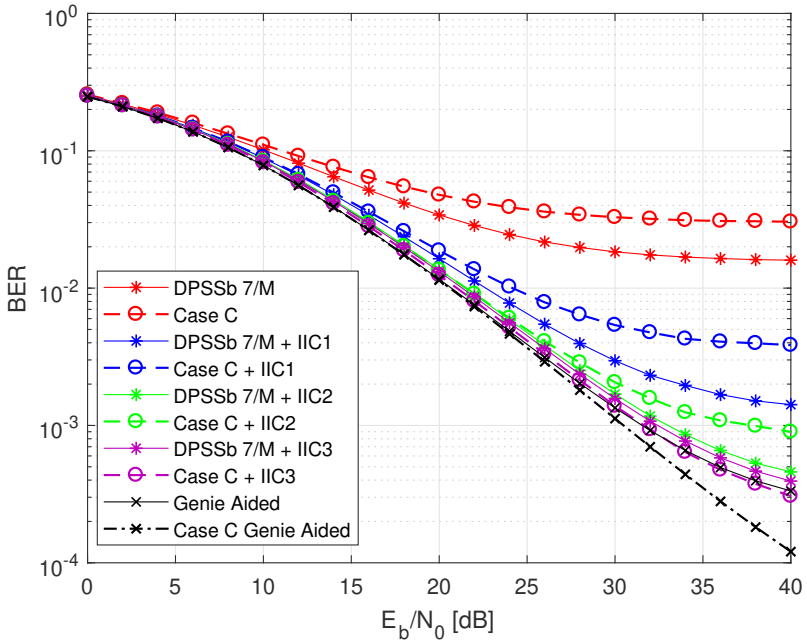

Figure 4.17: BER performance of QAM-FBMC system with 64QAM modulation, DPSSb $7/M$ filter and Case C [1] filter over pedestrian channel.

4.3 Hexagonal QAM-FBMC

In multicarrier systems, symbol duration and subcarrier spacing define the time-frequency lattice structure associated with the communication system. The major part of the work on system design have dealt with rectangular lattices. However, such approach shows not to be the best one for the case of time-frequency dispersive channels as discussed in [103]. With the aim of the transmitted signal to be distorted as little as possible, the authors in [104], proposed to use basic signals, which are localized in time and frequency with the same time frequency scale as the channel itself. This was the first time that different frequency and time scale was applied to communication systems, which leads to a lattice structure different from the traditional rectangular lattice.

Several lattice structures, including the hexagonal lattice, have been widely studied in [105]. The authors of [103], applied this hexagonal lattice structure to communication systems and provided an analysis of the optimality of the systems with lattices different from the rectangular. They have introduced the lattice OFDM (LOFDM) systems, which are based on general, non-rectangular, time-frequency lattices. They have also demonstrated that the LOFDM outperforms the classical OFDM.

Despite the investigation conducted, the prototype filter used in [103, 104] was Gaussian. As the Gaussian filter does not yield an orthogonal set of transmission filters, they used a standard method to orthogonalize these filters as in [106, 107]. More recently, in [108–110], the hexagonal lattice structure was studied over multicarrier faster than Nyquist systems (MFTN), and also OFDM. The authors evaluated the system performance also using Gaussian filter.

Although we find the study over hexagonal lattice in multicarier systems, to the best of our knowledge, there is no study over prototype filters specifically designed for multicarrier systems with hexagonal lattice structures.

We propose in this section a shifted structure of conventional QAM-FBMC. We present the QAM-FBMC system implemented over the hexagonal lattice structure (also known as quincunx), what we call HQAM-FBMC. In addition, we propose a novel prototype filter design for this structure based on the DPSS design presented in Section 4.2.2. Then, we optimize the proposed filter in order to overcome the intrinsic interference of the HQAM-FBMC system. We also provide a performance comparison of the QAM-FBMC system using its optimized DPSSb filter proposed in 4.2.2, and the proposed HQAM-FBMC system also with its optimized HDPSSb prototype filter.

4.3.1 System model

In this section we present the system model for the standard QAM-FBMC, with rectangular lattice, exemplified in Figure 4.18 (a). We also present the proposed system model for QAM-FBMC with hexagonal lattice, as exemplified in Figure 4.18 (b), which we called HQAM-FBMC.

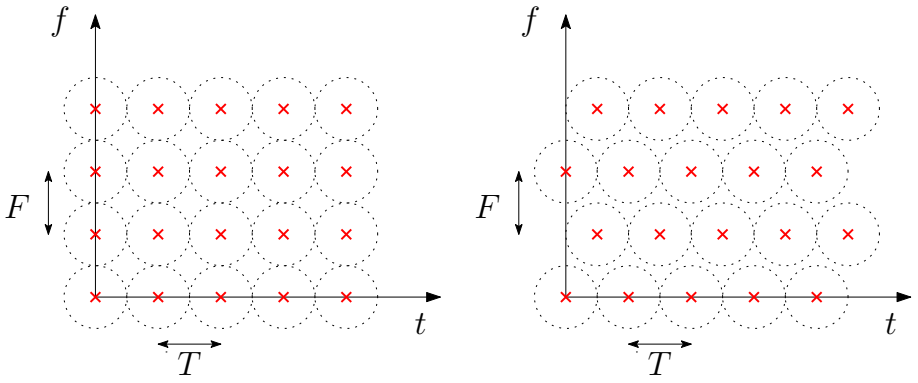

Figure 4.18: Time-frequency lattice structure, (a) rectangular and (b) hexagonal.

The hexagonal lattice consists of time shifting (or frequency) the signal related to the rectangular lattice. Let us consider a baseband HQAM-FBMC signaling system with M subchannels. By defining $d_{k',n'}$ as the transmitted symbol allocated at the k'-th subcarrier and transmitted in the n'-th HQAM-FBMC symbol, therefore, the transmitted HQAM-FBMC signal can be expressed as [108]

$$s(t) = \sum_{n'} \sum_{k'=0}^{M-1} d_{k',n'} g\left(t - n'T - \frac{\mathrm{mod}(k',2)}{2}T\right) e^{j2\pi Fk't}, \tag{4.19}$$

where mod (.) represent the modulo operation, $g(t)$ is assumed to be an unit-energy prototype filter *i.e.*, $\int_{-\infty}^{\infty} |g(t)|^2 \mathrm{d}t = 1$, T is the symbol time, and F is the subcarrier frequency spacing.

Similarly to the case of rectangular lattice, considering AWGN channel, the continuous-time received signal can be described as

$$r(t) = s(t) + v(t). \tag{4.20}$$

The demodulated symbol at the k-th subcarrier and n-th symbol is given by

$$\begin{aligned}\tilde{d}_{k,n} &= \int_{-\infty}^{\infty} r(t) g^*(t - nT - \frac{\mathrm{mod}(k,2)}{2}T) e^{-j2\pi Fkt} \mathrm{d}t \\ &= \int_{-\infty}^{\infty} \sum_{n'} \sum_{k'=0}^{M-1} d_{k',n'} g\left(t - n'T - \frac{\mathrm{mod}(k',2)}{2}T\right) g^*\left(t - nT - \frac{\mathrm{mod}(k,2)}{2}T\right) e^{-j2\pi F(k-k')t} \mathrm{d}t \\ &\quad + v_{k,n}\end{aligned} \tag{4.21}$$

where $v_{k,n} = \int_{-\infty}^{\infty} v(t) g^*\left(t - nT - \frac{\mathrm{mod}(k,2)}{2}T\right) e^{-j2\pi F(k-k')t} \mathrm{d}t$.

Also, by setting $\Delta'_n = (n + 1/2\mathrm{mod}(k,2)) - (n' + 1/2\mathrm{mod}(k',2))$, we can derive the ambiguity function as

$$\begin{aligned}&A_g\left(\Delta'_n T, \Delta_k F\right) = \\ &= \int_{-\infty}^{+\infty} g\left(t - n'T - \frac{\mathrm{mod}(k',2)}{2}T\right) g^*\left(t - nT - \frac{\mathrm{mod}(k,2)}{2}T\right) \\ &\quad \times e^{-j2\pi F(k-k')(t + (\frac{\mathrm{mod}(k,2)}{2} - n' - \frac{\mathrm{mod}(k',2)}{2})T)} \mathrm{d}t \\ &= \int_{-\infty}^{+\infty} g\left(t - n'T - \frac{\mathrm{mod}(k',2)}{2}T\right) g^*\left(t - nT - \frac{\mathrm{mod}(k,2)}{2}T\right) \\ &\quad \times e^{-j2\pi F(k-k')t} \mathrm{d}t \; e^{-j2\pi(k-k')(\frac{\mathrm{mod}(k,2) - \mathrm{mod}(k',2)}{2} - n')}\end{aligned} \tag{4.22}$$

Thus, we can use Equation (4.22) for rewriting the demodulated symbol presented in Equation (4.21) as

$$\tilde{d}_{k,n} = d_{k,n} + \underbrace{\sum_{(k',n') \neq (k,n)} d_{k',n'} A_g\left(\Delta'_n T, \Delta_k F\right) e^{j2\pi(k-k')(\frac{\mathrm{mod}(k,2) - \mathrm{mod}(k',2)}{2} - n')}}_{\text{interference}} + v_{k,n} \tag{4.23}$$

Similarly to what we have done for the standard case, by defining the HQAM-FBMC intrinsic interference coefficients as $\Gamma_{\Delta'_n, \Delta_k} = A_g\left(\Delta'_n T, \Delta_k F\right) e^{-j2\pi\Delta_k(n' - \frac{1}{2}\mathrm{mod}(k',2))}$, the total interference observed at the receiver of a HQAM-FBMC system over the k-th subcarrier at the n-th time instant can be obtained weighting the neighbor symbols with these coefficients as follows:

$$I'_{k,n} = \sum_{(k',n') \in \Upsilon_{k,n}} d_{k',n'} \Gamma_{\Delta'_n, \Delta_k}, \tag{4.24}$$

where $\Upsilon_{k,n}$ is the set of (k', n') for which the interference coefficient is non-null,

As we can see, similar to the rectangular case, these coefficients are essential to calculate the intrinsic interference, since the quantity of $\Gamma_{\Delta_k,\Delta'_n}$, when $(k',n') \neq (k,n)$, is dedicated to the interference that comes from the surrounding symbols (k',n').

4.3.2 Proposed Hexagonal DPSSb prototype filter design

In this section, we propose a prototype filter design technique based on DPSS, specifically for the HQAM-FBMC. For this, we consider the spectral confinement, through the band and time parameter of DPSS, and minimize the intrinsic interference of the HQAM-FBMC system by using its ambiguity function.

We have used here the same approach as in Section 4.2.2, we start by designing a function that represents the desired prototype filter using the DPSS. We design the matrix $\mathbf{Q}(L,B)$ as presented in Equation (4.16), and select the eigenvectors $\boldsymbol{\phi}^{(p)}(L,B)$ whose eigenvalues $\lambda_p(L,B)$ are higher than a certain threshold ξ. Then, we write the desired filter as

$$\boldsymbol{g} = \sum_{p=0}^{N_e-1} w_p \boldsymbol{\phi}^{(p)}(L_g,B). \tag{4.25}$$

where $\boldsymbol{g} = [g[0], g[1], \ldots, g[L_g-1]]$ is the discrete response of $g(t)$ with $g[m] = g\left(m\frac{T}{M}\right)$, and w_p is the weight coefficient.

Taking into account the intrinsic interference of HQAM-FBMC systems described in Equation (4.24), and the definition of the desired filter, we propose an optimization problem to find the best prototype filter for HQAM-FBMC systems. In this sense, we want to find the optimal weights w_p of the prototype filter that minimize the energy of the interference coefficients $\Gamma_{\Delta_k\Delta'_n}$ subject to the filter energy constraint. We formulate our optimization problem as

$$\begin{aligned} \min_{\boldsymbol{\omega}} \quad & \sum_{\substack{(k',n') \\ \neq \\ (k,n)}} \left| \sum_m g\left[m - n'M - \tfrac{\mathrm{mod}(k',2)}{2}M\right] g^*\left[m - nM - \tfrac{\mathrm{mod}(k,2)}{2}M\right] e^{-j2\pi\Delta_k \frac{1}{M} m} \right|^2 \\ \text{s.t.} \quad & \boldsymbol{g}^{\mathrm{H}}\boldsymbol{g} = 1 \end{aligned} \tag{4.26}$$

where the cost function is the discrete version of the ambiguity function given in (4.22).

We have also solved the above optimization problem through the IP method [62]. Our obtained prototype filters are denoted HDPSS based filters (HDPSSb).

4.3.3 Optimization results

In order to make a fair comparison of standard QAM-FBMC and HQAM-FBMC, we optimized the HDPSSb filter for different values of bandwidth. As in [111], we have set $B = 1.7/M$, $B = 3/M$, and $B = 7/M$. The number of subcarriers was defined as $M = 128$, and the overlapping factor of the filter was chosen as $K = 4$. Thus, the proposed filters have length $L_g = KM = 512$. Besides, We established the threshold as $\xi = 0.99$ for the eigenvalues, it means that we selected only eigenvalues greater than 0.99.

In Figure 4.19, Figure 4.20, and Figure 4.21, we present the ambiguity function of the optimized HDPSSb filters. As we can notice, the interference spreads differently for each one, and as expected, by increasing the optimized bandwidth we also increase the interference spreading in the frequency domain.

The red marks in Figure 4.19, Figure 4.20, and Figure 4.21, represent the hexagonal lattice structure of the HQAM-FBMC system. These points, except for the central one ($(\Delta_k, \Delta_n) = (0, 0)$), indicate where we should sample the ambiguity function in order to obtain the intrinsic interference coefficients which will be used compute the system intrinsic interference.

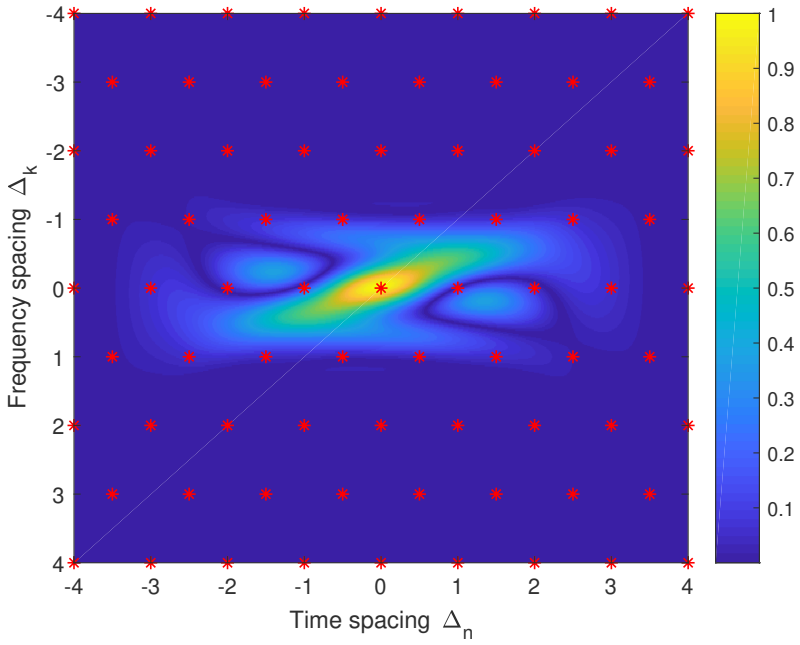

Figure 4.19: Ambiguity surface of the proposed HDPSSb filter $1.7/M$, ($|A_g(T, F)|$).

In order to compare the prototype filters, we present in Table 4.2 some characteristics of the DPSSb filters [111] and the proposed HDPSSb filters. We also compare the inter-symbol interference (ISI) observed in a QAM-FBMC system when using DPSSb prototype filters, with the ISI observed in HQAM-FBMC system when using HDPSSb filters. Besides, we evaluate their OOBE considering their bandwidth and

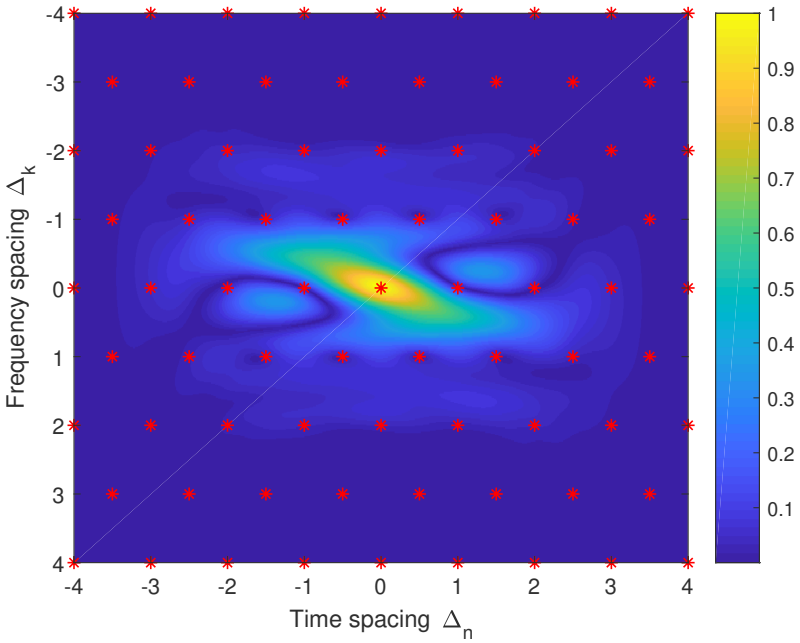

Figure 4.20: Ambiguity surface of the proposed HDPSSb filter $3/M$, ($|A_g(T,F)|$).

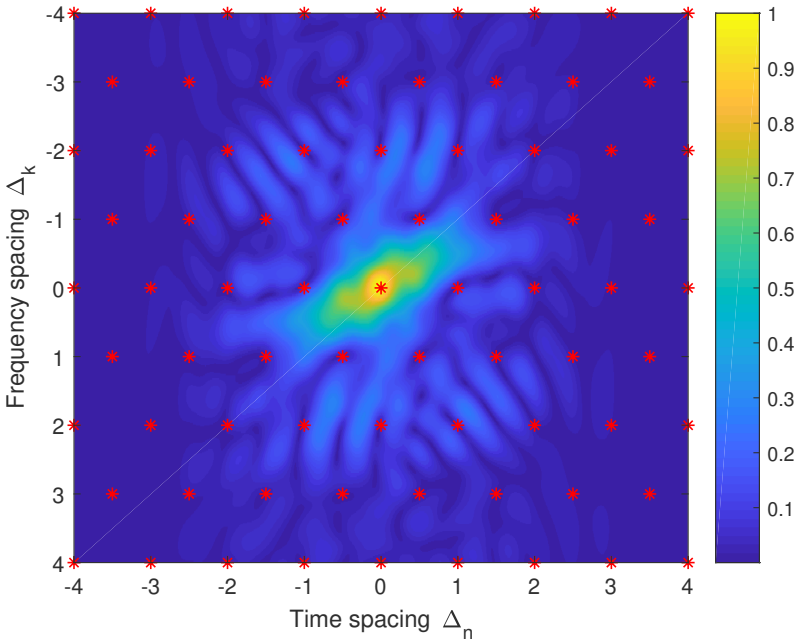

Figure 4.21: Ambiguity surface of the proposed HDPSSb filter $7/M$, ($|A_g(T,F)|$).

we also classify them by the nature of their coefficients.

Similarly to what happens in the case of DPSSb filters, when optimizing HDPSSb filters, by increasing the desired transmission bandwidth it is possible to decrease the ISI of the optimized prototype filter. However, it happens at a cost of OOBE increase. We can also observe that the ISI level achieved is approximately the same, for both filters DPSSb and HDPSSb, with the same bandwidth.

Table 4.2: ISI and OOBE of different systems and filters.

Filter	ISI	Coefficient	OOBE
DPSSb 7/M	-18.95 dB	Complex	4.89e-05
HDPSSb (proposed) 7/M	-18.12 dB	Complex	2.70e-05
DPSSb 3/M	-14.47 dB	Complex	3.30e-05
HDPSSb (proposed) 3/M	-14.44 dB	Complex	3.55e-05
DPSSb 1.7/M	-12.60 dB	Complex	3.54e-04
HDPSSb (proposed) 1.7/M	-12.64 dB	Complex	3.43e-04

4.3.4 Performance evaluation

In order to evaluate how much the use of hexagonal lattice improves the QAM-FBMC system, in this section we compare the system performance of QAM-FBMC using the DPSSb filter proposed in [111] with the system performance of HQAM-FBMC using our proposed HDPSSb and optimized prototype filters. Furthermore, the performances were compared through the bit error rate (BER) of the systems over Additive White Gaussian Noise (AWGN) channel and pedestrian channel.

In Figure 4.22 and Figure 4.23 we compare the performance of QAM-FBMC and HQAM-FBMC over AWGN channel. Both systems used optimized filters with bandwidth $B = 1.7/M$, however, the modulation in Figure 4.22 was 4-QAM, and in Figure 4.23 it was 16-QAM. As we can see, the results for QAM-FBMC and HQAM-FBMC are pretty much the same.

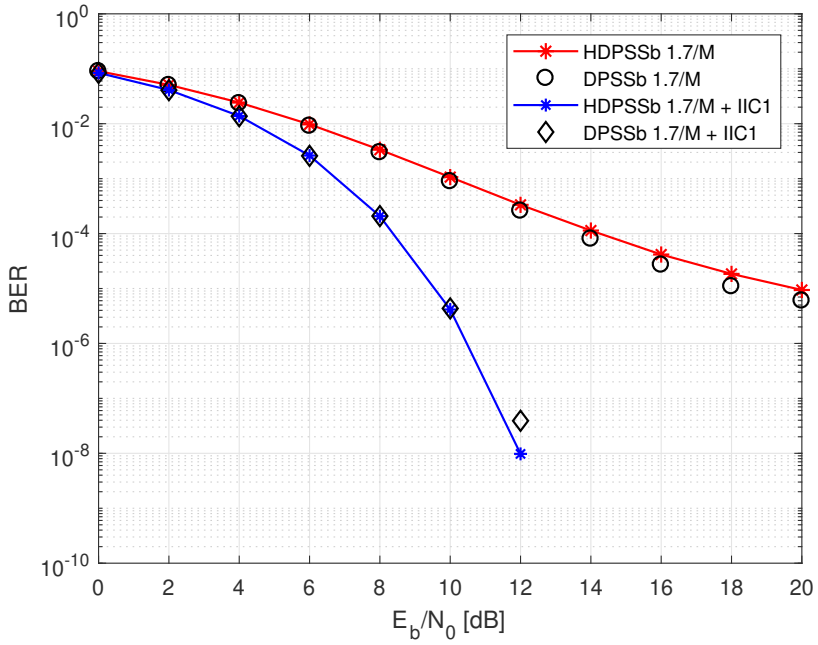

Figure 4.22: BER performance of QAM-FBMC system with 4QAM modulation with DPSSb 1.7/M filter and HQAM-FBMC with HDPSSb filter over AWGN channel.

We have also used the intrinsic interference cancellation (IIC) technique in order

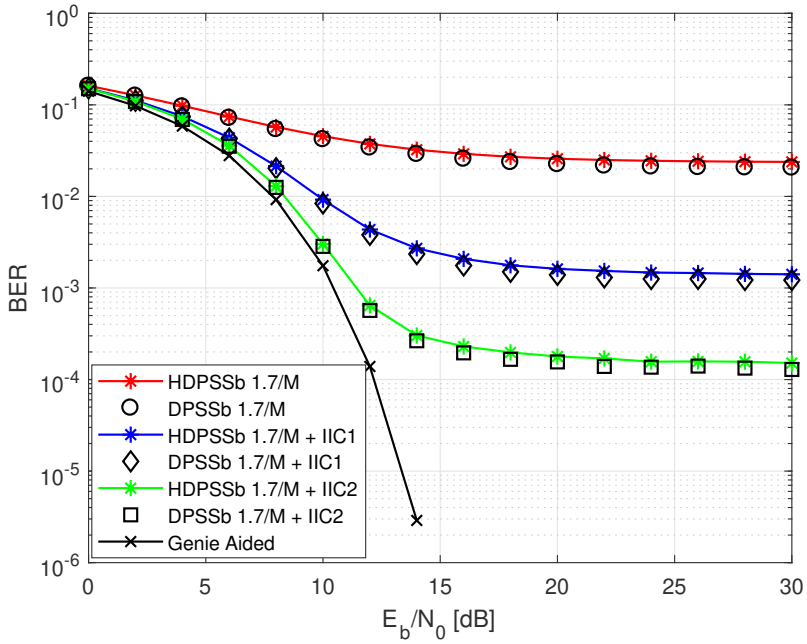

Figure 4.23: BER performance of QAM-FBMC system with 16QAM modulation with DPSSb 1.7/M filter and HQAM-FBMC with HDPSSb 1.7/M filter over AWGN channel.

to improve the overall system performance. Once again, for each IIC iteration both systems achieve the same results.

We have also evaluated and compared the system performance over pedestrian channel. The results were obtained by using several instantaneous channel realizations. In Figure 4.24, Figure 4.25 and 4.26 we compare the performance of QAM-FBMC and HQAM-FBMC using the optimized filter with bandwidth $B = 1.7/M$, 4-QAM, 16-QAM and 64-QAM modulations respectively. Comparing the results, for 4-QAM they are almost the same for HQAM-FBMC and QAM-FBMC. In the case of 16-QAM, the results of HQAM-FBMC match perfectly with those of QAM-FBMC, even considering the IIC procedure.

The optimized filter with bandwidth $3/M$ was also evaluated over pedestrian channel with 4QAM, 16QAM, and 64QAM as presented in Figure 4.27, Figure 4.28 and Figure 4.29 respectively.

Once again, the results of QAM-FBMC with the optimized DPSSb filter are pretty much the same as the results of HQAM-FBMC using the optimized HDPSSb filter in the case of 4QAM modulation. Besides, for the case of 16-QAM and 64-QAM, the evaluated performances are exactly the same.

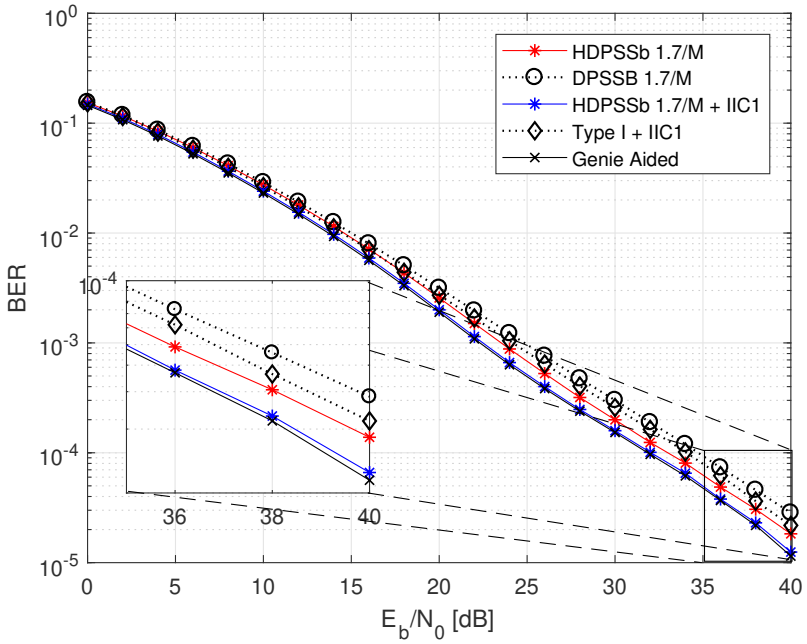

Figure 4.24: BER performance of QAM-FBMC system with 4QAM modulation with DPSSb 1.7/M filter and HQAM-FBMC with HDPSSb 1.7/M filter over pedestrian channel.

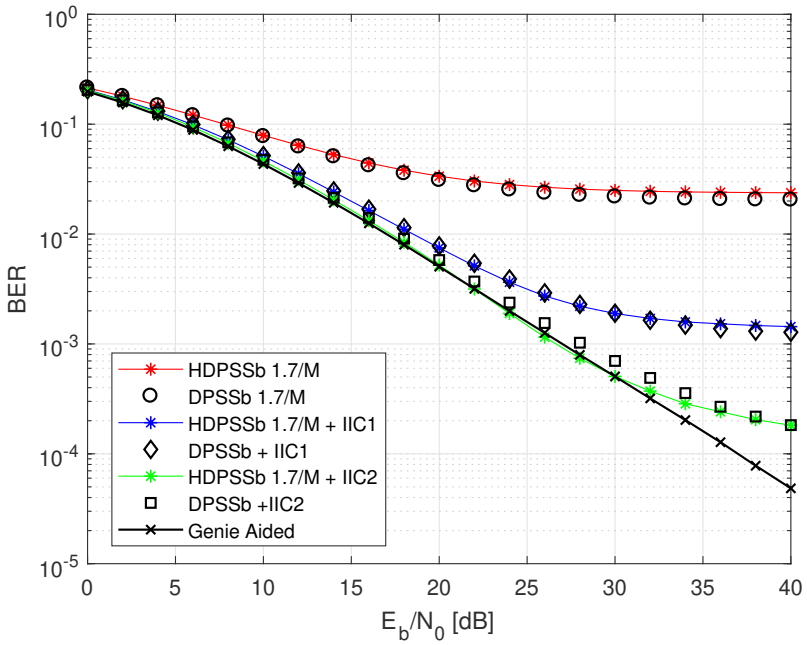

Figure 4.25: BER performance of QAM-FBMC system with 16QAM modulation with DPSSb 1.7/M filter and HQAM-FBMC with HDPSSb 1.7/M filter over pedestrian channel.

We have also analyzed the performance of HDPSSb $B = 7/M$ optimized filter for 4-QAM, 16-QAM, and 64-QAM modulations in Figure 4.30, Figure 4.31, and Figure 4.32 respectively. As we can notice, the performance is almost the same for HQAM-FBMC and QAM-FBMC.

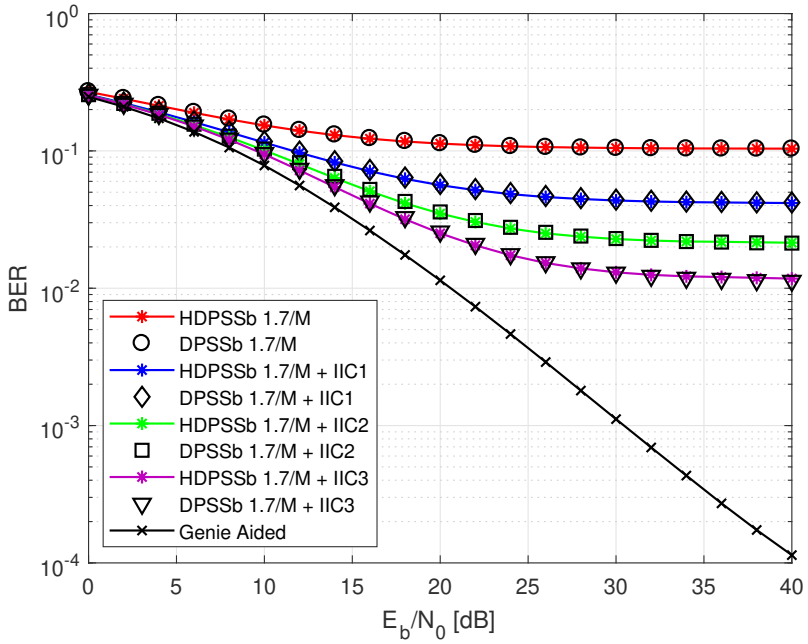

Figure 4.26: BER performance of QAM-FBMC system with 64QAM modulation with DPSSb 1.7/M filter and HQAM-FBMC with HDPSSb 1.7/M filter over pedestrian channel.

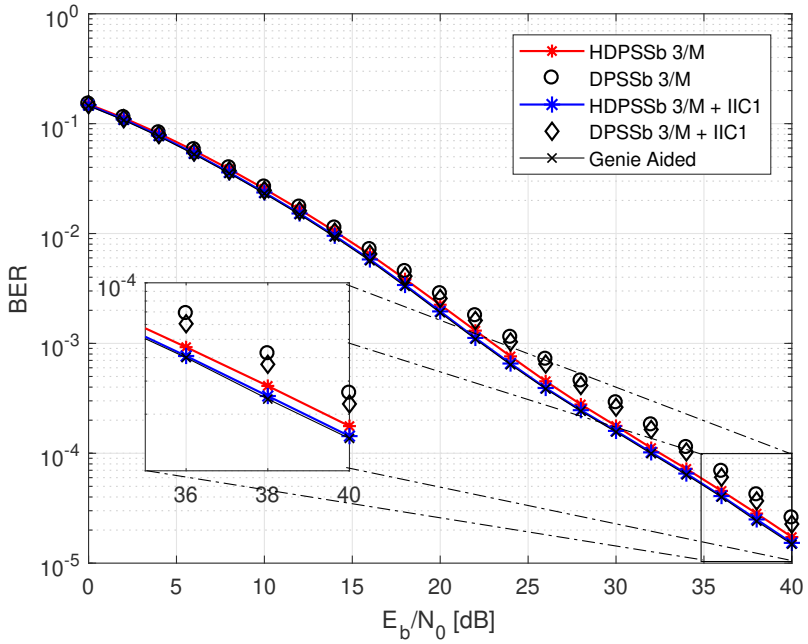

Figure 4.27: BER performance of QAM-FBMC system with 4QAM modulation with DPSSb 3/M filter and HQAM-FBMC with HDPSSb 3/M filter over pedestrian channel.

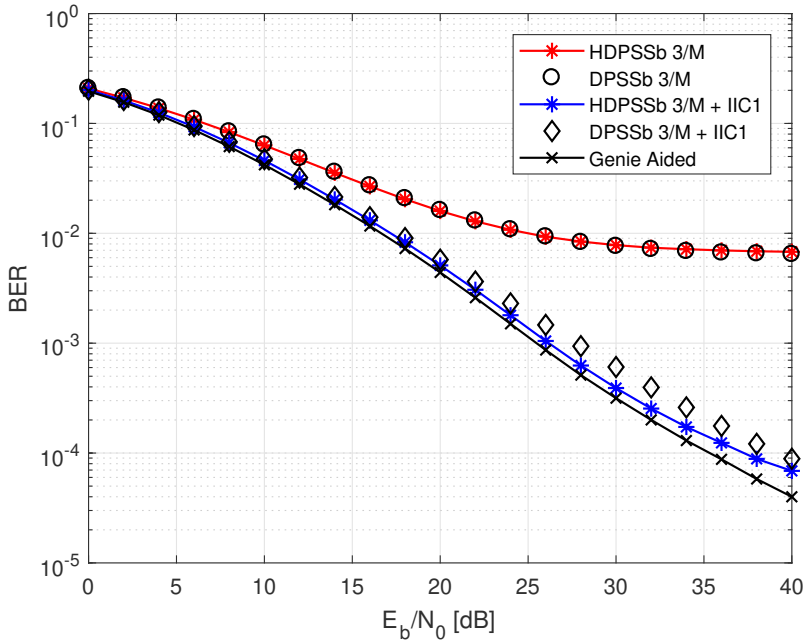

Figure 4.28: BER performance of QAM-FBMC system with 16QAM modulation with DPSSb $3/M$ filter and HQAM-FBMC with HDPSSb $3/M$ filter over pedestrian channel.

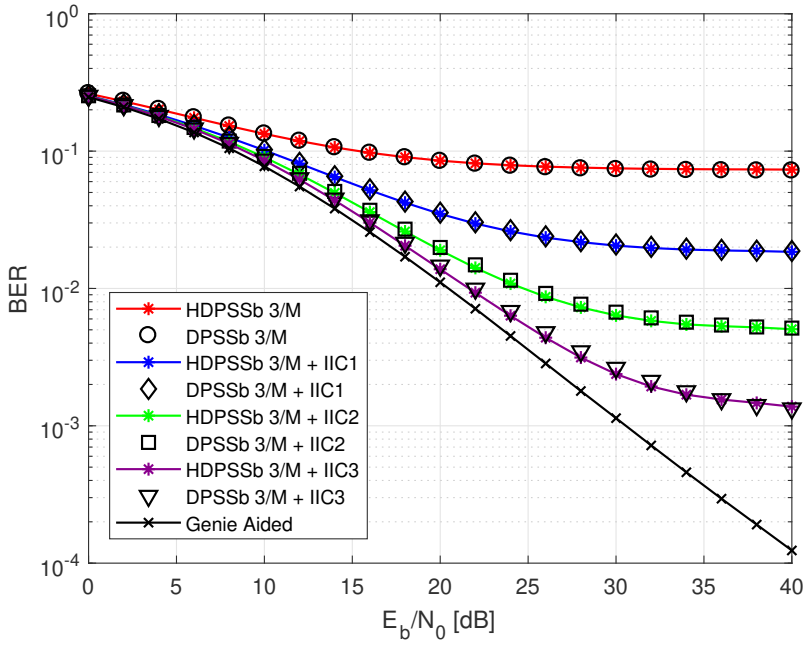

Figure 4.29: BER performance of QAM-FBMC system with 64QAM modulation with DPSSb $3/M$ filter and HQAM-FBMC with HDPSSb $3/M$ filter over pedestrian channel.

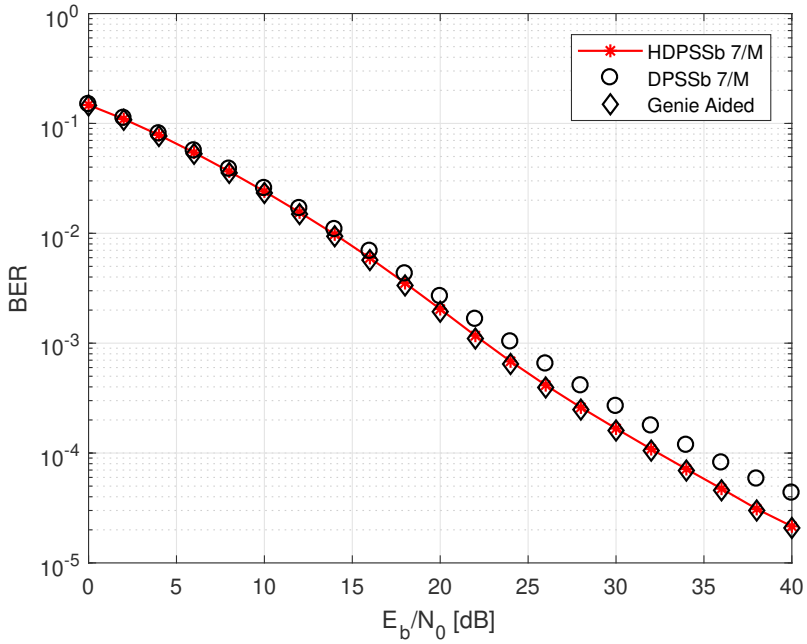

Figure 4.30: BER performance of QAM-FBMC system with 4QAM modulation with DPSSb $7/M$ filter and HQAM-FBMC with HDPSSb $7/M$ filter over pedestrian channel.

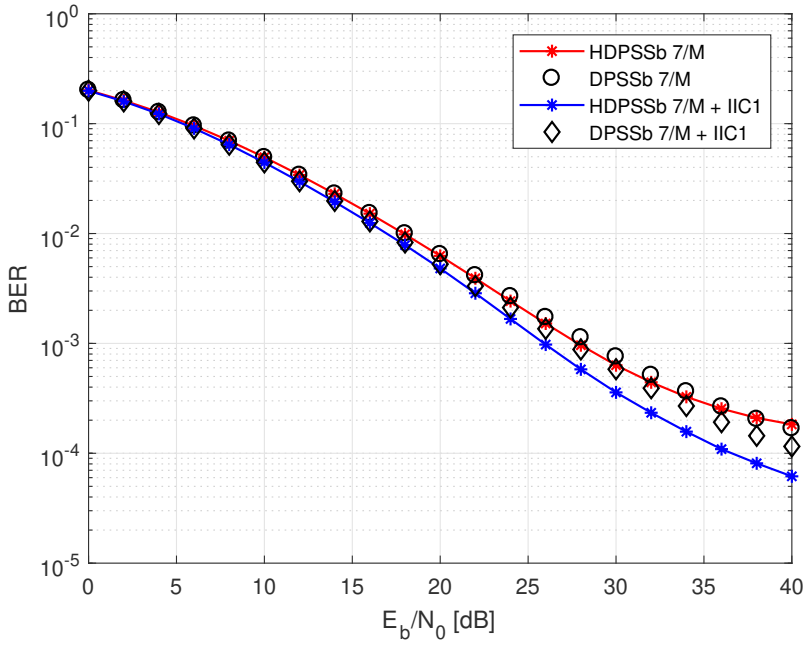

Figure 4.31: BER performance of QAM-FBMC system with 16QAM modulation with DPSSb $7/M$ filter and HQAM-FBMC with HDPSSb $7/M$ filter over pedestrian channel.

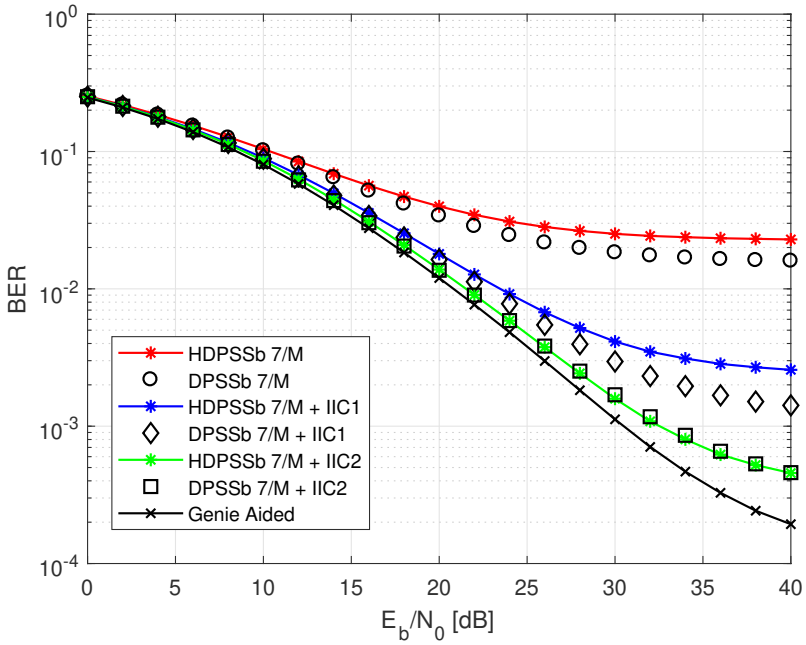

Figure 4.32: BER performance of QAM-FBMC system with 64QAM modulation with DPSSb 7/M filter and HQAM-FBMC with HDPSSb 7/M filter over pedestrian channel.

4.4 Bit error rate in QAM-FBMC

The choice of the prototype filter will directly impact the intrinsic interference of the system and consequently its bit error rate (BER). In this sense, several works have been done in order to evaluate the performance of multicarrier systems through their bit error probability (BEP). Closed form expressions have been provided for OFDM and OQAM-FBMC over AWGN channel [90] and over Rayleigh fading channel [91, 92]. However, to the best of our knowledge, the BEP analysis specifically for QAM-FBMC has not yet been investigated.

To evaluate the performance of the QAM-FBMC systems we propose in this section a mathematical expression of its BEP. We derive a BEP expression for QAM-FBMC system over AWGN channel taking into account the intrinsic interference generated due to non-orthogonality of the prototype filter. After that, we derive the BEP expression for QAM-FBMC over Rayleigh fading channel, by also considering the intrinsic interference generated by the prototype filter. The main contribution of this work lies in deriving a general expression of the BEP, which consider any modulation level, specifically for QAM-FBMC systems by considering AWGN and Rayleigh channels. Additionally, the expression of the BEP has been obtained using the intrinsic interference regardless the prototype filter choice.

4.4.1 Intrinsic interference probability

Let us recall the received symbol expression presented in (4.7)

$$\tilde{d}_{k,n} = d_{k,n} + \underbrace{\sum_{(k',n')\neq(k,n)} d_{k',n'} A_g(\Delta_n T, \Delta_k F)}_{\text{interference}} + v_{k,n}. \tag{4.27}$$

It is known, that the interference comes from the surrounding symbols for which the interference coefficients are not-null. By defining $\Upsilon_{k,n}$ as the set of (k', n') for which the interference coefficient is not-null, we can rewrite Equation (4.27) as

$$\tilde{d}_{k,n} = d_{k,n} + \underbrace{\sum_{(k',n')\in\Upsilon_{k,n}} d_{k',n'} A_g(\Delta_n T, \Delta_k F)}_{\text{interference}} + v_{k,n}. \tag{4.28}$$

Thus, the total interference over the k-th subcarrier at the n-th time instant, that comes from the surrounding symbols (k', n') presented in (4.8) can be simplified as

$$I_{k,n} = \sum_{(k',n')\in\Upsilon_{k,n}} d_{k',n'} \Gamma_{\Delta_k,\Delta_n}. \tag{4.29}$$

As we can see, the quantity of $\Gamma_{\Delta_k,\Delta_n}$ ponders the interference that comes from the surrounding symbols.

Let us now consider the transmission over a time invariant frequency selective channel $h(t)$ whose impulse response (the response at a time t to an impulse at zero) is given by ([112], Eq. (3.6))

$$h(t) = \sum_{i=0}^{L_h-1} h_i \delta\Big(t - \tau_i\Big), \tag{4.30}$$

where h_i is the channel path gain, and τ_{L_h-1} is the maximum delay spread of the channel. Thus, the continuous time received signal $r(t)$ is obtained convolving the baseband input signal $s(t)$ with the channel impulse response:

$$r(t) = h(t) \star s(t) + v(t), \tag{4.31}$$

where $\star$ represents the convolution operation. Hence we can modify (4.3) to represent the received signal as

$$\begin{aligned} r(t) &= \sum_{i=0}^{L_h-1} h_i \delta\left(t - \tau_i\right) \star s(t) + v(t) \\ &= \int_{-\infty}^{\infty} \sum_{i=0}^{L_h-1} h_i \delta\left(\tau - \tau_i\right) s(t-\tau) \mathrm{d}\tau + v(t) \qquad (4.32) \\ &= \sum_{i=0}^{L_h-1} h_i \int_{-\infty}^{\infty} \delta\left(\tau - \tau_i\right) s(t-\tau) \mathrm{d}\tau + v(t) \\ &= \sum_{i=0}^{L_h-1} h_i s(t - \tau_i) + v(t) \\ &= \sum_{i=0}^{L_h-1} h_i \sum_{n'} \sum_{k'=0}^{M-1} a_{k',n'} g\left(t - n'T - \tau_i\right) e^{j2\pi F k'(t-\tau_i)} + v(t). \qquad (4.33) \end{aligned}$$

Assuming that the bandwidth occupied by the filter is smaller than the coherence bandwidth of the channel, we can make the following approximation $g(t-n'T-\tau_i) \approx g(t-n'T)$. Consequently, Equation (4.33) becomes

$$\begin{aligned} r(t) &= \sum_{n'} \sum_{k'=0}^{M-1} d_{k',n'} g(t - n'T) e^{j2\pi F k' t} \sum_{i=0}^{L_h-1} h_i e^{-j2\pi k' \tau_i} + v(t) \\ &= \sum_{n'} \sum_{k'=0}^{M-1} d_{k',n'} g(t - n'T) e^{j2\pi F k' t} H_{k'} + v(t), \qquad (4.34) \end{aligned}$$

where $H_{k'} = \sum_{i=0}^{L_h-1} h_i e^{-j2\pi k' \tau_i}$.

The demodulated signal $y_{k,n}$ at the n-th symbol and k-th subcarrier is given by

$$\begin{aligned}
y_{k,n} &= \int_{-\infty}^{\infty} r(t) g^*(t - nT) e^{-j2\pi Fkt} dt \\
&= \int_{-\infty}^{\infty} \left(\sum_{n'} \sum_{k'=0}^{M-1} d_{k',n'} g(t - n'T) e^{j2\pi Fk't} H_{k'} + v(t) \right) g^*(t - nT) e^{-j2\pi Fkt} dt \\
&= \sum_{n'} \sum_{k'=0}^{M-1} H_{k'} d_{k',n'} \int_{-\infty}^{\infty} g(t - n'T) g^*(t - nT) e^{-j2\pi F(k-k')t} dt + v_{k,n} \\
&= H_k d_{k,n} + \underbrace{\sum_{(k',n') \neq (k,n)} H_{k'} d_{k',n'} A_g(\Delta_n T, \Delta_k F)}_{\text{interference}} + v_{k,n},
\end{aligned}$$

where $v_{k,n} = \int_{-\infty}^{\infty} v(t) g^*(t - nT) e^{-j2\pi Fkt} dt$.

By considering that the set $\Upsilon_{k,n}$ is in the coherence bandwidth of the channel (*i.e*, $H_{k'} \approx H_k \ \ \forall (k', n') \in \Upsilon_{k,n}$), $H_{k'}/H_k \ \ 1$. Thus, using H_k to perform the equalization, the demodulated signal is given by

$$\begin{aligned}
\tilde{d}_{k,n} &= y_{k,n}/H_k \\
&\cong d_{k,n} + \underbrace{\sum_{(k',n') \in \Upsilon_{k,n}} d_{k',n'} \Gamma_{\Delta_n, \Delta_k}}_{\text{interference}} + \frac{v_{k,n}}{H_k}.
\end{aligned} \tag{4.35}$$

Let us define the interference as the undesired received signal. In the absence of the channel, all the observed interference comes from the prototype filter properties. Considering a transmission of a unitary pulse at the subcarrier k', at block n', we can observe that at the receiver the energy spreads over neighbor subcarriers, which are in the set $\Upsilon_{k,n}$. This procedure gives us the interference coefficients ($\Gamma_{\Delta_k, \Delta_n}$), which clearly depend on the applied prototype filter.

The interference coefficients related to a given prototype filter are a keypoint to derive the BEP for QAM-FBMC systems. Once we know these coefficients, we can determine the overall interference as a sum of contributions induced by the neighbors into the subcarrier of interest weighted by the interference coefficients as presented in Equation (4.29). Considering the subcarrier of interest k, the real and imaginary operators $\Re$ and $\Im$ respectively, we can write the real part of the observed interference as

$$\Re\{I_{k,n}\} = \sum_{(k',n') \in \Upsilon_{k,n}} \Re\{d_{k',n'}\} \Re\{\Gamma_{\Delta_k, \Delta_n}\} - \sum_{(k',n') \in \Upsilon_{k,n}} \Im\{d_{k',n'}\} \Im\{\Gamma_{\Delta_k, \Delta_n}\}. \tag{4.36}$$

We opt for working with the real part of the interference presented in Equation

(4.36), however, it is possible to do a similar process by considering the imaginary part of the interference.

Let us define the cardinality of $\Upsilon_{k,n}$ as N. Thus, the interference can be numerically obtained by considering all possibilities of $\Re\{d_{k',n'}\}$ and $\Im\{d_{k',n'}\}$ with $(k', n') \in \Upsilon$ weighted by the intrinsic interference coefficients as in Equation (4.36).

For a 2^{2l}-QAM modulation, we have $2^{l(2N)}$ possible combinations for the real interference values, $i_r^{(l)}$, $r = 1, \ldots, 2^{l(2N)}$.

It is possible to deduce the exact discrete probability density function (PDF), $\mathrm{P}^{(l)}(\omega)$, of the interference generated by a 2^{2l}-QAM constellation from the interference values $i_r^{(l)}$ as follows:

$$\mathrm{P}^{(l)}(\omega) = \frac{1}{2^{l(2N)}} \sum_{r=1}^{2^{l(2N)}} \mathbb{1}(i_r^{(l)} = \omega), \tag{4.37}$$

where $\mathbb{1}(.)$ is the indicator function. When N is too high, we can work with an approximation of the interference. For doing this, instead of considering all the $2^{l(2N)}$ possible combinations that will generate the interference, we consider γ ($\gamma < 2^{l(2N)}$) different random combinations for the real interference $i_r^{(l)}$, and compute the approximate PDF, $\mathrm{P}_{\mathrm{apx}}^{(l)}(\omega)$ as

$$\mathrm{P}_{\mathrm{apx}}^{(l)}(\omega) = \frac{1}{\gamma} \sum_{r=1}^{\gamma} \mathbb{1}(i_r^{(l)} = \omega). \tag{4.38}$$

4.4.2 Bit Error probabilityv(BEP)

Based on the provided analysis of the interference, in this section we derive a closed form expression of the bit error probability (BEP) for QAM-FBMC systems over AWGN and Rayleigh flat fading channels.

AWGN channel

Assuming 2^{2l}-QAM modulation with Gray encoding and AWGN channel, the BEP can be expressed as function of the average bit energy to noise energy E_b/N_0 as follows [93]:

$$\mathrm{BEP}_{\mathrm{QAM}}^{\mathrm{AWGN}} = \frac{2^l - 1}{2^l l} \mathrm{erfc}\left(\sqrt{\frac{\varphi E_b}{N_0}}\right), \tag{4.39}$$

where

$$\varphi = \frac{3l}{2^{2l} - 1}. \tag{4.40}$$

Let us define $\mathrm{BEP}_{\mathrm{QAM}}^{\mathrm{AWGN}}(\omega)$ the BEP in presence of a given interference value ω.

So that we have

$$\mathrm{BEP}_{\mathrm{QAM}}^{\mathrm{AWGN}}(\omega) = \frac{2^l - 1}{2^l l}\mathrm{erfc}\left(\frac{\sqrt{\varphi E_b}\,(1-\omega)}{\sqrt{N_0}}\right). \tag{4.41}$$

Considering Ω as a set of all distinct possible values of the real interference ω, obtained as described in Section 4.4.1 and its approximated distribution $\mathrm{P}_{\mathrm{apx}}^{(l)}(\omega)$, the BEP over AWGN channel can be written as

$$\begin{aligned}\mathrm{BEP}_{\text{QAM-FBMC}}^{\mathrm{AWGN}} &= \sum_{\omega\in\Omega} \mathrm{P}_{\mathrm{apx}}^{(l)}(\omega)\mathrm{BEP}_{\mathrm{QAM}}^{\mathrm{AWGN}}(\omega) \\ &= \sum_{\omega\in\Omega} \mathrm{P}_{\mathrm{apx}}^{(l)}(\omega)\frac{2^l - 1}{2^l l}\mathrm{erfc}\left(\frac{\sqrt{\varphi E_b}\,(1-\omega)}{\sqrt{N_0}}\right).\end{aligned} \tag{4.42}$$

One can notice, the BEP of QAM-FBMC systems is directly related to the interference calculated in the previous section, which is associated with the prototype filter choice.

Rayleigh channel

In this section the QAM-FBMC system is analysed over Rayleigh flat fading channel and we propose an expression to calculate its BEP.

The transmitted signal is randomly attenuated by the channel coefficients, however, in the flat channel case we have only one tap h. Therefore, we can rewrite the BEP expression given in Equation (4.42) for a specific channel realization h and considering 2^{2l}-QAM modulation as

$$\mathrm{BEP}_h = \sum_{\omega\in\Omega} \mathrm{P}_{\mathrm{apx}}^{(l)}(\omega)\frac{2^l - 1}{2^l l}\mathrm{erfc}\left(|h|\frac{\sqrt{\varphi E_b}(1-\omega)}{\sqrt{N_0}}\right), \tag{4.43}$$

where $|.|$ represents the absolute value operation.

As we would like to find the BEP averaged over all possible random values of h, it is necessary to evaluate the conditional probability density function BEP_h over the PDF of $\eta = |h|\frac{\sqrt{\varphi E_b}}{\sqrt{N_0}}$. As $p(|h|)$ the PDF of $|h|$ is a Rayleigh distribution, the variable η is also Rayleigh distributed. Thus, its PDF for a given SNR is [93]:

$$p\left(\eta\right) = \frac{1}{\varphi E_b/N_0} e^{\frac{-\eta}{\varphi E_b/N_0}}. \tag{4.44}$$

Let us recall the classical expression of the BEP when $|h|$ is a Rayleigh distributed random variable and the modulation is 2^{2l}-QAM [93]

$$\begin{aligned}
\mathrm{BEP}^{\mathrm{RAY}} &= \int_0^{\infty} \frac{2^l-1}{2^l l}\mathrm{erfc}(\eta) p\left(\eta\right) \mathrm{d}\eta \\
&= \frac{2^l-1}{2^l l}\left(1-\sqrt{\frac{\varphi E_b/N_0}{\varphi E_b/N_0+1}}\right) \\
&= \frac{2^l-1}{2^l l}\left(1-\sqrt{\frac{\varphi E_b}{\varphi E_b+N_0}}\right).
\end{aligned} \tag{4.45}$$

Including all the distinct values of the intrinsic interference, ω, and its distribution, $\mathrm{P}_{\mathrm{apx}}^{(l)}(\omega)$, we can derive the $\mathrm{BEP}_{\text{QAM-FBMC}}^{\mathrm{RAY}}$ as follows:

$$\begin{aligned}
\mathrm{BEP}_{\text{QAM-FBMC}}^{\mathrm{RAY}} &= \int_0^{\infty} \mathrm{BEP}_h \; p\left(|h|\right) \mathrm{d}|h| \\
&= \int_0^{\infty} \sum_{\omega\in\Omega} \mathrm{P}_{\mathrm{apx}}^{(l)}(\omega) \frac{2^l-1}{2^l l}\mathrm{erfc}\left(|h|\frac{\sqrt{\varphi E_b}(1-\omega)}{\sqrt{N_0}}\right) p\left(\eta\right) \mathrm{d}\eta \\
&= \int_0^{\infty} \sum_{\omega\in\Omega} \mathrm{P}_{\mathrm{apx}}^{(l)}(\omega) \frac{2^l-1}{2^l l}\mathrm{erfc}\left(\eta(1-\omega)\right) p\left(\eta\right) \mathrm{d}\eta \\
&= \sum_{\omega\in\Omega} \mathrm{P}_{\mathrm{apx}}^{(l)}(\omega) \frac{2^l-1}{2^l l}\left(1-\frac{\sqrt{\varphi E_b}(1-\omega)}{\sqrt{\varphi E_b(1-\omega)^2+N_0}}\right).
\end{aligned} \tag{4.46}$$

The expression (4.46) is obtained from Equation (4.45) and Equation (4.43), replacing $\sqrt{E_b}$ by $\sqrt{E_b}(1-\omega)$, or equivalently E_b by $E_b(1-\omega)^2$.

4.4.3 Numerical evaluation

In this section we present numerical results for the analytical BEP expression that we have derived for QAM-FBMC systems. The analytical results, obtained by evaluating the intrinsic interference as function of the prototype filter, are compared to the one obtained by simulations through both AWGN and Rayleigh channels.

In Figure 4.33, we present the bit error rate obtained by simulation and using Equation (4.42) considering 4-QAM and 16-QAM modulations through AWGN channel. The number of subcarriers was $M = 128$, the parameter γ was set as 10^6 and the applied prototype filter was Case C, taken from [1], which has overlapping factor $K = 4$. As we can notice, the theoretical BEP matches perfectly the simulated results, which confirms the effectiveness of the proposed method.

We also evaluated the BEP over flat fading Rayleigh channel through the proposed Equation (4.46) considering 4-QAM modulation and using Case C prototype filter as presented in Figure 4.34. It is possible to verify the effectiveness of the proposed method since the theoretical and the simulated results are the same. In addition, we also present the theoretical and simulated results when using 16-

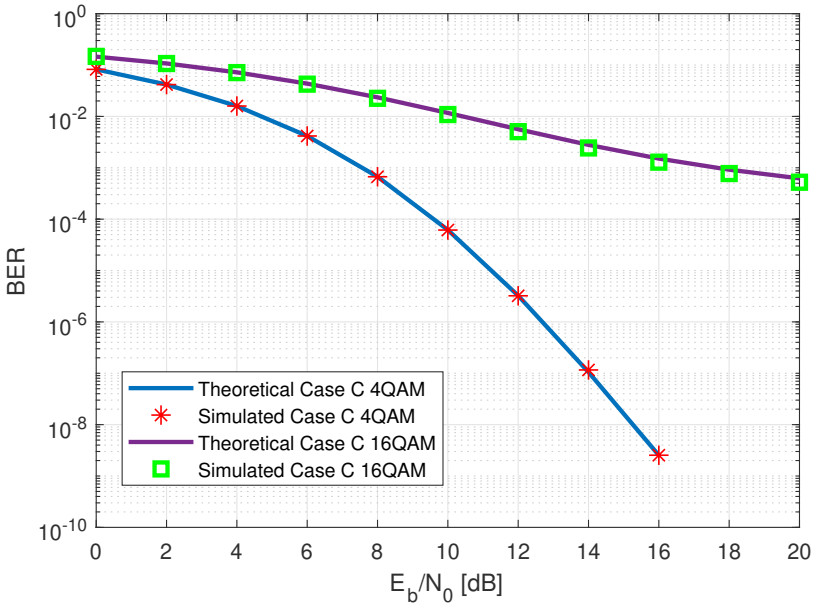

Figure 4.33: Simulated and theoretical Bit Error Probability of QAM-FBMC system when using Case C filter [1], 4QAM, and 16-QAM modulation under AWGN channel.

QAM modulation. Therefore, we can confirm the suitability of the proposed method through different modulation levels.

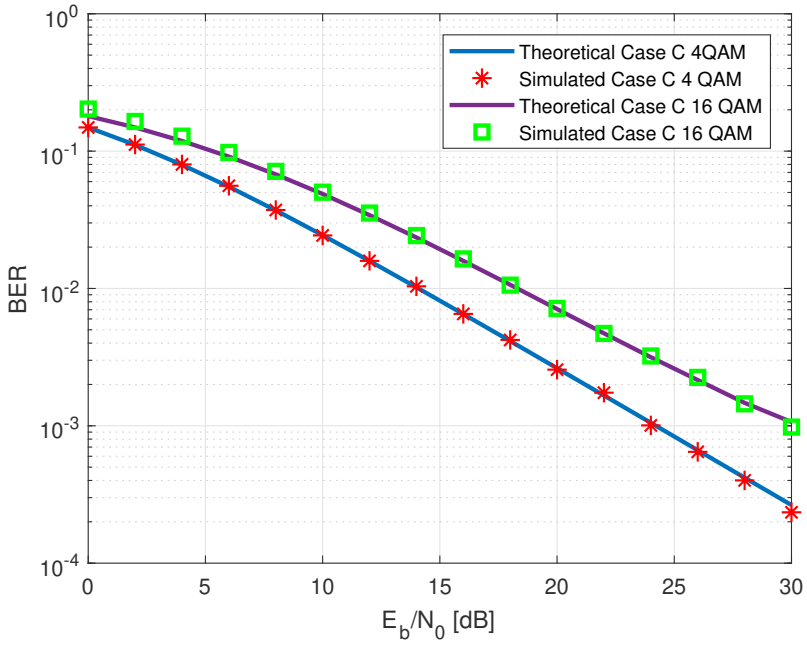

Figure 4.34: Simulated and theoretical Bit Error Probability of QAM-FBMC system when using Case C filter [1], 4-QAM, and 16-QAM modulation under Rayleigh channel.

For the sake of comparison, we also evaluated the proposed method over Pedestrian and Vehicular-A channels, defined by 3GPP [113], with very good agreement

between the results of our method and simulations, as also evidenced in Figure 4.35.

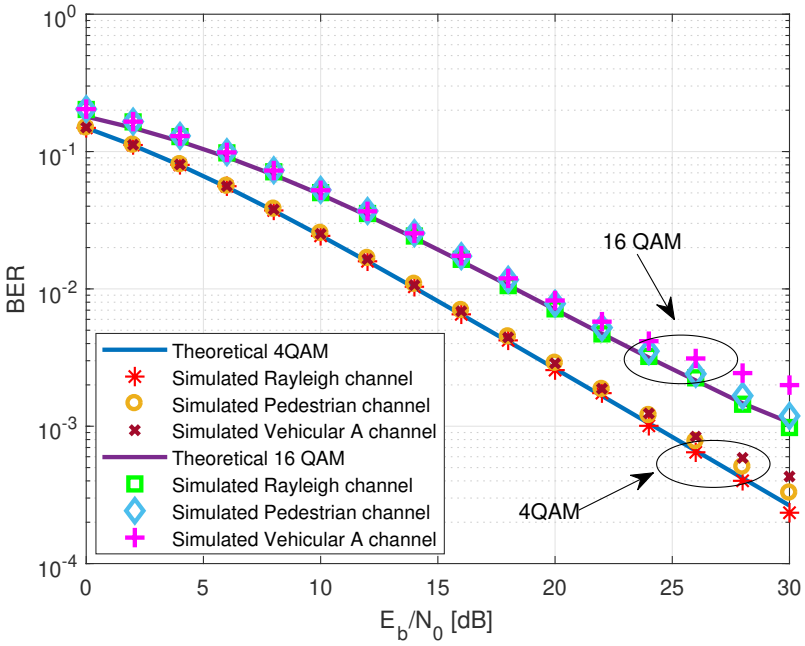

Figure 4.35: Simulated and theoretical Bit Error Probability of QAM-FBMC system when using Case C filter [1], 4-QAM and 16-QAM modulation under Rayleigh channel, pedestrian channel and Vehicular A channel.

As expected, for the poor frequency selective channels, the proposed method is still applicable. This fact can be explained thanks to the coherence band of the channel, that comprises the neighbor subcarriers for which the interference coefficients are not-zero. However for the strong frequency selective channels, such as Vehicular A, this hypothesis is no more true. That is why the curves does not match perfectly, although they are very close.

4.5 Chapter conclusions

In this chapter, we propose a novel method for prototype filter designed specifically for QAM-FBMC systems which is based on discrete prolate spheroidal sequences, DPSS. We consider the spectral confinement through the band-time parameter of DPSS and minimize the intrinsic interference coefficients of QAM-FBMC system. As a result, the obtained filters achieve smaller ISI than the competitors found in literature. Furthermore, our proposed design shows to be flexible considering their adjustable parameters as passband width, overlapping factor, and filter length.

The proposed DPSSb filter's performances were evaluated through the BER of the system and compared to the know filters performances such as Case C and Type

I. Besides, we consider different modulation levels, AWGN channel and pedestrian channel. For all the considered scenario the DPSSb optimized filters show high interference attenuation and, as expected, significantly improve the BER performance. In addition, since the bandwidth of the desired filter is adjustable through the DPSS parameters, the proposed procedure shows to be flexible in terms of spectrum confinement.

We have also proposed and analyze a novel structure of QAM-FBMC systems based on a hexagonal lattice (HQAM-FBMC). Differently from the works found in the literature, where Gaussian filters are used, we applied a prototype filter specifically designed considering the hexagonal lattice. We proposed a prototype filter design based on DPSS, which leads to the filters named HDPSSb prototype filters. The proposed filters were also optimized to reduce intrinsic interference in HQAM-FBMC.

Moreover, we have also analyzed the gain of using hexagonal lattice in QAM-FBMC systems. Comparing the simulation results of the performances of QAM-FBMC system using its optimized filters (DPSSb) with the performance of HQAM-FBMC, also using its optimized filters (HDPSSb), we can notice that, in terms of BER, there is no significant enhancement. Both systems, when using their optimized filters, present the same results.

We also analyze the intrinsic interference distribution of the system and derive an expression for the bit error probability of QAM-FBMC systems over both AWGN and Rayleigh flat fading channels. We present the intrinsic interference of the system related to the applied prototype filter, which is used to derive the BEP expression in the presence of a channel. The proposed expressions agree with simulated results, which confirms the applicability of the proposed method regardless the applied prototype filter.

Even though the proposed method assumes weak frequency selectivity, simulation results confirmed its suitability for predicting BEP for 3GPP Pedestrian and Vehicular channels. Thus, by applying our proposed method, now it is possible to predict the system performance, which allows us to enhance the QAM-FBMC system at the design stage. Hence, we certify that this method is an important tool for the QAM-FBMC design.

Chapter 5

QAM-FBMC modulation with short filters

USUALLY the FBMC systems implementation uses prototype filters with a duration higher than the FBMC symbol, *e.g*, overlapping factor $K = 4$, which leads to a filter 4 times higher than the FBMC symbol duration. Meantime, it is worth notice that different overlapping factors can also be considered. Actually, the usage of low overlapping factor *e.g.* $K = 1$, can be significantly advantageous.

Recently, the authors of [48] analyzed the applicability of short filters (K=1) to FBMC systems and also provide a prototype filter designed for OQAM-FBMC. Indeed, short filters enables particularities to support short frame sizes for low latency communications, reduce the transmitter power consumption, and reduce the computational complexity, since the polyphase network implementation highly depends on the prototype filter length.

In light of the advantages brought by short filters, in this chapter, we not only present the well-known short prototype filters found in the literature, but we also present a new short prototype filter design for beyond 5G systems. We present a waveform design for QAM-FBMC systems that applies one prototype filter, considering the total interference reduction while keeping spectral confinement, represented by the OOBE limitation. As we focus on the low latency, necessary for 5G systems, differently from the previously approach, the overlapping factor enforced for short filters was $K = 1$, which leads to a filter with the same duration as the QAM-FBMC symbol. We formulated two approaches: with and without the channel knowledge and minimized the total interference, subject to the OOBE constraint.

As the prototype filter choice directly impacts the intrinsic interference and consequently the BER of the system, similarly to what we have done in Chapter 4, in this chapter we analyze the intrinsic interference of the system and evaluate the bit error probability by using the equations presented in Chapter 4.

However, as QAM-FBMC cannot completely satisfy the orthogonality condition,

a residual interference is still observed and degrades system performance. Therefore, more elaborated receiver is needed. In [43] the authors proposed an MMSE receiver specifically for the QAM-FBMC system which uses $K+1$ symbols to detect the symbol of interest. However, their proposal consider a system with long filters (overlapping factor $K=4$). To the best of our knowledge, there is no specific work considering the design of QAM-FBMC receivers with short filters.

Knowing the needs of QAM-FBMC systems, we design different receivers for QAM-FBMC systems that applies short prototype filters. We propose a receiver that performs equalization before the analysis filter-bank (time domain equalizer - TDE) and compare it to the well known (frequency domain equalizer - FDE), which performs channel equalization after the analysis filter-bank. We also include iterative interference cancellation (IIC) scheme [40] to the receiver and evaluate the overall system performance. Furthermore, we propose a new receiver based on MMSE including inter-block interference (IBI) cancellation. In addition, we compare the performance of the proposed receivers with the state of the art in the presence of fading channels. Likewise, we extend the proposed MMSE receiver for the case of two users.

5.1 QAM-FBMC system model

Let us recall the discrete-time representation of the baseband transmitted QAM-FBMC signal presented in Chapter 4

$$s[m] = \sum_{k'=0}^{M-1} \sum_{n'} d_{k',n'} g\left[m - n'M\right] e^{j\frac{2\pi}{M}k'm}, \tag{5.1}$$

where $d_{k',n'}$ are complex symbols from a 2^{2l}-QAM constellation with average energy E_s, and $2l$ is the number of bits per symbol, allocated on the k'-th subcarrier and sent in the n-th QAM-FBMC symbol. $g[m]$ is the real valued prototype filter with length $L_g = KM$, where M is the number of subcarriers and K is the overlapping factor. As we consider the overlapping factor $K=1$, we will use $L_g = M$ for the rest of this chapter. The simplified system block representation is presented in Figure 5.1.

Considering just a pulse transmitted at the subcarrier k' and assuming an ideal channel, the demodulated symbol, received at the subcarrier k at the receiver side can be described as

$$\hat{d}_k = \boldsymbol{r}\mathbf{G}_k\mathbf{E}^{k'}\boldsymbol{g}, \tag{5.2}$$

where $\boldsymbol{g} \in \mathbb{R}^{L_g \times 1}$ is the transmitter short prototype filter impulse response, and $\mathbf{E} \in \mathbb{C}^{L_g \times L_g}$ is a diagonal matrix responsible for shifting the prototype filter to the

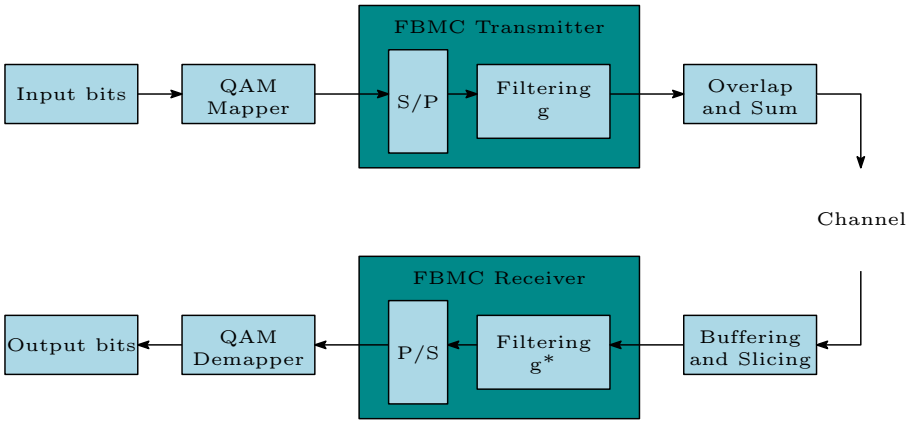

Figure 5.1: QAM-FBMC transceiver structure.

subcarrier k'. The matrix $\mathbf{E}$ can be defined by $\mathbf{E} = \text{diag}\left(1 \quad e^{j\frac{2\pi}{M}} \quad \dots \quad e^{j\frac{2\pi}{M}(L_g-1)}\right)$. $\boldsymbol{r} = \begin{bmatrix}0 & \dots & 0 & 1 & 0 & \dots & 0\end{bmatrix} \in \mathbb{R}^{1\times 2Lg-1}$ consists in a vector of zeros with just one element at the position L_g, and represents the downsampling operation. The matrix $\mathbf{G}_k \in \mathbb{C}^{(2L_g-1\times L_g)}$ is a Toeplitz matrix that multiplied by the received signal represents the convolution between the received signal and the receiver filter at the subcarrier k as a matrix multiplication. The relation between the transmitter filter and the receiver filter can be described as

$$g_{\text{RX}}[m] = g^*_{\text{TX}}[(L_g - 1) - m], \tag{5.3}$$

where * denotes the conjugate operation.

Let us define $\bar{\boldsymbol{g}}$ as

$$\bar{\boldsymbol{g}} = \left[\left(\mathbf{E}^k \boldsymbol{g}\right)^{\text{H}} \mathbf{0}_{(1\times L_g-1)}\right]^{\text{T}}, \tag{5.4}$$

where $\mathbf{E}^k\boldsymbol{g}$ represents the receiver filter at the subcarrier k.

So, we can express the $\mathbf{G}_k$ matrix as function of $\bar{\boldsymbol{g}}$ in the following manner

$$\mathbf{G}_k = [\bar{\boldsymbol{g}}_0 \quad \bar{\boldsymbol{g}}_1 \quad \dots \quad \bar{\boldsymbol{g}}_{L_g-1}], \tag{5.5}$$

where $\bar{\boldsymbol{g}}_m$ are the m-th cyclic shift versions of $\bar{\boldsymbol{g}}$ of dimension $(2Lg-1)\times 1$.

5.2 Protype filter

The QAM-FBMC system considered in this work is based on one low-pass prototype filter which is exponentially modulated to generate the other filters of the filterbank. Differently from the OQAM-FBMC, in QAM-FBMC there is no orthogonality to be kept, which means that there is no PR constraint to obey. However, low interference is still necessary at the receiver in order to recover the transmitted signal.

Based on this, we propose a filter design technique that addresses the time/frequency localization problem as an optimization problem. Aiming to obtain the smallest interference as possible for a given limit of the OOBE level, the proposed technique provides flexibility to control these parameters, essential for filter design.

After briefly presenting possible solutions of short filters found in literature, we will present a novel short prototype filter design specifically developed to meet the needs of QAM-FBMC systems. In our proposal, the interference can be minimized restrict to the OOBE radiation. A performance comparison confirms that the proposed filter outperforms the existing ones.

5.2.1 Near to perfect reconstruction filter - NPR1

Although the NPR1 (described in Subsection 3.4.2) was essentially developed to attempt the OQAM-FBMC characteristics, we have also analyzed its applicability to the QAM-FBMC systems.

5.2.2 Hamming window

Hamming is a commonly used window defined by the following expression [61]

$$g[m] = 0.54 - 0.46\cos\left(2\pi\frac{m}{L_g}\right), \quad m \in \quad 0, \dots L_g \tag{5.6}$$

The main advantage of Hamming window is that its transition bandwidth is larger than the rectangular one. Furthermore, the ratio between the main lobe and the secondary one is much larger when compared to rectangular filter, and its OOBE is also smaller than that for rectangular filter.

5.2.3 Gaussian filter

Gaussian pulse shape filters are interesting, since its frequency response is also a Gaussian function. The analytical expression of its impulse response can be defined as [52]

$$g[m] = \frac{\sqrt{\pi}}{\rho} e^{-\left(\frac{\pi}{\rho} m\right)^2}, \tag{5.7}$$

where the relation between the time and frequency localization is determined by the coefficient ρ.

The parameter ρ is determined by the Bandwidth-Time (BT) product, where B is the -3dB bandwidth of the baseband Gaussian filter, and T is the symbol

duration. In that manner ρ can be defined as

$$\rho = \frac{1}{BT}\sqrt{\frac{ln(2)}{2}}. \tag{5.8}$$

As ρ increases, the spectral occupancy of the Gaussian filter decreases, and the impulse response spreads in the time domain, leading to increased ISI at the receiver. On the other hand, as ρ decreases, the frequency response spreads over adjacent subcarriers causing inter carrier interference (ICI). Figure 5.2 exemplifies the effect of changing ρ in the resulting impulse response of the obtained filters. The Gaussian filters impulse response is presented for different values of ρ. Here it is possible to identify the effects of changing ρ in time domain.

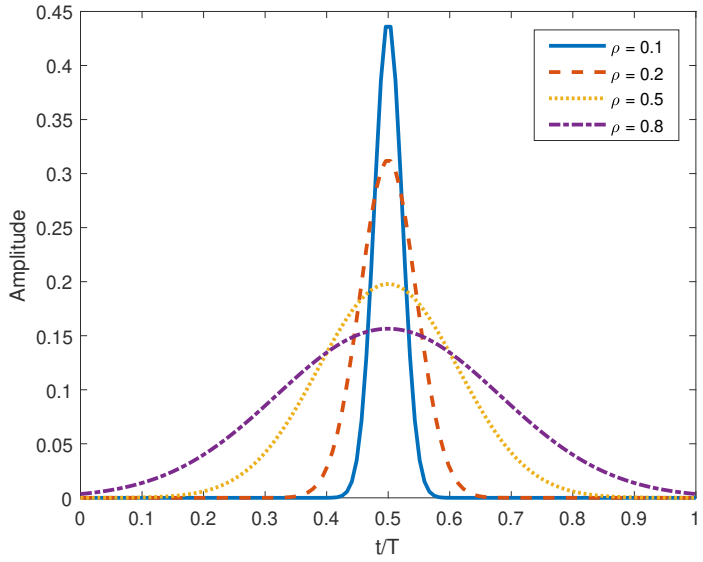

Figure 5.2: Impulse response of the Gaussian filter for different ρ.

The impulse response of the Gaussian filter leads us to a transfer function $G[f]$ which is strongly dependent upon ρ. These transfer functions are given by [52]

$$G[f] = e^{-\rho^2 f^2}. \tag{5.9}$$

Although its good time/frequency characteristics, the Gaussian filter has no zero crossing, therefore it does not satisfy the Nyquist criterion, then it introduces interference in the system. We also have approximations in the design of Gaussian filters that might introduce extra interference. It is worth to notice that in order to have a finite-time (FIR) representation of a Gaussian filter, it is necessary to truncate the theoretically infinite response of the ideal Gaussian filter, which causes high side lobes in frequency and consequently aliasing.

5.2.4 A novel short prototype filter design

In this Section we present a novel short prototype filter design specially developed for QAM-FBMC systems. Also working from an optimization point of view, we propose to minimize the total interference at the receiver subject to OOBE limitation.

With this purpose, we describe the OOBE through an expression and set a threshold for its acceptable value. We also define the total interference in two situations, with and without channel, and minimize two different objective functions as follows.

Out-of-band energy - OOBE

In this section we present the OOBE expression in a classical approach. The function that describes the total energy of the desired lowpass prototype filter is [61]

$$E = \int_{-0.5}^{0.5} |G(f)|^2 \mathrm{d}f, \tag{5.10}$$

where $G(f)$ is the frequency response of the prototype filter. It is also worth noticing that the filter is normalized such that $E = 1$. As the OOBE parameter is useful to quantify the spectrum confinement, we set Ω_p as the passband frequency edge, so that we define the OOBE function as

$$\mathrm{OOBE} = 2 \int_{\Omega_p}^{0.5} |G(f)|^2 \mathrm{d}f. \tag{5.11}$$

Defining $\boldsymbol{g} \in \mathbb{R}^{L_g \times 1}$ as the desired prototype filter coefficient vector, we can also rewrite the OOBE defined in Equation (5.11), in matrix form, as [114]

$$\mathrm{OOBE} = \quad \boldsymbol{g}^{\mathrm{H}} \mathbf{Q} \boldsymbol{g}, \tag{5.12}$$

where $\mathbf{Q} \in \mathbb{R}^{(L_g \times L_g)}$ is a symmetric and positive-definite matrix represented in (3.24).

Intrinsic interference

By sending a pulse, with unitary amplitude, at subcarrier k', and observing the received information at subcarrier k, for $k' \neq k$, and $\Delta_k = k - k'$, similarly to described in (5.2), we can obtain the interference coefficients $\mathit{\Gamma}_{\Delta_k}$ defined by

$$\mathit{\Gamma}_{\Delta_k} = \boldsymbol{r} \mathbf{G}_k \mathbf{E}^{k'} \boldsymbol{g}. \tag{5.13}$$

As we can notice, the expression of the interference coefficients $\mathit{\Gamma}_{\Delta_k}$ is exactly the same as in (5.2), except for the fact that the transmitter and receiver subcarriers

are not the same $k' \neq k$.

These coefficients, obtained from each pair k' and k, represent the interference coefficient vector, and strongly depends on the used prototype filter.

Similarly to the derivations given in [39] and using the definition given in Equation (5.13), the power of the interference can be obtained by

$$\begin{aligned}
E_I &= \sum_{k' \neq k} |\Gamma_{\Delta_k}|^2 \\
&= \left(\sum_{k' \neq k} \boldsymbol{r}\mathbf{G}_k\mathbf{E}^{k'}\boldsymbol{g} \right)^{\mathrm{H}} \left(\sum_{k' \neq k} \boldsymbol{r}\mathbf{G}_k\mathbf{E}^{k'}\boldsymbol{g} \right) \\
&= \sum_{k' \neq k} \left(\boldsymbol{g}^{\mathrm{H}}\mathbf{E}^{-k'}\mathbf{G}_k^{\mathrm{H}}\boldsymbol{r}^{\mathrm{H}} \right) \left(\boldsymbol{r}\mathbf{G}_k\mathbf{E}^{k'}\boldsymbol{g} \right) \\
&= \sum_{k' \neq k} \boldsymbol{g}^{\mathrm{H}} \left(\mathbf{E}^{-k'}\mathbf{G}_k^{\mathrm{H}}\boldsymbol{r}^{\mathrm{H}}\boldsymbol{r}\mathbf{G}_k\mathbf{E}^{k'} \right) \boldsymbol{g} \\
&= \boldsymbol{g}^{\mathrm{H}} \Bigg(\underbrace{\sum_{k' \neq k} \mathbf{E}^{-k'}\mathbf{G}_k^{\mathrm{H}}\boldsymbol{r}^{\mathrm{H}}\boldsymbol{r}\mathbf{G}_k\mathbf{E}^{k'}}_{\mathbf{Q}_1} \Bigg) \boldsymbol{g} \\
&= \boldsymbol{g}^{\mathrm{H}}\mathbf{Q}_1\boldsymbol{g}.
\end{aligned} \tag{5.14}$$

Interference in the presence of a channel

To calculate the overall system interference, we reformulate the approach previously used including the channel effects. Assuming that the channel length is $L_h \leq L_g$, and as we define the overlapping factor $K = 1$, and considering just a pulse transmitted at the subcarrier k', the coefficients Γ_{Δ_k} described in Equation (5.13) should be modified to also represent the inter-block interference (IBI). It becomes a vector of two interference coefficients (2×1), and the downsample operation is performed by a matrix $\boldsymbol{R}_{\Delta_k}$.

We define the toeplitz channel matrix $\mathbf{H} \in \mathbb{R}^{(L_g+L_h-1)\times L_g}$ as

$$\mathbf{H} = \left[\mathbf{h}_0 \quad \mathbf{h}_1 \quad \ldots \quad \mathbf{h}_{Lg-1} \right], \tag{5.15}$$

where $\mathbf{h}_m$ are cyclic shifted versions of dimension $L_g + L_h - 1$ of the impulse channel response $\mathbf{h}$.

Analogously to Equation (5.13), the interference coefficients can then be rewritten as

$$\boldsymbol{\Gamma}_{\Delta_k} = \boldsymbol{R}_{\Delta_k}\mathbf{G}'_k\mathbf{H}\mathbf{E}^{k'}\boldsymbol{g}, \tag{5.16}$$

where $\mathbf{G}'_k$ of dimension $(2L_g + L_h - 2 \times L_g + L_H - 1)$ is constructed from (5.5) by

adapting the Equation (5.4) as

$$\bar{\boldsymbol{g}} = \left[\left(\mathbf{E}^{k'} \tilde{\boldsymbol{g}} \right)^{\mathrm{T}} \mathbf{0}_{(1 \times L_g + L_h - 2)} \right]^{\mathrm{T}}. \tag{5.17}$$

Knowing that the total interference depends on the not-zero coefficients $\boldsymbol{\Gamma}_{\Delta_k}$, around the considered transmission position k', we also redefine the downsampling operation by setting the matrix $\boldsymbol{R}_{\Delta_k}, \in \mathbb{R}^{2 \times 2L_g + L_h - 1}$ as

$$\boldsymbol{R}_{\Delta_k} = \begin{cases} \begin{bmatrix} 0 \ \ldots \ 1 \ \ldots \ 0 \ \ldots \ 0 \\ 0 \ \ldots \ 0 \ \ldots \ 1 \ \ldots \ 0 \end{bmatrix}, & \text{if} \quad \Delta_k \neq 0 \\ \\ \begin{bmatrix} 0 \ \ldots \ 0 \ \ldots \ 0 \ \ldots \ 0 \\ 0 \ \ldots \ 0 \ \ldots \ 1 \ \ldots \ 0 \end{bmatrix}, & \text{if} \quad \Delta_k = 0, \end{cases} \tag{5.18}$$

where the not-null elements are at the positions $(1, L_g)$ and $(2, 2L_g)$, for $\Delta_k \neq 0$, and $(2, 2L_g)$, for $\Delta_k = 0$. In this case, even if $\Delta_k = 0$ we still observe the IBI.

Following the same reasoning, and considering the interference different for each subcarrier due to the channel, we can write the average power of the interference as

$$E_{Ic} = \boldsymbol{g}^{\mathrm{H}} \left(\frac{1}{M} \sum_{k',k} \mathbf{E}^{-k'} \mathbf{H}^{\mathrm{H}} \mathbf{G}_k'^{\mathrm{H}} \boldsymbol{R}_{\Delta_k}^{\mathrm{H}} \boldsymbol{R}_{\Delta_k} \mathbf{G}_k' \mathbf{H} \mathbf{E}^{k'} \right) \boldsymbol{g}. \tag{5.19}$$

By using Equation (5.19) and assuming that the power delay profile (PDP) of the channel is known, we can now determine the expected value of the interference as

$$\mathcal{E}\{E_{Ic}\} = \boldsymbol{g}^{\mathrm{H}} \mathcal{E} \left\{ \frac{1}{M} \sum_{k',k} \mathbf{E}^{-k'} \mathbf{H}^{\mathrm{H}} \mathbf{G}_k'^{\mathrm{H}} \boldsymbol{R}_{\Delta_k}^{\mathrm{H}} \boldsymbol{R}_{\Delta_k} \mathbf{G}_k' \mathbf{H} \mathbf{E}^{k'} \right\} \boldsymbol{g}. \tag{5.20}$$

Since the convolution is an associative and commutative operation, we can exchange the convolution with the channel and the reception filter. For doing this, it is necessary to adjust the matrix sizes, by increasing the number of zeros in $\mathbf{H}$. The obtained matrix is $\bar{\mathbf{H}}$, whose dimension is $(2L_g + L_h - 2 \times 2L_g - 1)$. Besides, we remove zeros from $\mathbf{G}_k$ which gives us $\bar{\mathbf{G}}_k \in \mathbb{R}^{(2L_g - 1) \times L_g}$. So that we have

$$\mathcal{E}\{E_{Ic}\} = \boldsymbol{g}^{\mathrm{H}} \frac{1}{M} \sum_{k',k} \mathbf{E}^{-k'} \bar{\mathbf{G}}_k^{\mathrm{H}} \mathcal{E} \left\{ \bar{\mathbf{H}}^{\mathrm{H}} \boldsymbol{R}_{\Delta_k}^{H} \boldsymbol{R}_{\Delta_k} \bar{\mathbf{H}} \right\} \bar{\mathbf{G}}_k \mathbf{E}^{k'} \boldsymbol{g}. \tag{5.21}$$

Let the matrix $\mathbf{T}_{\Delta_k}$ be defined by

$$\mathbf{T}_{\Delta_k} = \mathcal{E} \left\{ \bar{\mathbf{H}}^{\mathrm{H}} \boldsymbol{R}_{\Delta_k}^{\mathrm{H}} \boldsymbol{R}_{\Delta_k} \bar{\mathbf{H}} \right\}, \tag{5.22}$$

by applying the expectation of the channel, and assuming that the taps are uncor-

related, we can notice that the matrix $\mathbf{T}_{\Delta_k}$ is sparse with a few elements in the diagonal.

Finally, we can rewrite the Equation (5.21) as

$$\begin{aligned}\mathcal{E}\{E_{Ic}\} &= \boldsymbol{g}^{\mathrm{H}} \underbrace{\left(\frac{1}{M} \sum_{k',k} \mathbf{E}^{-k'} \bar{\mathbf{G}}_k^{\mathrm{H}} \mathbf{T}_{\Delta_k} \bar{\mathbf{G}}_k \mathbf{E}^{k'} \right)}_{\mathbf{Q}_2} \boldsymbol{g} \\ &= \boldsymbol{g}^{\mathrm{H}} \mathbf{Q}_2 \boldsymbol{g}. \end{aligned} \tag{5.23}$$

Optimization problem formulation

In order to reduce the total interference as much as possible and keep the out-of-band energy smaller than a given threshold, we address the filter design procedure as an optimization problem. We propose an iterative procedure where we optimize the transmitter and receiver filters iteratively. In each iteration, we solve the following optimization problem subject to an inequality constraint.

This section describes two proposed objective functions. Given the description of the interference presented in Section 5.2.4 and setting θ as the maximum accepted value of OOBE, we define the filter design as an optimization problem described by

$$\begin{aligned} \text{Case} \quad \text{I}: \qquad & \min_{\boldsymbol{g}} \quad \boldsymbol{g}^{\mathrm{H}} \mathbf{Q}_1 \boldsymbol{g} \\ & \text{s.t.} \quad \boldsymbol{g}^{\mathrm{H}} \boldsymbol{g} = 1 \\ & \qquad \boldsymbol{g}^{\mathrm{H}} \mathbf{Q} \boldsymbol{g} \leq \theta \end{aligned} \tag{5.24}$$

whereby we minimize the observed interference neglecting the channel effects.

In a second approach, we also propose an optimization problem based on the total interference described in Section 5.2.4, considering the channel power delay profile

$$\begin{aligned} \text{Case} \quad \text{II}: \qquad & \min_{\boldsymbol{g}} \quad \boldsymbol{g}^{\mathrm{H}} \mathbf{Q}_2 \boldsymbol{g} \\ & \text{s.t.} \quad \boldsymbol{g}^{\mathrm{H}} \boldsymbol{g} = 1 \\ & \qquad \boldsymbol{g}^{\mathrm{H}} \mathbf{Q} \boldsymbol{g} \leq \theta \end{aligned} \tag{5.25}$$

For solving both optimization problems above, we use the IP method [62]. Our optimized prototype filter is denoted OPF when we optimize the problem described in Case I, and OPFC when we optimize the Case II.

The proposed procedure to find the best prototype filter for QAM-FBMC system consists of initializing a known filter at the receiver and finding a transmitter filter

that minimizes the cost function. Iteratively, we swap transmitter and receiver filters (convolution is commutative), according to the relation described in Equation (5.3), update the cost function and optimize again the transmitter filter until convergence. Algorithm (2) exemplifies the procedure adopted to solve the problem in Case I, which can also be used to solve Case II.

Algorithm 2 Prototype Filter Design

procedure FILTER DESIGN(M, QMF)
  $\boldsymbol{g}_r \leftarrow$ QMF, dif $\leftarrow \infty$, int $\leftarrow \infty$, $\epsilon \geq 10^{-7}$
  compute $\boldsymbol{g}$ according to Equation (5.3)
  while dif $\geq \epsilon$ **do**
    draw $\mathbf{Q}_1$ (or $\mathbf{Q}_2$)
    $\boldsymbol{g} \leftarrow$ solution of problem Case I (or Case II)
    interf $= \boldsymbol{g}^{\mathrm{H}}\mathbf{Q}_1\boldsymbol{g}$
    compute $\boldsymbol{g}$ according to Equation (5.3)
    dif $=$ int $-$ interf
    int $\leftarrow$ interf
  end while
  return $\boldsymbol{g}$
end procedure

5.2.5 Numerical evaluation

Numerical experiments were conducted in order to evaluate the proposed method. For the sake of comparison, we used the QMF filter, which applied to FBMC leads to a modulation known as Lapped-OFDM, as presented in [55]. We also compared our designed filters with Near Perfect Reconstruction 1 filter (NPR1), presented in [48], Gaussian filters [115] and with the Hamming window.

Firstly, we evaluate the applicability of Gaussian filters to the QAM-FBMC. Differently from the NPR1 or Hamming window, there is not just one Gaussian filter to be tested, since its design depends on ρ parameter. Thus, we have designed several different Gaussian filters, by varying ρ, and analyzed its particular characteristics. In Figure 5.3 we present the interference observed in a QAM-FBMC system with $M = 128$ subcarriers and 4-QAM modulation when applying each one of 1000 different Gaussian filters, with length $L_g = M$, designed by changing ρ. As we can notice, the interference observed at the receiver decreases when ρ increases. We also verify the OOBE behavior of those filters, and we notice an inverse relation between the interference and OOBE.

Besides, we picked up 6 different Gaussian filters, with different ρ, to analyze its frequency response as presented in Figure 5.4. As we can notice, by changing ρ, we change the OOBE and consequently the decay rate in the rejection region.

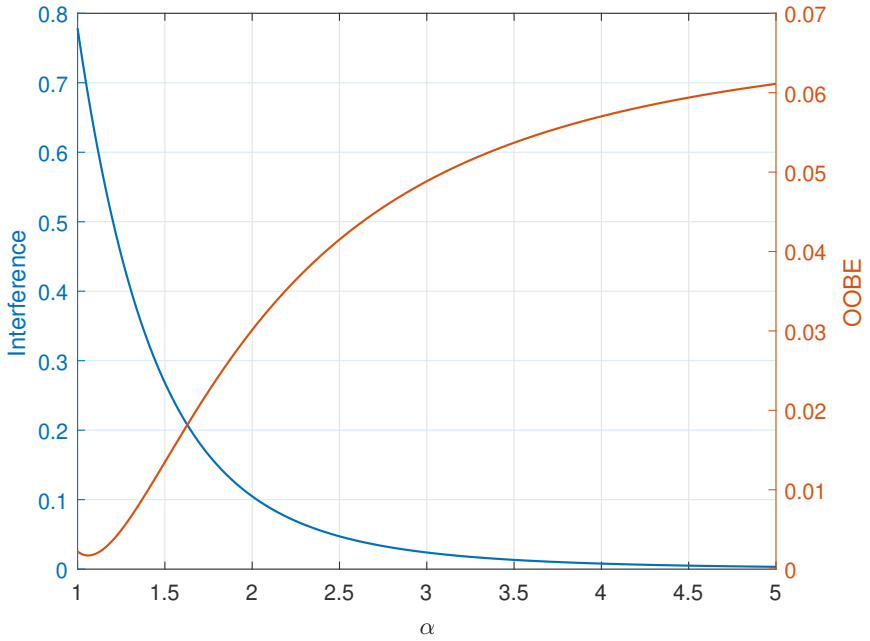

Figure 5.3: OOBE and interference evaluation as function of ρ.

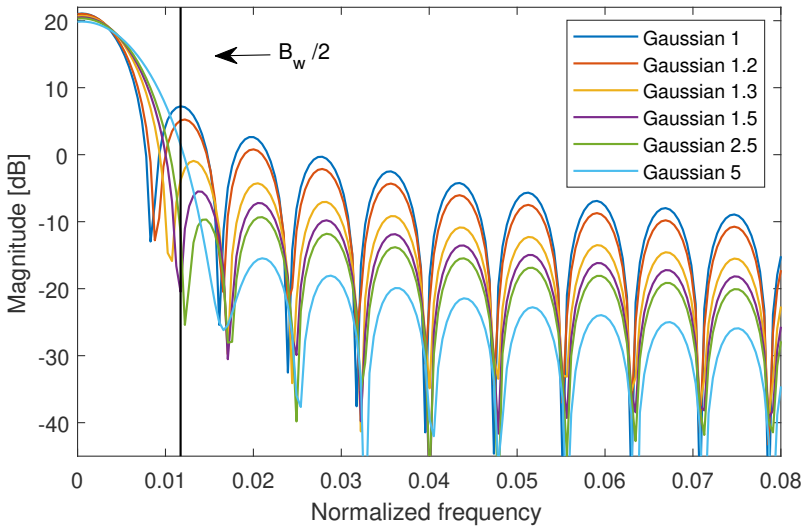

Figure 5.4: Frequency response of different Gaussian filters.

In the context of 4G/LTE standard, the 3GPP technical specification [113] defines the multipath fading channel model Extended Vehicular-A (EVA), whose power delay profile - PDP varies slowly [116], which was used in this work. We evaluated the effects of this channel on the average power of the total interference observed in the QAM-FBMC system and on the stopband energy. As, for each instantaneous channel realization, the interference is different, the presented results are the average for 1000 realizations. Moreover, we compared the bit error rate performance using different prototype filters.

The optimization procedure was applied to the problems defined by Case I and by Case II considering a QAM-FBMC system and LTE parameters with $M = 128$ subcarriers, 4-QAM modulation, overlapping factor $K = 1$ and filter length $L_g = M$.

Aiming to play a fair comparison with Hamming and NPR1, the OOBE constraint was defined in such a way that the optimized filters with and without channel information have the same OOBE as NPR1 (α), QMF (β) and Hamming (γ). As the Gaussian filter is also parameterizable, we designed a large set of Gaussian filters and picked up those with OOBE equal to α, β and γ, which correspond to the same OOBE as NPR, QMF and Hamming respectively: $\alpha = 8.2\ 10^{-3}$, $\beta = 5.1\ 10^{-3}$ and $\gamma = 2.7\ 10^{-3}$. We have also added OPF and OPFC filters with OOBE $= 4\ 10^{-3}$, $6\ 10^{-3}$ and $7\ 10^{-3}$.

In Figure 5.5, we present the average total interference power obtained by using 1000 different instantaneous channels (designed based on the 3GPP EVA model), and sending 200 symbols. As we can notice, in all cases the optimized filters proposed outperform the NPR1, QMF Gaussian and Hamming filters in terms of total interference. The designed prototype filters presented in this work are available online at [63].

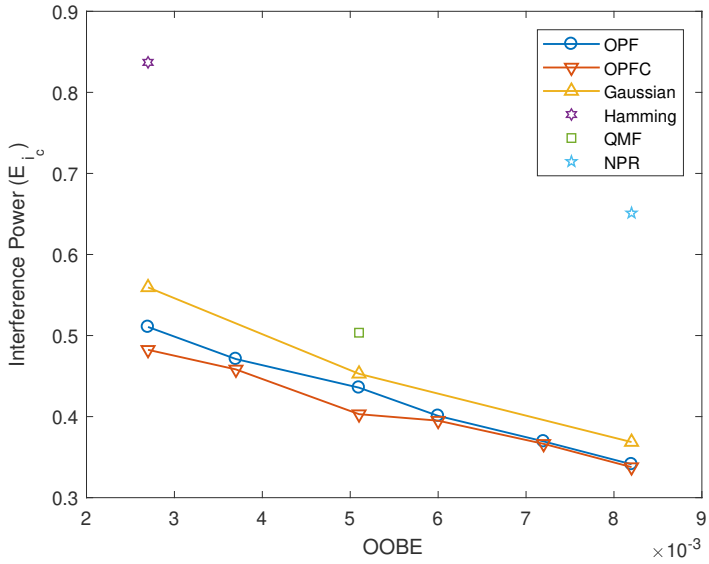

Figure 5.5: Average interference power,E_{Ic}, in QAM-FBMC system and OOBE of the OPF, OPFC, NPR, QMF, Gaussian and Hamming filters.

In Figure 5.6 we present the BER performance evaluation. The BER has been evaluated considering a simple receiver composed of an one-tap equalizer and detector per subcarrier. In this case, the presented BER is also the average value obtained for 1000 different instantaneous channels realized based on the power delay profile, and sending 200 symbols. As seen, in all experiments, the optimized filters undoubtedly outperform the NPR1, QMF Gaussian and Hamming filters. The BER

performance can be significantly improved by mitigating the interference terms using an iterative interference cancellation (IIC) receiver [39]. After equalization, the receiver uses the decided symbols in an attempt to estimate the interference terms. The estimated interference is removed from the received signal and the decision is performed again.

We have also provided in Figure 5.6, the performance of the iterative interference cancellation - IIC receiver for both OPFC α and Gaussian α filters. We compared the obtained results to the Genie-Aided bound, which assumes perfect interference estimation and its cancellation.

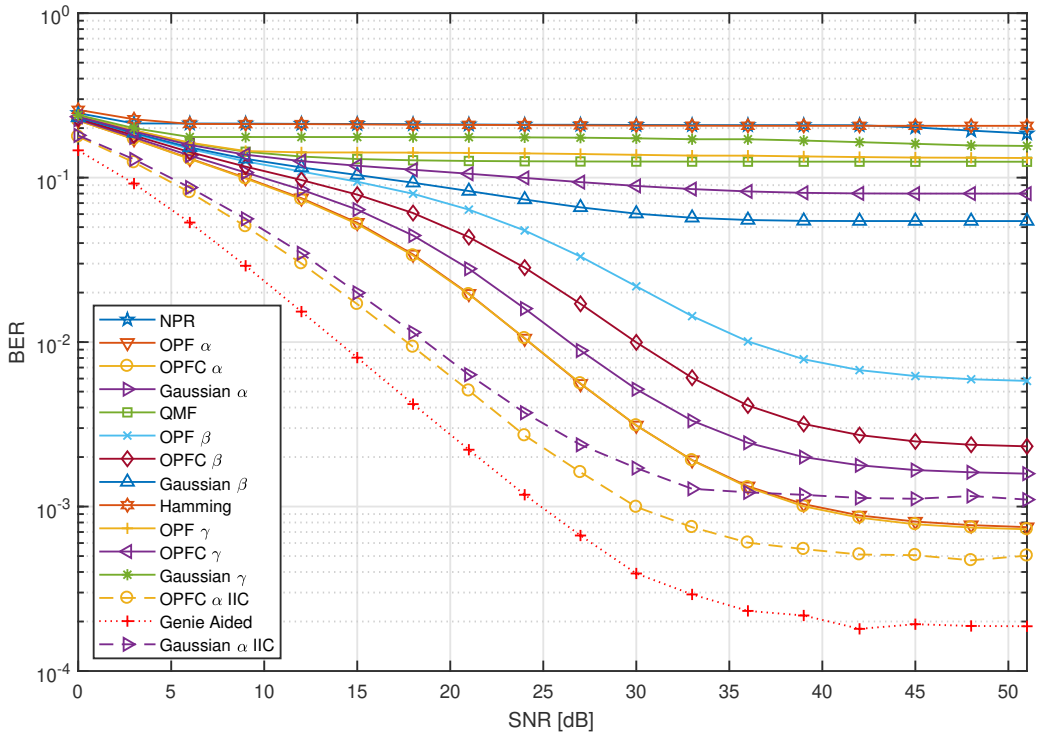

Figure 5.6: Average BER evaluated using OPF, OPFC, NPR, QMF Gaussian and Hamming filters with 1000 instantaneous channels.

It is possible to verify the system improvement when applying the IIC receiver. Besides, the performance limitation observed is due to the interference generated by the short filters ($K = 1$). We also present in Figure 5.7, and Figure 5.9 the magnitude of frequency response of the NPR1 and Hamming filters, and compare with Gaussian α and γ, and the optimized ones. Despite having the same OOBE, the energy distribution is different for each one. Besides, even if the frequency responses of the optimized filters are close to those of the Gaussian filters, they provide better performance. It is also worth noticing that, notwithstanding the slow side-lobe fall-off-rate observed in the optimized filter's frequency response, the total interference observed in the system is the smallest one, and it outperforms the other ones in terms of BER.

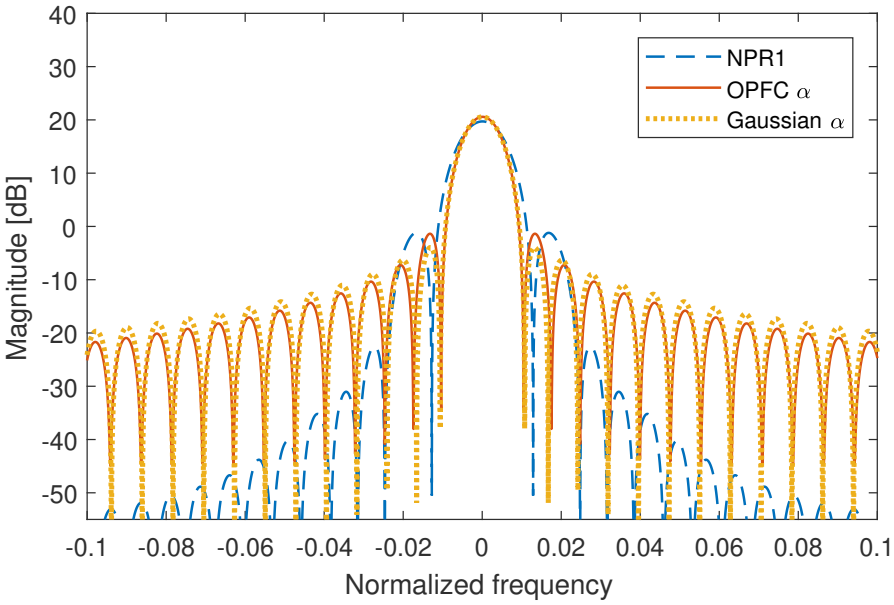

Figure 5.7: Magnitude frequency response of NPR1, OPFC-α and Gaussian-α.

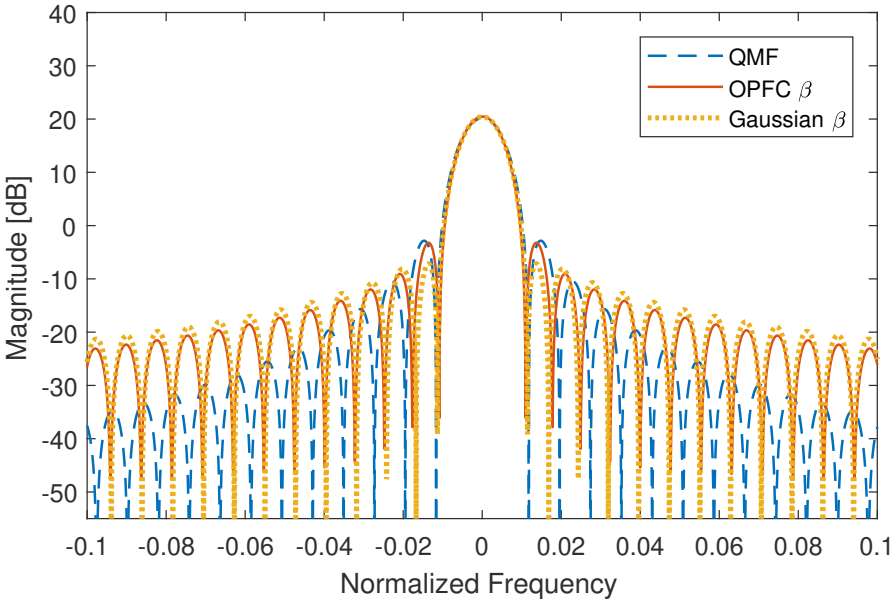

Figure 5.8: Magnitude frequency response of QMF, OPFC-β and Gaussian-β

We also evaluated in Figures 5.10 and 5.11 the simulated Complementary Cumulative Distribution Function (CCDF) of PAPR related to a threshold value PAPR_0 of the different filters. As we can notice, the obtained filters OPFC also outperform the other ones in terms of PAPR.

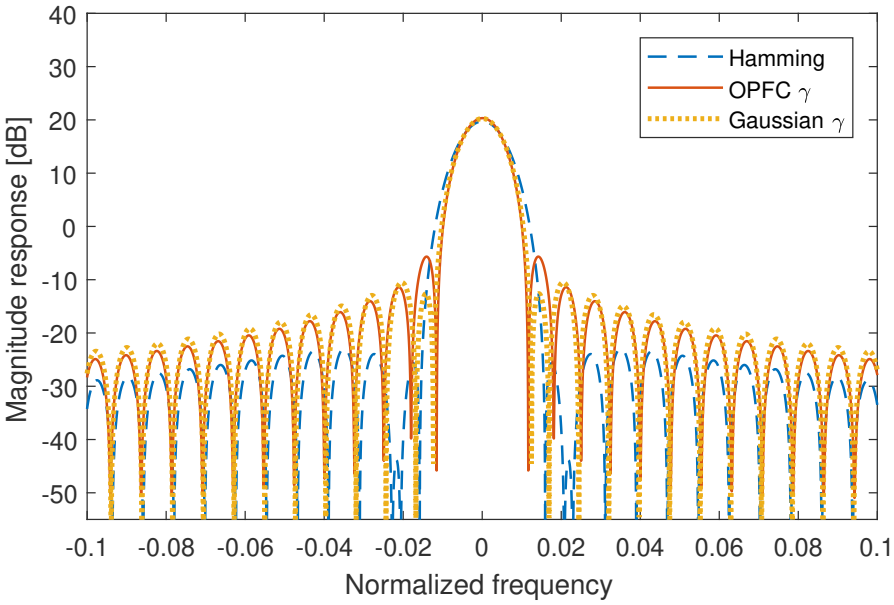

Figure 5.9: Magnitude frequency response of Hamming, OPFC-γ and Gaussian-γ

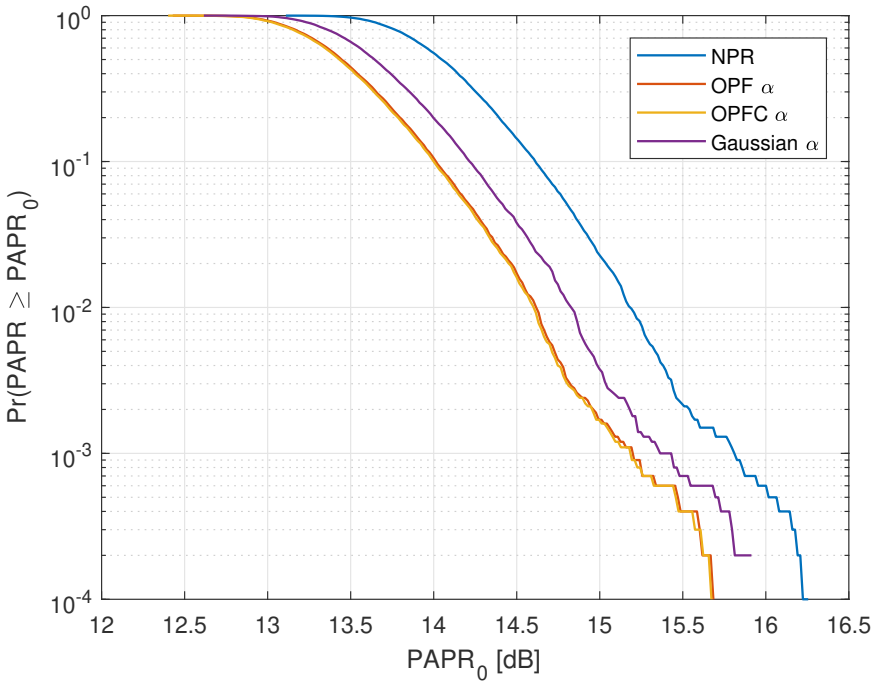

Figure 5.10: PAPR evaluation using NPR1, OPFC-α and Gaussian-α.

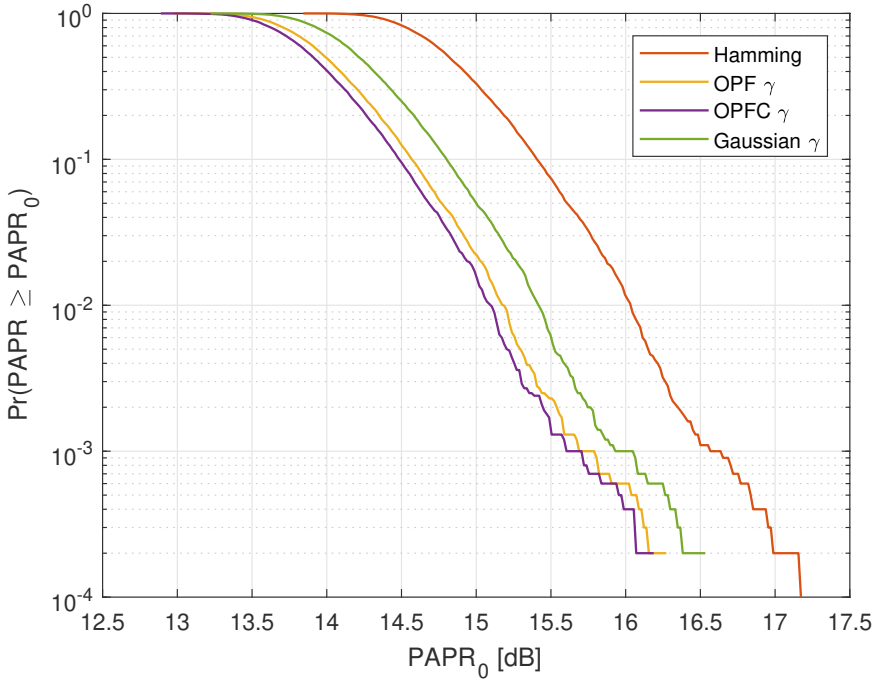

Figure 5.11: PAPR evaluation using Hamming, OPFC-γ and Gaussian-γ

5.3 Bit error rate in QAM-FBMC systems

Similarly to what we have done for QAM-FBMC systems that apply long filters ($K = 4$) in Chapter 4, we also evaluate the BEP of the system when applying short filters ($k = 1$).

Let us recall the expression of the transmitted signal $s[m]$ presented in Equation 5.1. By using the FFT, it is possible to rewrite the matrix approach. Considering the input data $\boldsymbol{d}_n = [d_{0,n}\ d_{1,n}\ \ldots\ d_{M-1,n}]^{\mathrm{T}}$, the block representation of the n-th transmitted QAM-FBMC symbol $\boldsymbol{s}_n = [s[nM]\ s[nM+1]\ \ldots\ s[nM+M-1]]^{\mathrm{T}}$ is given by

$$\boldsymbol{s}_n = \mathbf{G}\mathbf{W}^{\mathrm{H}}\boldsymbol{d}_n, \tag{5.26}$$

where $\mathbf{W}$ is the FFT matrix, $\mathbf{G} = \mathrm{diag}(\boldsymbol{g})$ and $\boldsymbol{g} \in \mathbb{R}^{L_g \times 1}$ is the transmitter short prototype filter impulse response. Here, the index n will be omitted without loss of generality in order to simplify the notation.

For the case of AWGN channel, the received signal is written as

$$\boldsymbol{y} = \mathbf{G}\mathbf{W}^{\mathrm{H}}\boldsymbol{d} + \boldsymbol{v}, \tag{5.27}$$

where $\boldsymbol{v}$ represents the Gaussian noise with zero mean and variance σ^2. Thus, the

demodulated symbol at the receiver can be described as:

$$\begin{aligned}\tilde{\boldsymbol{d}} =& \mathbf{W}\mathbf{G}^{\mathrm{H}}\boldsymbol{y} \\ =& \mathbf{W}\mathbf{G}^{\mathrm{H}}\mathbf{G}\mathbf{W}^{\mathrm{H}}\boldsymbol{d} + \mathbf{W}\mathbf{G}^{\mathrm{H}}\boldsymbol{v}.\end{aligned} \tag{5.28}$$

Despite having unitary norm-2, the transmitter and receiver filters are not orthogonal, thus the correlation matrix $\mathbf{W}\mathbf{G}^{\mathrm{H}}\mathbf{G}\mathbf{W}^{\mathrm{H}}$ is different from the identity matrix. There are elements outside of the principal diagonal slightly different from zero, which represents the intrinsic interference coefficients. Thus, we can write:

$$\tilde{\boldsymbol{d}} = \boldsymbol{d} + \underbrace{\left(\mathbf{W}\mathbf{G}^{\mathrm{H}}\mathbf{G}\mathbf{W}^{\mathrm{H}} - \mathbf{I}\right)\boldsymbol{d}}_{\text{interference}} + \tilde{\boldsymbol{v}}, \tag{5.29}$$

where $\tilde{\boldsymbol{v}} = \mathbf{W}\mathbf{G}^{\mathrm{H}}\boldsymbol{v}$, and $\mathbf{I}$ is the identity matrix.

Here, the matrix $\mathbf{W}\mathbf{G}^{\mathrm{H}}\mathbf{G}\mathbf{W}^{\mathrm{H}} - \mathbf{I}$ is composed of interference coefficients Γ_{Δ_k}. Since we are considering a filter of overlapping factor $K = 1$, and AWGN channel, there is not IBI. Besides, as $\mathbf{W}\mathbf{G}^{\mathrm{H}}\mathbf{G}\mathbf{W}^{\mathrm{H}} - \mathbf{I}$ is a circulant matrix, the interference coefficients are the same for all subcarriers.

Furthermore, we can separate the real and the imaginary parts of the received information at the subcarrier k, thus we have

$$\Re\{\tilde{d}_k\} = \Re\{d_k\} + \underbrace{\sum_{\substack{k'=0 \\ k'\neq k}}^{M-1} \Re\{\Gamma_{\Delta_k}\}\Re\{d_{k'}\} - \sum_{\substack{k'=0 \\ k'\neq k}}^{M-1} \Im\{\Gamma_{\Delta_k}\}\Im\{d_{k'}\}}_{\text{interference}}, + \Re\{\tilde{v}\} \tag{5.30}$$

and

$$\Im\{\tilde{d}_k\} = \Im\{d_k\} + \underbrace{\sum_{\substack{k'=0 \\ k'\neq k}}^{M-1} \Re\{\Gamma_{\Delta_k}\}\Im\{d_{k'}\} + \sum_{\substack{k'=0 \\ k'\neq k}}^{M-1} \Im\{\Gamma_{\Delta_k}\}\Re\{d_{k'}\}}_{\text{interference}} + \Im\{\tilde{v}\}. \tag{5.31}$$

Similarly to what we have done in Chapter 4, we opt for working with the real part of the interference presented in Equation (5.30).

For the case of Rayleigh channel, we include its effect on the received signal, thus by adapting Equation (5.27) we have:

$$\mathbf{y} = \mathbf{H}\mathbf{G}\mathbf{W}^{\mathrm{H}}\boldsymbol{d} + \boldsymbol{v}, \tag{5.32}$$

where $\mathbf{H}$ represents the channel matrix. Let us define $\tilde{\mathbf{H}}$ as a circulant approximation matrix of $\mathbf{H}$. From $\tilde{\mathbf{H}}$, it is possible to define a diagonal matrix $\bar{\mathbf{H}}$ by applying the

FFT matrix $\mathbf{W}$ as follows:

$$\bar{\mathbf{H}} = \mathbf{W}\tilde{\mathbf{H}}\mathbf{W}^{H}. \tag{5.33}$$

Thus, by using $\bar{\mathbf{H}}$ to perform the equalization, the demodulated signal is given by

$$\begin{aligned}\tilde{\boldsymbol{d}} =& \bar{\mathbf{H}}^{-1}\mathbf{W}\mathbf{G}^{\mathrm{H}}\boldsymbol{y} \\ =& \bar{\mathbf{H}}^{-1}\mathbf{W}\mathbf{G}^{\mathrm{H}}\left(\mathbf{H}\mathbf{G}\mathbf{W}^{H}\boldsymbol{d}\right) + \bar{\mathbf{H}}^{-1}\mathbf{W}\mathbf{G}^{\mathrm{H}}\boldsymbol{v} \\ =& \boldsymbol{d} + \underbrace{\left(\bar{\mathbf{H}}^{-1}\mathbf{W}\mathbf{G}^{\mathrm{H}}\mathbf{H}\mathbf{G}\mathbf{W}^{\mathrm{H}} - \mathbf{I}\right)\mathbf{d}}_{\text{interference}} + \bar{\mathbf{H}}^{-1}\tilde{\boldsymbol{v}}.\end{aligned} \tag{5.34}$$

The matrix $\bar{\mathbf{H}}^{-1}\mathbf{W}\mathbf{G}^{\mathrm{H}}\mathbf{H}\mathbf{G}\mathbf{W}^{\mathrm{H}} - \mathbf{I}$ is a nonzero matrix, and the non zero elements are responsible for introducing interference to the system. In this case, the interference coefficients include the channel effects. Thus, the received information at the subcarrier k can be described by

$$\tilde{d}_k = d_k + \sum_{\substack{k'=0 \\ k'\neq k}}^{M-1} \Gamma_{\Delta_k} d_{k'} + \bar{H}_k^{-1}\tilde{v}_k, \tag{5.35}$$

where $\bar{H}_k$ is the channel frequency response over the k-th subcarrier. In this case, assuming that the frequency response channel is almost flat over the frequency response of the prototype filter, Γ_{Δ_k} does not depend on the channel response.

Regarding the real part of the received information we have

$$\begin{aligned}\Re\{\tilde{d}_k\} = \Re\{d_k\} + \underbrace{\sum_{\substack{k'=0 \\ k'\neq k}}^{M-1} \Re\{\Gamma_{\Delta_k}\}\Re\{d_{k'}\} - \sum_{\substack{k'=0 \\ k'\neq k}}^{M-1} \Im\{\Gamma_{\Delta_k}\}\Im\{d_{k'}\}}_{\text{interference}} \\ + \Re\{H_k^{-1}\}\Re\{\tilde{v}_k\} - \Im\{H_k^{-1}\}\Im\{\tilde{v}_k\}.\end{aligned} \tag{5.36}$$

Equations (5.35) and (5.36) are applicable just for the case of flat channel over the narrowband frequency domain filter response, which is not a strong constraint. Thus, the calculated interference is the same as in the AWGN channel case.

5.3.1 Intrinsic interference probability

Since we are considering short filters ($K = 1$), in the absence of a channel, all the observed interference is inter-carrier (ICI), and it comes from the prototype filter properties. Considering a transmission of unitary pulse at the subcarrier k, at block n, we can observe at the receiver the energy spread over neighbor subcarriers, which is the intrinsic interference. This interference gives us the interference coefficient

table, which clearly depends on the applied prototype filter.

In Table 5.1 we present the observed interference to the subcarrier k at the receiver block n when the unitary pulse is sent at the transmission block n. For this, the OPF-α prototype filter proposed in Section 5.2.4 was applied, and no channel was considered.

Table 5.1: Main interference at the receiver of QAM-FBMC systems using OPF-α filter.

Δ_k	Γ_{Δ_k}
-5	-0.0028 + 0.0004j
-4	-0.0042 + 0.0004j
-3	-0.0067 + 0.0005j
-2	-0.0195 + 0.0010j
-1	-0.4100 + 0.0101j
0	1
+1	-0.4100 - 0.0101j
+2	-0.0195 - 0.0010j
+3	-0.0067 - 0.0005j
+4	-0.0042 - 0.0004j
+5	-0.0028 - 0.0004j

Since we opt for working with overlapping factor $K = 1$, the interference between different blocks is zero. The observed interference depends only on the difference Δ_k and is indicated by the interference coefficients (Γ_{Δ_k}).

For the sake of comparison, we present also in Table 5.2 the main interference table observed when using OPF-β filter.

Table 5.2: Main interference table at the receiver of QAM-FBMC system using OPF-β filter.

Δ_k	Γ_{Δ_k}
-5	-0.0018 + 0.0002j
-4	-0.0024 + 0.0002j
-3	-0.0015 + 0.0001j
-2	0.0059 - 0.0003j
-1	-0.4646 + 0.0114j
0	1
+1	-0.4646 - 0.0114j
+2	0.0059 + 0.0003j
+3	-0.0015 - 0.0001j
+4	-0.0024 - 0.0002j
+5	-0.0018 - 0.0002j

The interference coefficients related to a given prototype filter are a keypoint to derive the BEP for FBMC systems. Once we know these coefficients, we can deter-

mine the overall interference as a sum of the contributions induced by all neighbors into the subcarrier of interest weighted by the interference coefficients.

Once again, considering Υ as the set for which the interference coefficients are not-zero, and its cardinality N, we can deduce the exact discrete PDF $\mathrm{P}^{(l)}(\omega)$ of the interference generated by a 2^{2l}-QAM constellation as

$$\mathrm{P}^{(l)}(\omega) = \frac{1}{2^{l(N)}} \sum_{r=1}^{2^{l(N)}} \mathbb{1}(i_r^{(l)} = \omega). \tag{5.37}$$

In order to be able to visualize the real part of the interference probability distribution, in Figure 5.12 we discretized the probability distribution. In this case, the probability density function (PDF) of the real part of the interference observed in a QAM-FBMC system is exemplified when using the short prototype filter OPF-α and $M = 128$ subcarriers.

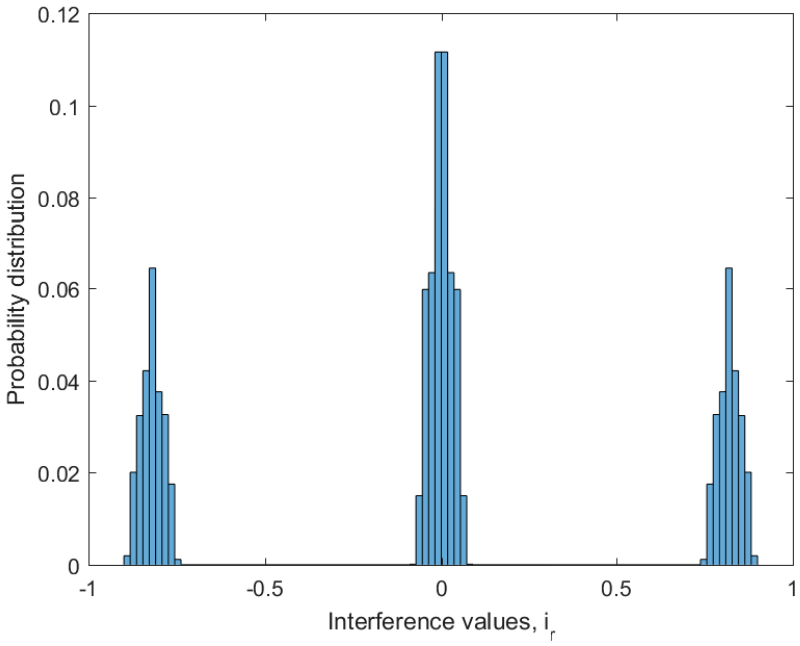

Figure 5.12: Real interference probability distribution of 4-QAM-FBMC using OPF-α filter.

We also present the probability distribution of the real interference for the case OPF-γ in Figure 5.13. Thus, we can cerify that the interference distribution, which is the same for the real and imaginary parties, is slightly different, when changing prototype filters.

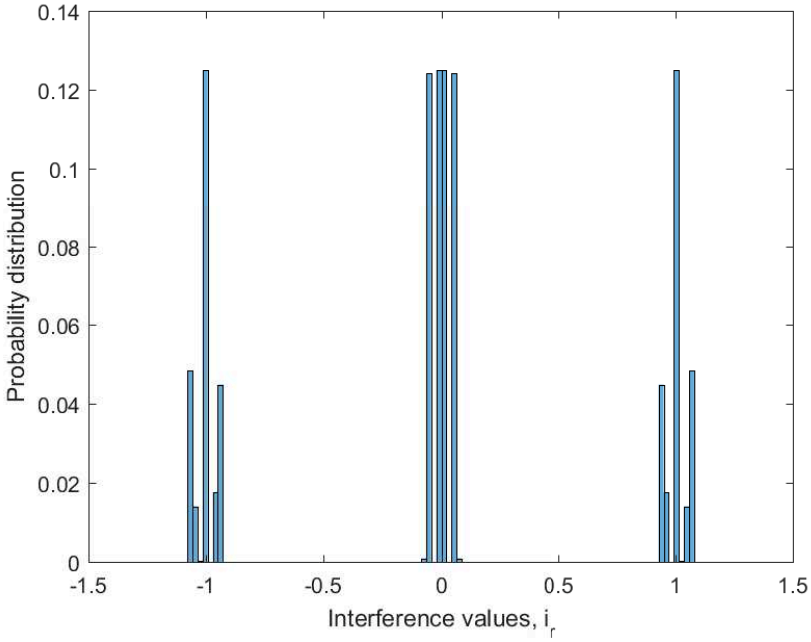

Figure 5.13: Real interference probability distribution of 4-QAM-FBMC using OPF-γ filter.

5.3.2 Bit Error probability (BEP)

Once we know the interference distribution for the case of short filters, we can apply the BEP as calculated in Chapter 4 for both AWGN and Rayleigh channels.

AWGN channel

Including all the distinct values of the intrinsic interference, ω, and its distribution, $\mathrm{P}^{(l)}(\omega)$, we derived the $\mathrm{BEP}^{\mathrm{AWGN}}_{\text{QAM-FBMC}}$ as

$$\mathrm{BEP}^{\mathrm{AWGN}}_{\text{QAM-FBMC}} = \sum_{\omega\in\Omega} \mathrm{P}^{(l)}(\omega)\frac{2^l-1}{2^l l}\mathrm{erfc}\left(\frac{\sqrt{\varphi E_b}\,(1-\omega)}{\sqrt{N_0}}\right). \tag{5.38}$$

One can notice, the BEP for QAM-FBMC systems is directly related to the interference calculated previously, which is related to the prototype filter.

Rayleigh channel

We derived also the $\mathrm{BEP}^{\mathrm{RAY}}_{\text{QAM-FBMC}}$ as follows

$$\mathrm{BEP}^{\mathrm{RAY}}_{\text{QAM-FBMC}} = \sum_{\omega\in\Omega} \mathrm{P}^{(l)}(\omega)\frac{2^l-1}{2^l l}\left(1-\frac{\sqrt{\varphi E_b}(1-\omega)}{\sqrt{\varphi E_b(1-\omega)^2+N_0}}\right). \tag{5.39}$$

As we can notice, the provided BEP derivations still applicable in the case of short filters.

5.3.3 Numerical evaluation

In this section we present numerical results for the analytical BER expression that we have derived for the QAM-FBMC system. The analytical results, obtained by evaluating the intrinsic interference as function of the prototype filter, are compared to the one obtained by simulations through both AWGN and Rayleigh channels.

In Figure 5.14, we present the bit error rate obtained by simulation and using Equation (5.38) considering 4-QAM modulation and AWGN channel. In all cases, the number of subcarriers was $M = 128$ and the short prototype filters applied were OPF-α and Gaussian-α, both with overlapping factor $K = 1$, and the same OOBE. As we can notice, the theoretical BEP matches the simulated results for both filters, which confirms the applicability of the proposed method, despite the choice of the prototype filters and its overlapping factor.

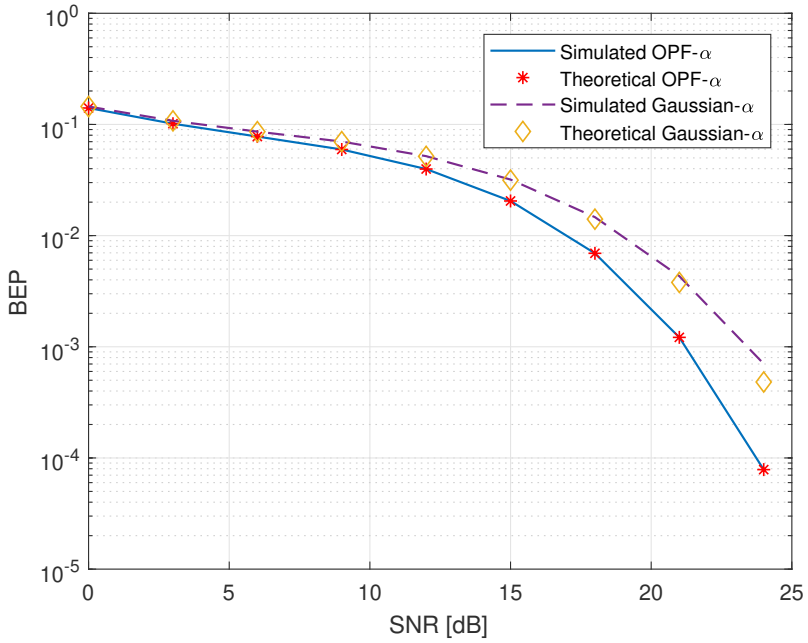

Figure 5.14: Simulated and theoretical Bit Error Probability of QAM-FBMC system when using OPF-α filter and Gaussian-α filter under AWGN channel

Furthermore, we evaluate the proposed method by using different Gaussian filters in Figure 5.15. Once again the BEP matches the simulated results, and we endorse the applicability of the proposed method for different prototype filters.

We also evaluated the BEP over flat fading Rayleigh channel through the proposed Equation (5.39) considering 4-QAM modulation and using the OPF-α filter as presented in Figure 5.16. It is possible to verify the effectiveness of the proposed method even through the fading channel, since the theoretical and the simulated results are the same.

For the sake of comparison, we also evaluated the proposed method over pedes-

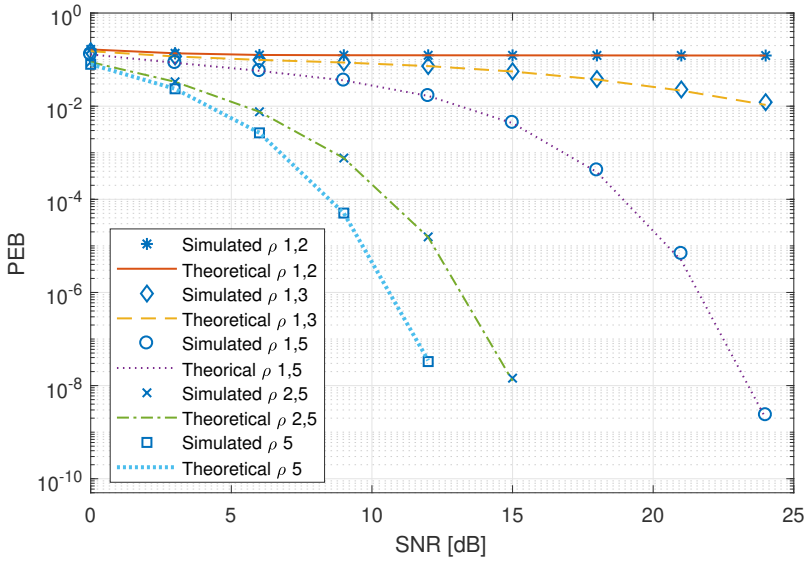

Figure 5.15: Simulated and theoretical Bit Error Probability of QAM-FBMC system when using Gaussians filters with $\rho = 1,2$ $\rho = 1,3$ $\rho = 1,5$ $\rho = 2,5$ and $\rho = 5$.

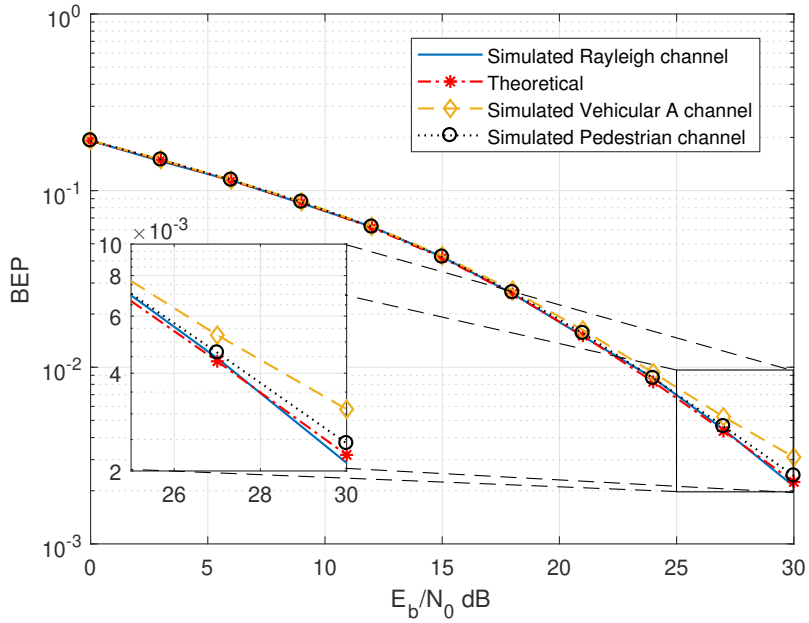

Figure 5.16: Simulated and theoretical Bit Error Probability of QAM-FBMC system using OPF-α filter under Rayleigh channel, Vehicular-A channel and Pedestrian channel

trian and Vehicular-A channels with very good agreement between the results of our method and simulations, as also evidenced in Figure 5.16. As expected, for the low to moderate selective channels we can still use the proposed expressions.

5.4 Receiver schemes for QAM-FBMC

Even though interference can be significantly reduced through the well localized prototype filters, advanced receivers are still needed to overcome the residual interference observed at the reception. Knowing that, we propose an MMSE-based receiver associated to inter-block interference (IBI) cancellation, developed to minimize the interference in QAM-FBMC systems.

Let us recall the block representation of the system presented in Equation (5.26). By considering the previous transmitted block $\boldsymbol{s}_{n-1}$ we can define the transmitted vector $\bar{\boldsymbol{s}}_n$ as the concatenation of $\boldsymbol{s}_n$ and $\boldsymbol{s}_{n-1}$

$$\bar{\boldsymbol{s}}_n = \begin{bmatrix} \boldsymbol{s}_{n-1} \\ \boldsymbol{s}_n \end{bmatrix} = \begin{bmatrix} \mathbf{G}\mathbf{W}^{\mathrm{H}} & \mathbf{0}_{M\times M} \\ \mathbf{0}_{M\times M} & \mathbf{G}\mathbf{W}^{\mathrm{H}} \end{bmatrix} \begin{bmatrix} \boldsymbol{d}_{n-1} \\ \boldsymbol{d}_n \end{bmatrix}. \tag{5.40}$$

Considering also a channel defined by its impulse response composed of $L_h \leq M$ non zero taps, $\boldsymbol{h} = [h_0\ h_1 \dots h_{L_h}\ \mathbf{0}_{2M-L_h-1\times 1}]^T$, we can define the $2M \times 2M$ channel convolution matrix $\mathbf{H}$ as follows

$$\mathbf{H} = [\boldsymbol{h}_0 \quad \boldsymbol{h}_1 \ \dots \ \boldsymbol{h}_{2M-1}], \tag{5.41}$$

where $\boldsymbol{h}_i$ is the shifted version of $\boldsymbol{h}$ by i elements. The channel matrix $\mathbf{H}$ can also be decomposed in four $M \times M$ submatrices as

$$\mathbf{H} = \begin{bmatrix} \mathbf{H}_0 & \mathbf{0}_{M\times M} \\ \mathbf{H}_1 & \mathbf{H}_0 \end{bmatrix}. \tag{5.42}$$

Thus, combining the block representation of the transmitter, presented in Equation (5.40), and the channel effects, the received signal $\bar{\boldsymbol{y}}_n$ can be written as

$$\begin{aligned} \bar{\boldsymbol{y}}_n &= \begin{bmatrix} \boldsymbol{y}_{n-1} \\ \boldsymbol{y}_n \end{bmatrix} \\ &= \begin{bmatrix} \mathbf{H}_0 & \mathbf{0}_{M\times M} \\ \mathbf{H}_1 & \mathbf{H}_0 \end{bmatrix} \begin{bmatrix} \boldsymbol{s}_{n-1} \\ \boldsymbol{s}_n \end{bmatrix} + \begin{bmatrix} \boldsymbol{v}_{n-1} \\ \boldsymbol{v}_n \end{bmatrix} \\ &= \begin{bmatrix} \mathbf{H}_0 & \mathbf{0}_{M\times M} \\ \mathbf{H}_1 & \mathbf{H}_0 \end{bmatrix} \begin{bmatrix} \mathbf{G}\mathbf{W}^{\mathrm{H}} & \mathbf{0}_{M\times M} \\ \mathbf{0}_{M\times M} & \mathbf{G}\mathbf{W}^{\mathrm{H}} \end{bmatrix} \begin{bmatrix} \boldsymbol{d}_{n-1} \\ \boldsymbol{d}_n \end{bmatrix} + \begin{bmatrix} \boldsymbol{v}_{n-1} \\ \boldsymbol{v}_n \end{bmatrix}, \end{aligned} \tag{5.43}$$

where $\boldsymbol{v}$ is the noise vector.

Finally, the n-th received vector $\boldsymbol{y}_n$ can be rewritten as follows

$$\begin{aligned} \boldsymbol{y}_n &= \mathbf{T}\mathbf{H}\bar{\boldsymbol{s}}_n + \boldsymbol{v}_n \\ &= \mathbf{H}_1\mathbf{G}\mathbf{W}^{\mathrm{H}}\boldsymbol{d}_{n-1} + \mathbf{H}_0\mathbf{G}\mathbf{W}^{\mathrm{H}}\boldsymbol{d}_n + \boldsymbol{v}_n, \end{aligned} \tag{5.44}$$

where $\mathbf{T} = [\mathbf{0}_{M\times M}\ \mathbf{I}_M]$.

5.4.1 Time Domain channel equalization

In this section, we present a version of the QAM-FBMC receiver in which the equalization is performed in the time domain just after receiving the transmitted signal, as depicted in Figure 5.17.

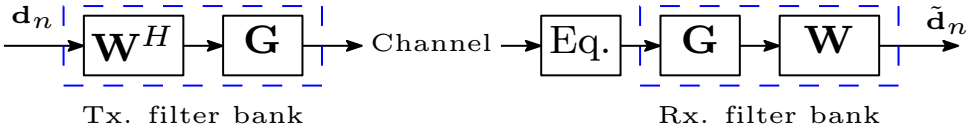

Figure 5.17: Simplified time-domain-equalization (TDE) receiver structure.

Let us define a circulant channel submatrix $\tilde{\mathbf{H}}_0$ as an approximation of $\mathbf{H}_0$. From $\tilde{\mathbf{H}}_0$, it is possible to define a diagonal matrix $\bar{\mathbf{H}}_0$ by applying the FFT as follows:

$$\bar{\mathbf{H}}_0 = \mathbf{W}\tilde{\mathbf{H}}_0\mathbf{W}^{\mathrm{H}}. \tag{5.45}$$

For this proposal, we define the equalizer as the inverse of the channel matrix $\tilde{\mathbf{H}}_0$. Thus, we can write the estimated symbol as

$$\begin{aligned}\tilde{\boldsymbol{d}}_n =& \mathbf{W}\mathbf{G}\tilde{\mathbf{H}}_0^{-1}\boldsymbol{y}_n \\ =& \mathbf{W}\mathbf{G}\tilde{\mathbf{H}}_0^{-1}\mathbf{H}_0\mathbf{G}\mathbf{W}^{\mathrm{H}}\boldsymbol{d}_n + \mathbf{W}\mathbf{G}\tilde{\mathbf{H}}_0^{-1}\mathbf{H}_1\mathbf{G}\mathbf{W}^{\mathrm{H}}\boldsymbol{d}_{n-1} + \mathbf{W}\mathbf{G}\tilde{\mathbf{H}}_0^{-1}\boldsymbol{v}_n \\ =& \mathbf{H}_{eq}\boldsymbol{d}_n + \tilde{\boldsymbol{v}}_n,\end{aligned} \tag{5.46}$$

where the matrix $\mathbf{H}_{eq}$ is defined as

$$\mathbf{H}_{eq} = \mathbf{W}\mathbf{G}\tilde{\mathbf{H}}_0^{-1}\mathbf{H}_0\mathbf{G}\mathbf{W}^{\mathrm{H}}, \tag{5.47}$$

and $\tilde{\boldsymbol{v}}_n$ is given by $\mathbf{W}\mathbf{G}\tilde{\mathbf{H}}_0^{-1}\mathbf{H}_1\mathbf{G}\mathbf{W}^{\mathrm{H}}\boldsymbol{d}_{n-1} + \mathbf{W}\mathbf{G}\tilde{\mathbf{H}}_0^{-1}\boldsymbol{v}_n$.

It is possible to improve further the receiver's performance by applying the iterative interference cancellation (IIC) scheme proposed in [40]. In this case, after equalization, the receiver uses the decided symbols, $\boldsymbol{d}'_n$, in an attempt to estimate the interference terms as

$$\boldsymbol{d}'_n = \mathrm{dec}(\tilde{\boldsymbol{d}}_n). \tag{5.48}$$

Then the interference term is estimated from $\boldsymbol{d}'_n$ and removed from $\tilde{\boldsymbol{d}}_n$ as follows:

$$\check{\boldsymbol{d}}_n = \tilde{\mathbf{d}}_n - (\mathbf{H}_{eq} - \mathbf{I}_M)\,\mathbf{d}'_n. \tag{5.49}$$

After interference cancellation, the decision is made again, and finally we have

$$\hat{\boldsymbol{d}}_n = \mathrm{dec}(\check{\boldsymbol{d}}_n). \tag{5.50}$$

5.4.2 MMSE receiver

In order to enhance the QAM-FBMC system performance, we propose in this section an MMSE-based receiver, which is directly applied to the received symbol $\boldsymbol{y}_n$, as depicted in Figure 5.18. An improvement in the system performance is expected since we are not using the ZF as in TDE receiver.

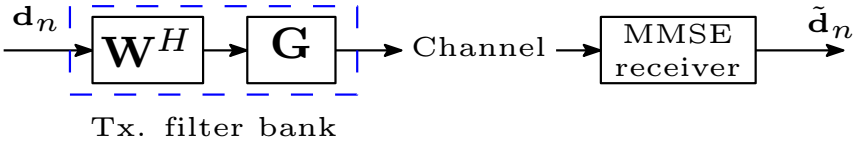

Figure 5.18: Simplified MMSE-based receiver structure.

Compared to the TDE presented in Section 5.4.1, where the equalization is a simple channel inversion based in a diagonal approximation of the channel $\tilde{\mathbf{H}}_0^{-1}$, in our proposal it is performed by the MMSE filter. For this, the equalization takes into account the noise and interference terms. Besides, as the IBI can still be observed, we also apply the IBI cancellation technique.

In this case we can write the estimated symbol as

$$\begin{aligned}\tilde{\boldsymbol{d}}_n &= \boldsymbol{y}_n \\ &= \mathbf{H}_0\mathbf{G}\mathbf{W}^{\mathrm{H}}\boldsymbol{d}_n + \mathbf{H}_1\mathbf{G}\mathbf{W}^{\mathrm{H}}\boldsymbol{d}_{n-1} + \boldsymbol{v}_n \\ &= \mathbf{H}_{eq}\boldsymbol{d}_n + \tilde{\boldsymbol{v}}_n,\end{aligned} \tag{5.51}$$

where $\mathbf{H}_{eq}$ is defined by

$$\mathbf{H}_{eq} = \mathbf{H}_0\mathbf{G}\mathbf{W}^{\mathrm{H}}, \tag{5.52}$$

and $\tilde{\boldsymbol{v}}_n$ can be written as $\mathbf{H}_1\mathbf{G}\mathbf{W}^{\mathrm{H}}\boldsymbol{d}_{n-1} + \boldsymbol{v}_n$.

In order to deal with the interference terms, we apply the filter $\mathbf{Q}_n$, based on the MMSE criterion as follows

$$\check{\boldsymbol{d}}_n = \mathbf{Q}_n^{\mathrm{H}}\tilde{\boldsymbol{d}}_n, \tag{5.53}$$

where the matrix $\mathbf{Q}_n$ is given by

$$\mathbf{Q}_n = \left(\mathbf{H}_{eq}\mathbf{H}_{eq}^{\mathrm{H}} + \frac{\mathbf{R}_{\tilde{\boldsymbol{v}}_n\tilde{\boldsymbol{v}}_n}}{\sigma_{d_n}^2}\right)^{-1}\mathbf{H}_{eq}. \tag{5.54}$$

$\mathbf{R}_{\tilde{\boldsymbol{v}}_n\tilde{\boldsymbol{v}}_n} = E\left\{\tilde{\boldsymbol{v}}_n\tilde{\boldsymbol{v}}_n^{\mathrm{H}}\right\}$ is the correlation matrix of $\tilde{\boldsymbol{v}}_n$, which can be obtained by

$$\begin{aligned}\mathbf{R}_{\tilde{\boldsymbol{v}}_n\tilde{\boldsymbol{v}}_n} &= (\mathbf{H}_1\mathbf{G}\mathbf{W}^{\mathrm{H}})(\mathbf{H}_1\mathbf{G}\mathbf{W}^{\mathrm{H}})^{\mathrm{H}}\sigma_{d_{n-1}}^2 + \sigma_{\boldsymbol{v}_n}^2\mathbf{I}_M \\ &= \mathbf{H}_1\mathbf{G}^2\mathbf{H}_1^{\mathrm{H}}\sigma_d^2 + \sigma_{\boldsymbol{v}_n}^2\mathbf{I}_M. \end{aligned} \tag{5.55}$$

From Equation (5.54) it is possible to develop the matrix $\mathbf{Q}_n^{\mathrm{H}}$ as follows

$$\begin{aligned}\mathbf{Q}_n^{\mathrm{H}} &= \mathbf{H}_{eq}^{\mathrm{H}}\left(\mathbf{H}_{eq}\mathbf{H}_{eq}^{\mathrm{H}} + \frac{\mathbf{R}_{\tilde{\boldsymbol{v}}_n\tilde{\boldsymbol{v}}_n}}{\sigma_{d_n}^2}\right)^{-\mathrm{H}} \\ &= \mathbf{W}\mathbf{G}\mathbf{H}_0^{\mathrm{H}}\left(\mathbf{H}_0\mathbf{G}^2\mathbf{H}_0^{\mathrm{H}} + \frac{\mathbf{R}_{\tilde{\boldsymbol{v}}_n\tilde{\boldsymbol{v}}_n}}{\sigma_{d_n}^2}\right)^{-1}. \end{aligned} \tag{5.56}$$

The MMSE filter can be seen as a time-domain channel equalization followed by the analysis filter-bank, $\mathbf{WG}$.

It is also possible to improve the performance of the receiver by canceling the interference, *i.e.*, the contribution of the previous block $\boldsymbol{d}_{n-1}$ in Equation (5.51), using the previously estimated vector $\tilde{\boldsymbol{d}}_{n-1}$ before applying the MMSE filter. Thus we have

$$\begin{aligned}\tilde{\boldsymbol{d}}_n &= \mathbf{H}_0\mathbf{G}\mathbf{W}^{\mathrm{H}}\boldsymbol{d}_n + \mathbf{H}_1\mathbf{G}\mathbf{W}^{\mathrm{H}}(\boldsymbol{d}_{n-1} - \tilde{\boldsymbol{d}}_{n-1}) + \boldsymbol{v}_n \\ &= \mathbf{H}_{eq}\boldsymbol{d}_n + \bar{\boldsymbol{v}}_n. \end{aligned} \tag{5.57}$$

Assuming perfect IBI cancellation, we have $\bar{\boldsymbol{v}}_n = \boldsymbol{v}_n$. Then, the MMSE filter is applied using Equation (5.54) and adapting $\mathbf{R}_{\tilde{\boldsymbol{v}}_n\tilde{\boldsymbol{v}}_n}$ as $\sigma_{\bar{\boldsymbol{v}}_n}^2\mathbf{I}_M$.

5.4.3 Frequency domain channel equalization

For the sake of comparison, we present in this section the well known frequency domain equalizer (FDE). In this case the equalization is performed in the frequency domain just after the filter-bank, as presented in the simplified representation of the full system in Figure 5.19.

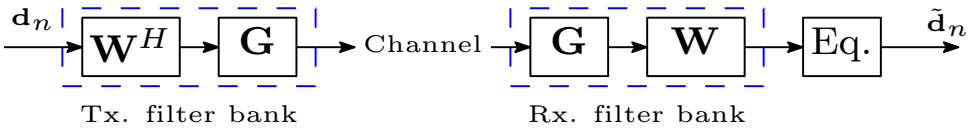

Figure 5.19: Simplified frequency domain equalizer structure.

We define the equalizer as the inverse of the channel matrix $\bar{\mathbf{H}}_0$, as presented in

Equation (5.45). Thus, the estimated symbol is given by

$$\begin{aligned}\tilde{\boldsymbol{d}}_n =&\bar{\mathbf{H}}_0^{-1}\mathbf{W}\mathbf{G}\boldsymbol{y}_n \\ =&\bar{\mathbf{H}}_0^{-1}\mathbf{W}\mathbf{G}\mathbf{H}_0\mathbf{G}\mathbf{W}^{\mathrm{H}}\boldsymbol{d}_n + \bar{\mathbf{H}}_0^{-1}\mathbf{W}\mathbf{G}\mathbf{H}_1\mathbf{G}\mathbf{W}^{\mathrm{H}}\boldsymbol{d}_{n-1} + \bar{\mathbf{H}}_0^{-1}\mathbf{W}\mathbf{G}\boldsymbol{v}_n \\ =&\mathbf{H}_{eq}\boldsymbol{d}_n + \tilde{\boldsymbol{v}}_n, \end{aligned} \tag{5.58}$$

where $\mathbf{H}_{eq}$ can be defined as

$$\mathbf{H}_{eq} = \bar{\mathbf{H}}_0^{-1}\mathbf{W}\mathbf{G}\mathbf{H}_0\mathbf{G}\mathbf{W}^{\mathrm{H}}. \tag{5.59}$$

Also, $\tilde{\boldsymbol{v}}_n$ can be written as

$$\tilde{\boldsymbol{v}}_n = \bar{\mathbf{H}}_0^{-1}\mathbf{W}\mathbf{G}\mathbf{H}_1\mathbf{G}\mathbf{W}^{\mathrm{H}}\boldsymbol{d}_{n-1} + \bar{\mathbf{H}}_0^{-1}\mathbf{W}\mathbf{G}\boldsymbol{v}_n. \tag{5.60}$$

Data detection can be performed directly from Equation (5.58). However, as in TDE, it can also be performed by applying IIC using Equations (5.48), (5.49) and (5.50).

5.4.4 Block-wise MMSE receiver

We also compare our proposal to the state of the art receiver, linear block-wise MMSE (BW-MMSE), recently presented in [43]. It was simplified by considering only the case of overlapping factor $K = 1$. Differently from our MMSE-based receiver presented in Section 5.4.2, in this work, the MMSE filter is computed considering both symbols $\boldsymbol{d}_{n-1}$ and $\boldsymbol{d}_n$. However, the MMSE filter is only applied to $\tilde{\boldsymbol{d}}_n$ after truncation. Following this approach, let us define $\bar{\boldsymbol{d}}_n$ as a concatenation of two consecutive symbols $\bar{\boldsymbol{d}}_n = [\boldsymbol{d}_{n-1}\ \boldsymbol{d}_n]^{\mathrm{T}}$. Thus, from Equation (5.44) we have, at the receiver

$$\begin{aligned}\boldsymbol{y}_n &= \mathbf{T}\mathbf{H}\bar{\mathbf{s}}_n + \boldsymbol{v}_n \\ &= \mathbf{T}\mathbf{H}\begin{bmatrix}\mathbf{G}\mathbf{W}^{\mathrm{H}} & \mathbf{0}_{M\times M} \\ \mathbf{0}_{M\times M} & \mathbf{G}\mathbf{W}^{\mathrm{H}}\end{bmatrix}\bar{\boldsymbol{d}}_n + \boldsymbol{v}_n \\ &= \bar{\mathbf{H}}_{eq}\bar{\boldsymbol{d}}_n + \boldsymbol{v}_n. \end{aligned} \tag{5.61}$$

Then a filter matrix $\bar{\mathbf{Q}}_n$, based on the MMSE criterion, is applied at the received symbol as follows:

$$\breve{\boldsymbol{d}}_n = \bar{\mathbf{Q}}_n^{\mathrm{H}}\boldsymbol{y}_n, \tag{5.62}$$

where the matrix $\bar{\mathbf{Q}}_n$ is given by

$$\bar{\mathbf{Q}}_n = \left(\bar{\mathbf{H}}_{eq} \bar{\mathbf{H}}_{eq}^{\mathrm{H}} + \frac{\sigma^2_{\boldsymbol{v}_n}}{\sigma^2_{\bar{\boldsymbol{d}}_n}} \mathbf{I}_M \right)^{-1} \bar{\mathbf{H}}_{eq}. \tag{5.63}$$

5.4.5 Extension to the two-user case

Due to the advantages observed in our proposed MMSE-based receiver, we decide to extend it to the two-user case in an up-link transmission. We assume that the first half of the transmitter bandwidth is allocated to a first user and that the second half is allocated to a second user. Thus, the relations between input data and transmitted vectors are given by

$$\boldsymbol{s}_n^1 = \mathbf{G}\mathbf{W}_{\mathrm{L}}^{\mathrm{H}} \boldsymbol{d}_n^1 \quad \text{and} \quad \boldsymbol{s}_n^2 = \mathbf{G}\mathbf{W}_{\mathrm{R}}^{\mathrm{H}} \boldsymbol{d}_n^2, \tag{5.64}$$

where $\boldsymbol{d}_n^1 = [d_{0,n}^1 \; d_{1,n}^1 \; \ldots \; d_{M/2-1,n}^1]^{\mathrm{T}}$ and $\boldsymbol{d}_n^2 = [d_{0,n}^2 \; d_{1,n}^2 \; \ldots \; d_{M/2-1,n}^2]^{\mathrm{T}}$ are the input data vectors of users 1 and 2 respectively; and $\boldsymbol{s}_n^1 = [s^1[nM] \; s^1[nM+1] \; \ldots \; s^1[nM+M-1]]^{\mathrm{T}}$ and $\boldsymbol{s}_n^2 = [s^2[nM] \; s^2[nM+1] \; \ldots \; s^2[nM+M-1]]^{\mathrm{T}}$ their respective transmitted vectors. Besides, $\mathbf{W}_{\mathrm{L}}^{\mathrm{H}} = \mathbf{W}^{\mathrm{H}}[\mathbf{I}_{M/2} \; \mathbf{0}_{M/2}]^{\mathrm{T}}$ and $\mathbf{W}_{\mathrm{R}}^{\mathrm{H}} = \mathbf{W}^{\mathrm{H}}[\mathbf{0}_{M/2} \; \mathbf{I}_{M/2}]^{\mathrm{T}}$ represent the truncated IFFT matrices.

Following the derivation given in Equations (5.40), (5.42) and (5.43), the n-th received vector $\boldsymbol{y}_n$ can be written as

$$\boldsymbol{y}_n = \mathbf{H}_0^1 \mathbf{G}\mathbf{W}_{\mathrm{L}}^{\mathrm{H}} \boldsymbol{d}_n^1 + \mathbf{H}_1^1 \mathbf{G}\mathbf{W}_{\mathrm{L}}^{\mathrm{H}} \boldsymbol{d}_{n-1}^1 + \mathbf{H}_0^2 \mathbf{G}\mathbf{W}_{\mathrm{R}}^{\mathrm{H}} \boldsymbol{d}_n^2 + \mathbf{H}_1^2 \mathbf{G}\mathbf{W}_{\mathrm{R}}^{\mathrm{H}} \boldsymbol{d}_{n-1}^2 + \boldsymbol{v}_n, \tag{5.65}$$

where $\boldsymbol{v}_n$ is the noise vector.

Extending the proposed single user MMSE receiver to the considered case, we can apply an MMSE filter to the received vector $\boldsymbol{y}_n$ for the estimation of the data of user 1 without loss of generality. In this case we have

$$\begin{aligned} \tilde{\boldsymbol{d}}_n^1 &= \boldsymbol{y}_n \\ &= \mathbf{H}_{eq} \boldsymbol{d}_n^1 + \tilde{\boldsymbol{v}}_n^1, \end{aligned} \tag{5.66}$$

where $\mathbf{H}_{eq}$ is defined by

$$\mathbf{H}_{eq} = \mathbf{H}_0^1 \mathbf{G}\mathbf{W}_{\mathrm{L}}^{\mathrm{H}}. \tag{5.67}$$

In this case, the interference $\tilde{\boldsymbol{v}}_n^1$ is given by

$$\tilde{\boldsymbol{v}}_n^1 = \mathbf{H}_1^1 \mathbf{G}\mathbf{W}_{\mathrm{L}}^{\mathrm{H}} \boldsymbol{d}_{n-1}^1 + \mathbf{H}_0^2 \mathbf{G}\mathbf{W}_{\mathrm{R}}^{\mathrm{H}} \boldsymbol{d}_n^2 + \mathbf{H}_1^2 \mathbf{G}\mathbf{W}_{\mathrm{R}}^{\mathrm{H}} \boldsymbol{d}_{n-1}^2 + \boldsymbol{v}_n. \tag{5.68}$$

To deal with the interference term, we apply the filter $\mathbf{Q}_n^1$, based on the MMSE

criterion as follows:

$$\check{\mathbf{d}}_n^1 = \mathbf{Q}_n^{1H} \tilde{\mathbf{d}}_n^1, \tag{5.69}$$

where the matrix $\mathbf{Q}_n^1$ is given by Equation (5.54). However, $\mathbf{R}_{\tilde{\boldsymbol{v}}_n \tilde{\boldsymbol{v}}_n}$ must be adapted for user 1 as $\mathbf{R}_{\tilde{\boldsymbol{v}}_n^1 \tilde{\boldsymbol{v}}_{\boldsymbol{n}}^{\mathbf{1}}}$. So we have

$$\begin{aligned}\mathbf{R}_{\tilde{\boldsymbol{v}}_n^1 \tilde{\boldsymbol{v}}_{\boldsymbol{n}}^{\mathbf{1}}} =& (\mathbf{H}_1^1 \mathbf{G} \mathbf{W}_{\mathrm{L}}^{\mathrm{H}} \mathbf{W}_{\mathrm{L}} \mathbf{G} \mathbf{H}_1^{1\mathrm{H}} + \mathbf{H}_0^2 \mathbf{G} \mathbf{W}_{\mathrm{R}}^{\mathrm{H}} \mathbf{W}_R \mathbf{G} \mathbf{H}_0^{2\mathrm{H}} \\ &+ \mathbf{H}_1^2 \mathbf{G} \mathbf{W}_{\mathrm{R}}^{\mathrm{H}} \mathbf{W}_R \mathbf{G} \mathbf{H}_1^{2\mathrm{H}}) \sigma_{d_n}^2 + \sigma_{\boldsymbol{v}_n}^2 \mathbf{I}_M. \end{aligned} \tag{5.70}$$

Instead of estimating each user's data independently using the MMSE filters $\mathbf{Q}_n^1$ and $\mathbf{Q}_n^2$, it is possible to estimate both user's data jointly by applying the filter $\mathbf{Q}_n$ to the received vector $\boldsymbol{y}_n$. Finally, we can rewrite Equation (5.65) as

$$\mathbf{y}_n = \mathbf{H}_{eq} \begin{bmatrix} \boldsymbol{d}_n^1 \\ \boldsymbol{d}_n^2 \end{bmatrix} + \mathbf{H}_{ibi} \begin{bmatrix} \boldsymbol{d}_{n-1}^1 \\ \boldsymbol{d}_{n-1}^2 \end{bmatrix} + \boldsymbol{v}_n, \tag{5.71}$$

where

$$\begin{aligned} \mathbf{H}_{eq} =& [\mathbf{H}_0^1 \mathbf{G} \mathbf{W}_{\mathrm{L}}^{\mathrm{H}} \quad \mathbf{H}_0^2 \mathbf{G} \mathbf{W}_{\mathrm{R}}^{\mathrm{H}}] \\ \mathbf{H}_{ibi} =& [\mathbf{H}_1^1 \mathbf{G} \mathbf{W}_{\mathrm{L}}^{\mathrm{H}} \quad \mathbf{H}_1^2 \mathbf{G} \mathbf{W}_{\mathrm{R}}^{\mathrm{H}}]. \end{aligned} \tag{5.72}$$

Thus, the matrix $\mathbf{Q}_n$ is given by

$$\mathbf{Q}_n = \left(\mathbf{H}_{eq} \mathbf{H}_{eq}^{\mathrm{H}} + \mathbf{H}_{ibi} \mathbf{H}_{ibi}^{\mathrm{H}} \frac{\sigma_{\boldsymbol{v}_n}^2}{\sigma_{\boldsymbol{d}_n}^2} \mathbf{I}_M \right)^{-1} \mathbf{H}_{eq}. \tag{5.73}$$

We can easily show that the two approaches are equivalent. Indeed we can deduce the matrices $\mathbf{Q}_n^1$ and $\mathbf{Q}_n^2$ from $\mathbf{Q}_n$ by replacing the right term $\mathbf{H}_{eq}$ in equation (5.73) by $\mathbf{H}_0^1 \mathbf{G} \mathbf{W}_{\mathrm{L}}^{\mathrm{H}}$ and $\mathbf{H}_0^2 \mathbf{G} \mathbf{W}_{\mathrm{R}}^{\mathrm{H}}$ respectively.

5.4.6 Numerical evaluation

In this section we evaluate and compare the performance of our proposed MMSE-based QAM-FBMC and TDE receivers with the FDE and the BW-MMSE receivers [43]. We also evaluate the use of IIC and IBI cancellation techniques. For the sake of clarity, we also present the Genie-Aided performance, when the interference is supposed to be perfectly known. The QAM-FBMC symbol size was $M = 128$. Since the overlapping factor is $K = 1$, the filter has the same length as the FBMC symbol $L_g = 128$. The OPF-α filter, developed in Section 5.2.4 was used.

The 3GPP technical specification [113] defines the multipath fading channel model Extended Vehicular-A (EVA) which was used in this work. The presented

results are obtained by averaging over different channel realizations.

In Figure 5.20 we compare the system performance through their bit error rate (BER) for the TDE and FDE receivers, applying IIC and also Genie-Aided. As we can notice, by using the IIC approach we can improve significantly the system performance. We can also identify the gain between the TDE and FDE receivers, which indicates that performing the equalization before the filter-bank brings better results.

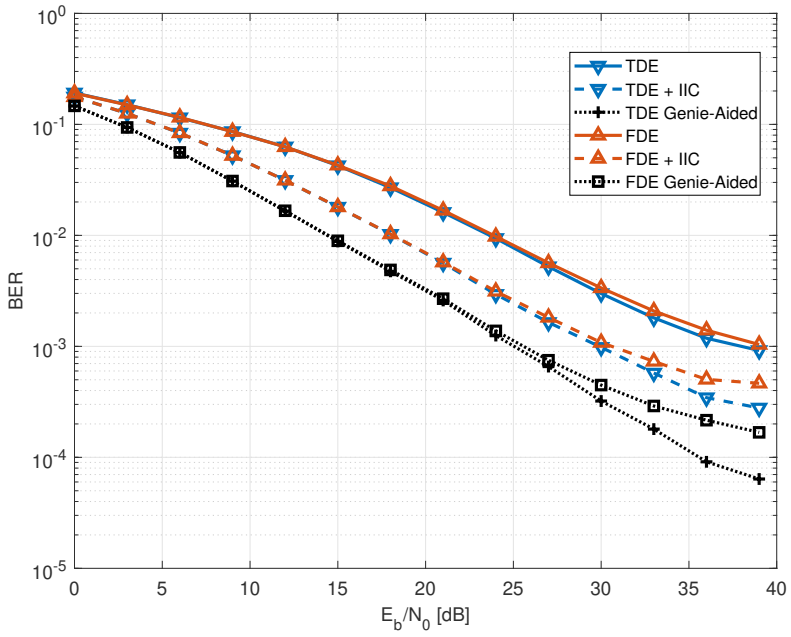

Figure 5.20: BER performance evaluation in QAM-FBMC systems applying the short filter OPF-α and different receivers through EVA channel.

We have also compared our MMSE-based receiver with and without IBI cancellation with the BW-MMSE from Han *et. al* as presented in Figure 5.21. For the sake of comparison, we have also included the FDE receiver.

The simulation shows that our MMSE-based receiver without IBI cancellation has the same performance as the BW-MMSE proposed in [43] adapted to the overlapping factor $K = 1$. However, by introducing the IBI cancellation, the performance of the proposed MMSE receiver is improved, achieving the best performance overall evaluated receivers

We have also evaluated the performance of the system in the case of two users as presented in Figure 5.22. We have considered the two presented receivers, for both individual and joint MMSE estimation. As expected, both receivers have the same performance, which is also the same as in the case of just one user.

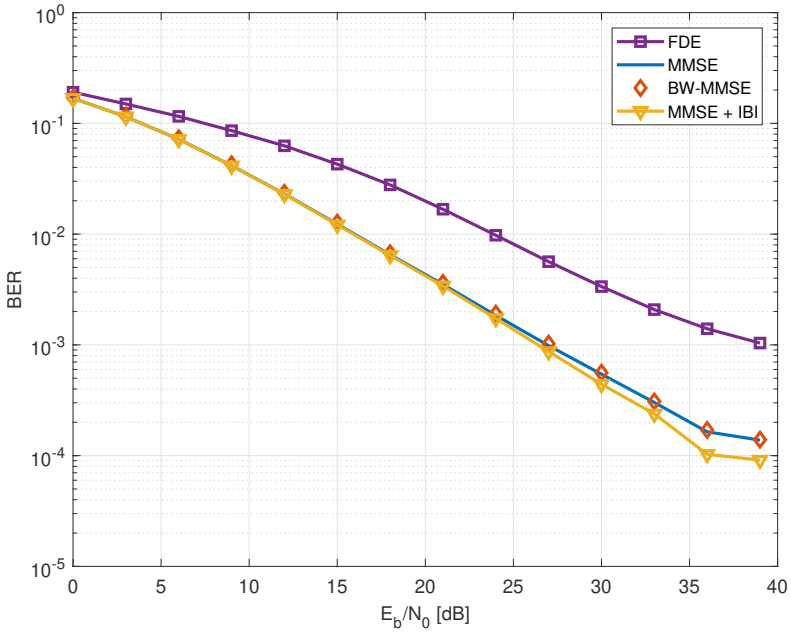

Figure 5.21: BER performance evaluation in QAM-FBMC systems applying OPF-α filter and different receivers based on MMSE and IBI cancellation.

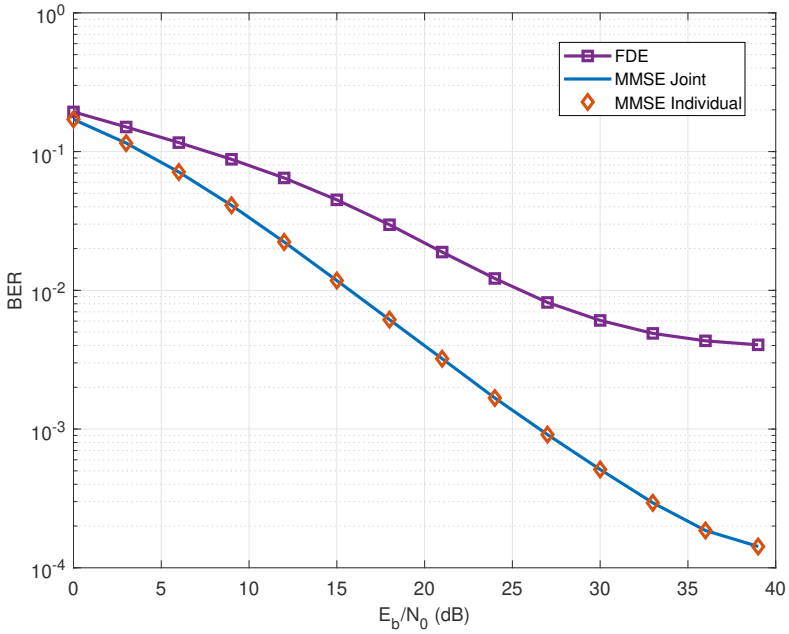

Figure 5.22: BER performance evaluation in QAM-FBMC systems applying the short filter OPF-α and different receivers for the case of two users through EVA channel.

5.5 Chapter Conclusions

In this chapter, we presented a new waveform design for QAM-FBMC systems using short filters to approach the main requirements for waveforms to be used in heterogeneous networks. The system model of QAM-FBMC was derived considering two hypotheses: assuming no channel knowledge and exploiting the knowledge of the PDP of the channel. We formulated the filter optimization problem by minimizing the interference subjected to the OOBE constraint to warrant spectral confinement. Performance evaluations showed that the observed interference is undoubtedly improved by the optimized filters, while keeping the same OOBE. The proposed filters showed also significant enhancement in BER compared to the other ones. Moreover, observing the frequency response of the obtained filters, we could verify that just using the fall-off-rate to confine the spectrum was not enough to mitigate the total interference.

In addition, we also analyze the intrinsic interference in the case of short filters, and evaluate the bit error probability of QAM-FBMC systems over both AWGN and Rayleigh channels by applying the expressions proposed in Chapter 4. The proposed expressions agree with simulated results, which confirms the applicability of the proposed method regardless the applied prototype filter and its overlapping factor. Even though the proposed method assumed weak frequency selectivity, simulation results confirmed its suitability for predicting BEP for 3GPP pedestrian and vehicular channels endorsing this method as an important tool for the QAM-FBMC design.

Finally, different receivers for QAM-FBMC system that applies short filters have been proposed in order to enhance its performance. Linear TDE receivers based on IIC and MMSE filters with IBI cancellation were presented and compared to the well known ones such as the FDE receivers. Besides, we evaluated the average performance over different fading channels EVA.

The evaluation results show that the proposed TDE IIC based receiver can improve the performance of QAM-FBMC systems compared to the classical FDE IIC based receiver. Despite the improvement brought by the IIC technique over TDE and FDE for the QAM-FBMC system, as expected, it is our proposed MMSE receiver, followed by the IBI cancellation, that presents the best performance compared to the conventional existing receivers and even to the state of the art receiver. Additionally, our proposed MMSE receiver proved to be applicable to the case of two or more users, achieving the same BER as in the case of just one user.

In summary, our proposed receiver proves to be applicable to the QAM-FBMC with short filters using just one block to perform the equalization. Thus, it is promising for future QAM-FBMC based communication systems.

5.5.1 Contributions

- The proposed prototype filter that is described in Section 5.2 has been published in [96]: I. Galdino, R. Zakaria, D. Le Ruyet, and M. L. R. d. Campos, "Short-Filter design for intrinsic interference reduction in QAM-FBMC modulation," *IEEE Communications Letters*, vol. 24, pp. 1487–1491, 2020.

- The applicability of Gaussian filters to QAM-FBMC described in Section 5.2 has been published in [117]: I. Galdino, R. Zakaria, D. Le Ruyet, and M. L. R. de Campos, "Avaliação da performance do sistema QAM-FBMC utilizando filtros Gaussianos curtos," in *XXXVII Simpósio Brasileiro de Telecomunicações e Pprocessamento de Sinais - SBrT*. SBrT, 2019, pp. 1–5.

- The bit error probability presented in Section 5.3 has been published in [118]: I. Galdino, D. Le Ruyet, R. Zakaria, and M. L. R. de Campos, "Probabilidade de erro de bit em sistemas QAM-FBMC," in *XXXVIII Simpósio Brasileiro de Telecomunicações e Processamento de Sinais - SBrT*. SBrT, 2020, pp. 1–5.

Chapter 6

Conclusions

6.1 Conclusions

This thesis mainly focused in the analysis and optimization of OQAM-FBMC and QAM-FBMC modulations as alternatives to OFDM in order to fulfil the requirements of futures mobile communication systems. The issue of filter design and optimization is the essence and the main motivation of this work.

In the first chapter we have presented the main characteristics of 5G networks. We discussed major user cases and the technologies that will be needed for these services. Due to the new services, OFDM modulation is not enough for providing the necessary conditions for the 5G network. Hence a completely new physical layer has been developed. Since the multicarrier modulation is the central theme of this thesis, some background on OFDM, OQAM-FBMC, and QAM-FBMC modulations have been introduced as a basis for the rest of this thesis.

In Chapter 2 we have addressed the OQAM-FBMC system. We have mainly analysed the intrinsic interference of the system, the out of pass band energy, and the perfect reconstruction condition. Then, we have introduced a new prototype filter design that minimizes the OOBE with a carefully chosen objective function without violating the orthogonality condition. We have evaluated the performance of the obtained filters and compared to the performance of known filters. Finally, we have also analysed the system behavior in the context of asynchronous access by considering multiple users. The obtained filters show to outperform the known filters.

The QAM-FBMC system have been studied in Chapter 3. We have presented the system model based on the ambiguity function and described the intrinsic interference through the interference coefficients. We proposed a novel prototype filter design that minimizes these coefficients. The discrete prolate spheroidal sequences were briefly introduced together with its major advantageous features. We proposed

a prototype filter based on DPSS and optimized it for reducing the intrinsic interference of the system. Compared to the state of the art filters, we proved to be possible to enhance the system performance through the use of the proposed filters. In addition, we evaluated the performance variation according to the chosen lattice structure of the system. For this, we proposed an hexagonal QAM-FBMC system (HQAM-FBMC). Similarly to what we have done for the standard QAM-FBMC, we proposed a prototype filter for the HQAM-FBMC system based on the DPSS, then we optimized it for reducing the intrinsic interference. Surprisingly, comparing the performance of QAM-FBMC systems with the performance of HQAM-FBMC, both with its optimized filters, there was no significant difference in terms of BER. We proved thus, that, in the conditions presented in this thesis, there is no gain in using hexagonal lattice. Finally, we have analysed the bit error probability of the system. As we did not find in the literature the expression of the BEP for QAM-FBMC systems, we have proposed one in order to predict the performance of the system. The accuracy of the proposed expression has been validated through various simulation results, also taking into account different channels.

Finally, Chapter 4, focused on the low latency desired for 5G. We firstly present the QAM-FBMC system model in a simplified matrix form, which uses short prototype filters. We, proposed a new prototype filter design that minimizes the intrinsic interference of the system subjected to an OOBE limitation. In this case, we also considered the information about the channel, and optimized a filter for a given channel distribution. The effectiveness of the filter was analyzed through the BER performance, and it showed to outperform the known filters. We have also performed a bit error probability analysis by using the expression proposed in Chapter 4. The proposed expressions agree with simulated results, which confirms the applicability of the proposed method regardless the applied prototype filter and its overlapping factor. Finally, as the filter length is directly related to the interference level in communication systems, with the use of short prototype filters we can observe an overall performance degradation. Based on that, different receivers for a QAM-FBMC system that applies short filters were proposed in order to enhance its performance. The results shoed that our proposed MMSE receiver, followed by the IBI cancellation, present the best performance compared to the conventional existing receivers and even to the state of the art receiver. In summary, our proposed receiver proves to be applicable to the QAM-FBMC with short filters using just one block to perform the equalization.

6.2 Future works

This thesis has addressed the OQAM-FBMC and QAM-FBMC systems applied to 5G/6G physical layer. We have mainly focused in prototype filter designed for enhancing the system performance. During this research, a number of interesting research topics, based on the issues studied in this thesis, came up and can also be addressed. Here, we provide some possible extension of the work, that have not been addressed in this thesis, as future works.

- All the proposed methods and receiver schemes make the simplifying assumption that channel state information is fully known at the receiver. It would be of interest to study the influence of channel estimation errors on the performance of the receivers proposed in Chapter 5, and adapt them for more realistic conditions.

- The authors of [2] have proposed the use of two prototype filters to reduce the interference in QAM-FBMC systems. It is of interest to study and design prototype filters for the case of QAM-FBMC with two or more filters. This approach should allow us to further reduce the inherent residual interference at a cost of an increase in the overall complexity.

- A more recent MCM called FFT-FBMC was proposed in [33]. The main idea of the FFT-FBMC is to precode the transmitted data in a subcarrier level by using an IFFT. By doing this, at the receiver the interference coming from the same subcarrier can be removed by a simple equalization due to the subcarrier IFFT/FFT precoding/decoding and cyclic prefix insertion. Furthermore, the interference that comes from the adjacent subcarriers can be avoided by applying good localized prototype filters. Based on this, several investigations can be conducted in order to provide the most appropriate prototype filter for the FFT-FBMC modulation.

- Currently, the implementation through the PPN is considered the most efficient one. However, by removing the phase terms of the transmitted symbols, it may be possible to have a more general implementation. Based on this, a new implementation proposal would be of interest, as long as its equivalence with the traditional implementation can be established.

References

[1] H. Kim, H. Han, and H. Park, "Waveform design for QAM-FBMC systems," in *IEEE 18th International Workshop on Signal Processing Advances in Wireless Communications (SPAWC)*, 2017, pp. 1–5.

[2] Y. H. Yun, C. Kim, K. Kim, Z. Ho, B. Lee, and J.-Y. Seol, "A new waveform enabling enhanced QAM-FBMC systems," in *IEEE 16th International Workshop on Signal Processing Advances in Wireless Communications (SPAWC)*, 2015, pp. 116–120.

[3] R. Nissel, S. Schwarz, and M. Rupp, "Filter Bank Multicarrier Modulation Schemes for Future Mobile Communications," *IEEE Journal on Selected Areas in Communications*, vol. 35, no. 8, pp. 1768–1782, 2017.

[4] Y. Medjahdi *et al.*, "On the road to 5G: Comparative study of physical layer in MTC context," *IEEE Access*, vol. 5, pp. 26 556–26 581, 2017.

[5] A. Dogra, R. K. Jha, and S. Jain, "A Survey on beyond 5G network with the advent of 6G: Architecture and Emerging Technologies," *IEEE Access*, 2020.

[6] A. F. Demir, M. Elkourdi, M. Ibrahim, and H. Arslan, "Waveform Design for 5G and Beyond," *arXiv preprint arXiv:1902.05999*, 2019.

[7] S. Acquah, A. Krampah-Nkoom, and M. O. Adjei, "Performance of the candidate modulation wave-forms for 5g communication systems," *International Journal of Scientific and Research Publications*, vol. 10, no. 6, pp. 597–644, 2020.

[8] A. Abrol and R. K. Jha, "Power optimization in 5G networks: A step towards GrEEn communication," *IEEE Access*, vol. 4, pp. 1355–1374, 2016.

[9] S.-Y. Lien, S.-L. Shieh, Y. Huang, B. Su, Y.-L. Hsu, and H.-Y. Wei, "5G new radio: Waveform, frame structure, multiple access, and initial access," *IEEE communications magazine*, vol. 55, no. 6, pp. 64–71, 2017.

[10] E. G. Larsson, O. Edfors, F. Tufvesson, and T. L. Marzetta, "Massive MIMO for next generation wireless systems," *IEEE communications magazine*, vol. 52, no. 2, pp. 186–195, 2014.

[11] J. Nam, J.-Y. Ahn, A. Adhikary, and G. Caire, "Joint spatial division and multiplexing: Realizing massive MIMO gains with limited channel state information," in *46th Annual Conference on Information Sciences and Systems (CISS)*. IEEE, 2012, pp. 1–6.

[12] "3GPP TS 138.211 - 3rd Generation Partnership project; Physical channels and modulation," 2020. [Online]. Available: https://www.3gpp.org/ftp/Specs/archive/38_series/38.211/

[13] B. Bertenyi, S. Nagata, H. Kooropaty, X. Zhou, W. Chen, Y. Kim, X. Dai, and X. Xu, "5g NR radio interface," *Journal of ICT Standardization*, vol. 6, no. 1, pp. 31–58, 2018.

[14] G. P. Fettweis and E. Matus, "Scalable 5G MPSoC architecture," in *IEEE Asilomar Conference on Signals, Systems, and Computers*, 2017, pp. 613–618.

[15] S. E. Elayoubi, M. Fallgren, P. Spapis, G. Zimmermann, D. Martín-Sacristán, C. Yang, S. Jeux, P. Agyapong, L. Campoy, Y. Qi *et al.*, "5G service requirements and operational use cases: Analysis and METIS II vision," in *IEEE European Conference on Networks and Communications (EuCNC)*, 2016, pp. 158–162.

[16] "3GPP TS 36.211 - 3rd Generation Partnership project; technical specification group radio access network physical channels and modulation," 2020. [Online]. Available: https://portal.3gpp.org/desktopmodules/Specifications/SpecificationDetails.aspx?specificationId=2425

[17] A. A. Esswie and K. I. Pedersen, "Opportunistic spatial preemptive scheduling for urllc and embb coexistence in multi-user 5g networks," *Ieee Access*, vol. 6, pp. 38 451–38 463, 2018.

[18] G. P. Fettweis, "The tactile internet: Applications and challenges," *IEEE Vehicular Technology Magazine*, vol. 9, no. 1, pp. 64–70, 2014.

[19] C. Bockelmann, N. Pratas, H. Nikopour, K. Au, T. Svensson, C. Stefanovic, P. Popovski, and A. Dekorsy, "Massive machine-type communications in 5G: Physical and MAC-layer solutions," *IEEE Communications Magazine*, vol. 54, no. 9, pp. 59–65, 2016.

[20] F. Boccardi, R. W. Heath, A. Lozano, T. L. Marzetta, and P. Popovski, "Five disruptive technology directions for 5G," *IEEE Communications Magazine*, vol. 52, no. 2, pp. 74–80, 2014.

[21] X. Zhang, L. Chen, J. Qiu, and J. Abdoli, "On the waveform for 5G," *IEEE Communications Magazine*, vol. 54, no. 11, pp. 74–80, 2016.

[22] H. Chen, R. Abbas, P. Cheng, M. Shirvanimoghaddam, W. Hardjawana, W. Bao, Y. Li, and B. Vucetic, "Ultra-reliable low latency cellular networks: Use cases, challenges and approaches," *IEEE Communications Magazine*, vol. 56, no. 12, pp. 119–125, 2018.

[23] D. Maaz, A. Galindo-Serrano, and S. E. Elayoubi, "URLLC User Plane Latency Performance in New Radio," in *25th International Conference on Telecommunications (ICT)*. IEEE, 2018, pp. 225–229.

[24] Z. Hou, C. She, Y. Li, L. Zhuo, and B. Vucetic, "Prediction and communication co-design for ultra-reliable and low-latency communications," *IEEE Transactions on Wireless Communications*, vol. 19, no. 2, pp. 1196–1209, 2019.

[25] F. Schaich and T. Wild, "Subcarrier spacing-a neglected degree of freedom?" in *IEEE International Workshop on Signal Processing Advances in Wireless Communications (SPAWC)*, 2015, pp. 56–60.

[26] S. Weinstein and P. Ebert, "Data transmission by frequency-division multiplexing using the discrete Fourier transform," *IEEE Transactions on Communication Technology*, vol. 19, no. 5, pp. 628–634, 1971.

[27] W. Henkel, G. Taubock, P. Odling, P. O. Borjesson, and N. Petersson, "The cyclic prefix of OFDM/DMT-an analysis," in *IEEE International Zurich Seminar on Broadband Communications Access-Transmission-Networking*, 2002, pp. 22–22.

[28] B. Farhang-Boroujeny, "OFDM versus filter bank multicarrier," *IEEE Signal Processing Magazine*, vol. 28, no. 3, pp. 92–112, 2011.

[29] H. Huawei, "F-ofdm scheme and filter design," in *R1-165425, 3GPP TSG RAN WG1 Meeting# 85*, 2016.

[30] M. G. Bellanger, "Specification and design of a prototype filter for filter bank based multicarrier transmission," in *IEEE International conference on Acoustics, Speech, and Signal Processing*, vol. 4, 2001, pp. 2417–2420.

[31] P. Siohan, C. Siclet, and N. Lacaille, "Analysis and design of OFDM/OQAM systems based on filterbank theory," *IEEE transactions on signal processing*, vol. 50, no. 5, pp. 1170–1183, 2002.

[32] H. Wang, W. Du, and L. Xu, "A new sparse adaptive channel estimation method based on compressive sensing for FBMC/OQAM transmission network," *Sensors*, vol. 16, no. 7, p. 966, 2016.

[33] R. Zakaria and D. Le Ruyet, "A novel filter-bank multicarrier scheme to mitigate the intrinsic interference: Application to MIMO systems," *IEEE Transactions on Wireless Communications*, vol. 11, no. 3, pp. 1112–1123, 2012.

[34] H. Lin, M. Gharba, and P. Siohan, "Impact of time and carrier frequency offsets on the FBMC/OQAM modulation scheme," *Signal Processing*, vol. 102, pp. 151–162, 2014.

[35] A. Viholainen, T. Ihalainen, T. H. Stitz, M. Renfors, and M. Bellanger, "Prototype filter design for filter bank based multicarrier transmission," in *Signal Processing Conference, 2009 17th European*. IEEE, 2009, pp. 1359–1363.

[36] M. Alard, "Construction of a multicarrier signal," 1996, patent WO96/35 278.

[37] F. Schaich, T. Wild, and Y. Chen, "Waveform contenders for 5G-suitability for short packet and low latency transmissions," in *2014 IEEE 79th Vehicular Technology Conference (VTC Spring)*. IEEE, 2014, pp. 1–5.

[38] C. Lélé, P. Siohan, and R. Legouable, "The alamouti scheme with CDMA-OFDM/OQAM," *EURASIP Journal on Advances in Signal Processing*, vol. 2010, pp. 1–13, 2010.

[39] R. Zakaria and D. Le Ruyet, "Intrinsic interference reduction in a filter bank-based multicarrier using QAM modulation," *Physical Communication*, vol. 11, pp. 15–24, 2014.

[40] R. Zakaria, D. Le Ruyet, and Y. Medjahdi, "On ISI cancellation in MIMO-ML detection using FBMC/QAM modulation," in *International Symposium on Wireless Communication Systems (ISWCS)*. IEEE, 2012, pp. 949–953.

[41] S. Van Beneden, J. Riani, J. W. Bergmans, and A. Immink, "Cancellation of linear intersymbol interference for two-dimensional storage systems," in *IEEE International Conference on Communications*, vol. 8. IEEE, 2006, pp. 3173–3178.

[42] H. Han and H. Park, "Design on the Waveform for QAM-FBMC System in the Presence of Residual CFO," in *16th Annual Consumer Communications & Networking Conference (CCNC)*. IEEE, 2019, pp. 1–2.

[43] H. Han, N. Kim, and H. Park, "Design of QAM-FBMC Waveforms Considering MMSE Receiver," *IEEE Communications Letters*, 2020.

[44] H. Nam, M. Choi, S. Han, C. Kim, S. Choi, and D. Hong, "A new filter-bank multicarrier system with two prototype filters for QAM symbols transmission and reception," *IEEE Transactions on Wireless Communications*, vol. 15, no. 9, pp. 5998–6009, 2016.

[45] C. Kim *et al.*, "QAM-FBMC: A New Multi-Carrier System for Post-OFDM Wireless Communications," in *2015 Global Communications Conference (GLOBECOM)*. IEEE, 2015, pp. 1–6.

[46] R. Zakaria and D. Le Ruyet, "On maximum likelihood MIMO detection in qam-fbmc systems," in *21st International Symposium on Personal, Indoor and Mobile Radio Communications*. IEEE, 2010, pp. 183–187.

[47] ——, "Theoretical analysis of the power spectral density for FFT-FBMC signals," *IEEE Communications Letters*, vol. 20, no. 9, pp. 1748–1751, 2016.

[48] J. Nadal, C. A. Nour, and A. Baghdadi, "Design and Evaluation of a Novel Short Prototype Filter for FBMC/OQAM Modulation," *IEEE access*, vol. 6, pp. 19 610–19 625, 2018.

[49] R. W. Chang, "Synthesis of Band-limited Orthogonal Signals for Multichannel Data Transmission," *Bell System Technical Journal*, vol. 45, no. 10, pp. 1775–1796, 1966.

[50] B. Saltzberg, "Performance of an Efficient Parallel Data Transmission System," *IEEE Transactions on Communication Technology*, vol. 15, no. 6, pp. 805–811, 1967.

[51] M. Bellanger and J. Daguet, "TDM-FDM transmultiplexer: Digital polyphase and FFT," *IEEE Transactions on Communications*, vol. 22, no. 9, pp. 1199–1205, 1974.

[52] A. Sahin, I. Guvenc, and H. Arslan, "A survey on multicarrier communications: Prototype filters, lattice structures, and implementation aspects," *IEEE Communications Surveys & Tutorials*, vol. 16, no. 3, pp. 1312–1338, 2013.

[53] [Online]. Available: http://www.ict-phydyas.org/

[54] H. S. Malvar, "Modulated QMF filter banks with perfect reconstruction," *Electronics Letters*, vol. 26, no. 13, pp. 906–907, 1990.

[55] M. Bellanger, D. Mattera, and M. Tanda, "Lapped-ofdm as an alternative to CP-OFDM for 5G asynchronous access and cognitive radio," in *Vehicular Technology Conference (VTC Spring), 2015 IEEE 81st.* IEEE, 2015, pp. 1–5.

[56] K. W. Martin, "Small side-lobe filter design for multitone data-communication applications," *IEEE Transactions on Circuits and Systems II: Analog and Digital Signal Processing*, vol. 45, no. 8, pp. 1155–1161, 1998.

[57] S. Mirabbasi and K. Martin, "Overlapped complex-modulated transmultiplexer filters with simplified design and superior stopbands," *IEEE Transactions on Circuits and Systems II: Analog and Digital Signal Processing*, vol. 50, no. 8, pp. 456–469, 2003.

[58] P. Vaidyanathan, "Quadrature mirror filter banks, M-band extensions and perfect-reconstruction techniques," *IEEE Assp Magazine*, vol. 4, no. 3, pp. 4–20, 1987.

[59] H. Liu, C. Yi, and Z. Yang, "Design perfect reconstruction cosine-modulated filter banks via quadratically constrained quadratic programming and least squares optimization," *Signal Processing*, vol. 141, pp. 199–203, 2017.

[60] D. Pinchon, P. Siohan, and C. Siclet, "Design techniques for orthogonal modulated filterbanks based on a compact representation," *IEEE Transactions on signal processing*, vol. 52, no. 6, pp. 1682–1692, 2004.

[61] P. S. Diniz, E. A. Da Silva, and S. L. Netto, *Digital signal processing: system analysis and design.* Cambridge University Press, 2010.

[62] S. Boyd and L. Vandenberghe, *Convex optimization.* Cambridge University press, 2004.

[63] [Online]. Available: www.smt.ufrj.br/~iandra.galdino/

[64] Q. Bai and J. A. Nossek, "On the effects of carrier frequency offset on cyclic prefix based OFDM and filter bank based multicarrier systems," in *11th International Workshop on Signal Processing Advances in Wireless Communications (SPAWC).* IEEE, 2010, pp. 1–5.

[65] I. Galdino, R. Zakaria, D. Le Ruyet, and M. L. R. de Campos, "Short Prototype Filter Design for OQAM-FBMC Modulation," *IEEE Transactions on Vehicular Technology*, vol. 69, no. 8, pp. 9163–9167, 2020.

[66] A. Gupta and R. K. Jha, "A survey of 5G network: Architecture and emerging technologies," *IEEE access*, vol. 3, pp. 1206–1232, 2015.

[67] S. E. Elayoubi *et al.*, "5G service requirements and operational use cases: Analysis and METIS II vision," in *European Conference on Networks and Communications (EuCNC)*. IEEE, 2016, pp. 158–162.

[68] M. Bellanger, D. Le Ruyet, D. Roviras, M. Terré, J. Nossek, L. Baltar, Q. Bai, D. Waldhauser, M. Renfors, T. Ihalainen *et al.*, "Fbmc physical layer: a primer," *PHYDYAS, January*, vol. 25, no. 4, pp. 7–10, 2010.

[69] R. Zakaria, D. Le Ruyet, and M. Bellanger, "Maximum likelihood detection in spatial multiplexing with fbmc," in *2010 European Wireless Conference (EW)*, 2010, pp. 1038–1041.

[70] M. Renfors, T. Ihalainen, and T. H. Stitz, "A block-alamouti scheme for filter bank based multicarrier transmission," in *2010 European Wireless Conference (EW)*, 2010, pp. 1031–1037.

[71] H. Han, H. Kim, N. Kim, and H. Park, "An enhanced QAM-FBMC scheme with interference mitigation," *IEEE Communications Letters*, vol. 20, no. 11, pp. 2237–2240, 2016.

[72] K. K.-C. Lee, "An Intrinsic Interference Mitigation Scheme for FBMC-QAM Systems," *IEEE Access*, vol. 7, pp. 51 907–51 914, 2019.

[73] R. Zakaria, D. Le Ruyet, and Y. Medjahdi, "On ISI cancellation in MIMO-ML detection using FBMC/QAM modulation," in *International Symposium on Wireless Communication Systems (ISWCS)*, 2012, pp. 949–953.

[74] S. Mahama, Y. J. Harbi, A. G. Burr, and D. Grace, "Iterative Interference Cancellation in FBMC-QAM Systems," in *Wireless Communications and Networking Conference (WCNC)*. IEEE, 2019, pp. 1–5.

[75] H. Han, G. Kwon, and H. Park, "MMSE-Interference Canceling Receiver for QAM-FBMC Systems," *IEEE Communications Letters*, 2020.

[76] D. Slepian and H. O. Pollak, "Prolate spheroidal wave functions, Fourier analysis and uncertainty—I," *Wiley Online Library - Bell System Technical Journal*, vol. 40, no. 1, pp. 43–63, 1961.

[77] H. J. Landau and H. O. Pollak, "Prolate spheroidal wave functions, Fourier analysis and uncertainty—II," *Wiley Online Library - Bell System Technical Journal*, vol. 40, no. 1, pp. 65–84, 1961.

[78] D. B. Percival, A. T. Walden *et al.*, *Spectral analysis for physical applications*. cambridge university press, 1993.

[79] I. C. Moore and M. Cada, "Prolate spheroidal wave functions, an introduction to the Slepian series and its properties," *Elsevier Academic Press - Applied and Computational Harmonic Analysis*, vol. 16, no. 3, pp. 208–230, 2004.

[80] H. Alıcı and J. Shen, "Highly accurate pseudospectral approximations of the prolate spheroidal wave equation for any bandwidth parameter and zonal wavenumber," *Springer - Journal of Scientific Computing*, vol. 71, no. 2, pp. 804–821, 2017.

[81] L.-L. Wang, "A review of prolate spheroidal wave functions from the perspective of spectral methods," *J. Math. Study*, vol. 50, no. 2, pp. 101–143, 2017.

[82] M. Boulsane, N. Bourguiba, and A. Karoui, "Discrete Prolate Spheroidal Wave Functions: Further spectral analysis and some related applications," *Springer - Journal of Scientific Computing*, vol. 82, no. 3, pp. 1–19, 2020.

[83] J. Mathews, J. Breakall, and G. Karawas, "The discrete prolate spheroidal filter as a digital signal processing tool," *IEEE Transactions on Acoustics, Speech, and Signal Processing*, vol. 33, no. 6, pp. 1471–1478, 1985.

[84] M. A. Davenport and M. B. Wakin, "Compressive sensing of analog signals using discrete prolate spheroidal sequences," *Elsevier - Applied and Computational Harmonic Analysis*, vol. 33, no. 3, pp. 438–472, 2012.

[85] F. Yin, C. Debes, and A. M. Zoubir, "Parametric Waveform Design Using Discrete Prolate Spheroidal Sequences for Enhanced Detection of Extended Targets," *IEEE Transactions on Signal Processing*, vol. 60, no. 9, pp. 4525–4536, 2012.

[86] Z. Zhu and M. B. Wakin, "Wall Clutter Mitigation and Target Detection Using Discrete Prolate Spheroidal Sequences," in *3rd International Workshop on Compressed Sensing Theory and its Applications to Radar, Sonar and Remote Sensing (CoSeRa)*. IEEE, 2015, pp. 41–45.

[87] S. Soman and M. Cada, "Design and simulation of a linear prolate filter for a baseband receiver," *Journal of Information Technology and Software Engineering*, vol. 7, p. 197, 2017.

[88] A. Triana, D. Pastor, and M. Varón, "Code Division Multiplexing Applied to FBG Sensing Networks: FBG Sensors Designed as Discrete Prolate

Spheroidal Sequences (DPSS-FBG Sensors)," *IEEE Journal of Lightwave Technology*, vol. 35, no. 14, pp. 2880–2886, 2017.

[89] B. P. Day, A. Evers, and D. E. Hack, "Multipath Suppression for Continuous Wave Radar via Slepian Sequences," *IEEE Transactions on Signal Processing*, vol. 68, pp. 548–557, 2020.

[90] Q. He and A. Schmeink, "Comparison and evaluation between FBMC and OFDM systems," in *WSA 2015; 19th International ITG Workshop on Smart Antennas*. IEEE, 2015, pp. 1–7.

[91] R. T. Kobayashi and T. Abrao, "Closed-Form Bit Error Probabilities for FBMC Systems," *IEEE Transactions on Vehicular Technology*, vol. 69, no. 2, pp. 1237–1244, 2020.

[92] R. Nissel and M. Rupp, "OFDM and FBMC-OQAM in Doubly-Selective Channels: Calculating the Bit Error Probability," *IEEE Communications Letters*, vol. 21, no. 6, pp. 1297–1300, 2017.

[93] J. G. Proakis and M. Salehi, *Digital communications*. McGraw-hill New York, 2001, vol. 4.

[94] A. Ron and Z. Shen, "Frames and stable bases for shift-invariant subspaces of l 2 (r d)," *Canadian Journal of Mathematics*, vol. 47, no. 5, pp. 1051–1094, 1995.

[95] P. M. Woodward, *Probability and Information Theory, with Applications to Radar*. Pergamon London, 1953.

[96] I. Galdino, R. Zakaria, D. Le Ruyet, and M. L. R. d. Campos, "Short-Filter design for intrinsic interference reduction in QAM-FBMC modulation," *IEEE Communications Letters*, vol. 24, pp. 1487–1491, 2020.

[97] D. Slepian, "Some comments on fourier analysis, uncertainty and modeling," *SIAM review*, vol. 25, no. 3, pp. 379–393, 1983.

[98] C. Flammer, "Spheroidal Wave Functions, A Stanford Research Inst," *Monograph. Stanford, Calif.: Stanford University Press*, 1957.

[99] A. Osipov, V. Rokhlin, and H. Xiao, *Prolate spheroidal wave functions of order zero*. Springer, New York, 2013, vol. 187.

[100] D. Slepian, "Prolate spheroidal wave functions, Fourier analysis, and uncertainty—V: The discrete case," *Bell System Technical Journal*, vol. 57, no. 5, pp. 1371–1430, 1978.

[101] T. Zemen and C. F. Mecklenbrauker, "Time-variant channel estimation using discrete prolate spheroidal sequences," *IEEE Transactions on signal processing*, vol. 53, no. 9, pp. 3597–3607, 2005.

[102] J. Kaiser and R. Schafer, "On the use of the I_0-sinh window for spectrum analysis," *IEEE Transactions on Acoustics, Speech, and Signal Processing*, vol. 28, no. 1, pp. 105–107, 1980.

[103] T. Strohmer and S. Beaver, "Optimal OFDM design for time-frequency dispersive channels," *IEEE Transactions on communications*, vol. 51, no. 7, pp. 1111–1122, 2003.

[104] B. Le Floch, M. Alard, and C. Berrou, "Coded orthogonal frequency division multiplex [tv broadcasting]," *Proceedings of the IEEE*, vol. 83, no. 6, pp. 982–996, 1995.

[105] J. H. Conway and N. J. A. Sloane, *Sphere packings, lattices and groups*. Springer Science & Business Media, 2013, vol. 290.

[106] H. Bölcskei, "Orthogonal frequency division multiplexing based on offset QAM," in *Advances in Gabor analysis*. Springer, 2003, pp. 321–352.

[107] T. Strohmer, "Approximation of dual gabor frames, window decay, and wireless communications," *Applied and Computational Harmonic Analysis*, vol. 11, no. 2, pp. 243–262, 2001.

[108] S. Peng, A. Liu, X. Pan, and H. Wang, "Hexagonal multicarrier faster-than-Nyquist signaling," *IEEE Access*, vol. 5, pp. 3332–3339, 2017.

[109] S. Peng, A. Liu, X. Tong, K. Wang, and G. Colavolpe, "Optimal multicarrier faster-than-Nyquist signaling under symbol-by-symbol detection," *Digital Signal Processing*, vol. 72, pp. 135–146, 2018.

[110] F.-M. Han and X.-D. Zhang, "Hexagonal multicarrier modulation: A robust transmission scheme for time-frequency dispersive channels," *IEEE Transactions on Signal Processing*, vol. 55, no. 5, pp. 1955–1961, 2007.

[111] I. Galdino, R. Zakaria, D. Le Ruyet, and M. L. R. de Campos, "Prototype Filter for QAM-FBMC Systems Based on Discrete Prolate Spheroidal Sequences (DPSS)," *IEEE Access*, 2021.

[112] A. Goldsmith, *Wireless communications*. Cambridge university press, 2005.

[113] "3GPP TS 36.104 - 3rd Generation Partnership project; Base Station (BS) radio transmission and reception," 2020. [Online]. Available: https://portal.3gpp.org/desktopmodules/Specifications/SpecificationDetails.aspx?specificationId=2412

[114] A. Antoniou and W.-S. Lu, *Practical optimization: algorithms and engineering applications*. Springer Science & Business Media, 2007.

[115] D. Demmer, R. Zakaria, J.-B. Doré, R. Gerzaguet, and D. Le Ruyet, "Filter-bank OFDM transceivers for 5G and beyond," in *IEEE 52nd Asilomar Conference on Signals, Systems, and Computers*, 2018, pp. 1057–1061.

[116] T. Cui and C. Tellamvura, "Power delay profile and noise variance estimation for OFDM," *IEEE communications letters*, vol. 10, pp. 25–27, 2006.

[117] I. Galdino, R. Zakaria, D. Le Ruyet, and M. L. R. de Campos, "Avaliação da performance do sistema QAM-FBMC utilizando filtros Gaussianos curtos," in *XXXVII Simpósio Brasileiro de telecomunicações e processamento desinais - SBrT*. SBrT, 2019, pp. 1–5.

[118] I. Galdino, D. Le Ruyet, R. Zakaria, and M. L. R. de Campos, "Probabilidade de erro de bit em sistemas QAM-FBMC," in *XXXVII Simpósio Brasileiro de telecomunicações e processamento desinais - SBrT*. SBrT, 2020, pp. 1–5.

Iandra GALDINO

Multicarrier Waveform Design in the Context of 5G/6G Communication Systems

Résumé: Le système Filter-Bank Multi-Carrier (FBMC) est une technologie prometteuse pour permettre de futures communications sans fil, par exemple 5G/6G. Par rapport au multiplexage par répartition orthogonale de la fréquence (OFDM), les systèmes FBMC ont une meilleure localisation de fréquence et, par conséquent, causent moins d'interférences aux systèmes voisins. Les systèmes FBMC peuvent être associés à différentes modulations telles que la modulation d'amplitude en quadrature, qui nous conduit au système QAM-FBMC, ou offset QAM appelé (OQAM-FBMC). Dans les deux cas, la conception du filtre prototype est une clé pour garantir de bonnes performances, car elle sera utilisée pour construire tous les filtres du banc de filtres. Dans cette thèse, nous abordons le problème de la conception de filtres prototypes pour les systèmes OQAM-FBMC et QAM-FBMC, à la lumière des procédures d'optimisation. Nous procédons à un choix judicieux de la fonction objectif à minimiser pour réduire les interférences intrinsèques tout en conservant le confinement spectral. Nous étudions également les performances des systèmes à porteuses multiples grâce à leur probabilité d'erreur sur les bits (BEP). Pour évaluer les performances des systèmes QAM-FBMC, nous proposons une expression mathématique de son BEP. Nous étudions comment le choix du filtre prototype affecte les interférences du système et par conséquent le BEP. Bien que plusieurs filtres prototypes aient été conçus pour les systèmes QAM-FBMC, une interférence résiduelle est toujours observée et dégrade les performances du système. Par conséquent, un récepteur plus élaboré est nécessaire. Ainsi, nous menons également une recherche sur les récepteurs afin de réduire les interférences et nous proposons un récepteur spécifiquement conçu pour les systèmes QAM-FBMC.

Mots clés: communication sans fil, 5G, systèmes multiporteuses, conception de formes d'onde.

Abstract: Filter-Bank Multi-Carrier (FBMC) system, is a promising technology to enable future wireless communications e.g., 5G/6G. When compared to the Orthogonal Frequency division Multiplexing (OFDM), FBMC systems have better frequency localization, and consequently, cause less interference to neighboring systems. FBMC systems can be associate to different modulations such as quadrature amplitude modulation, which leads us to the QAM-FBMC system, or offset QAM called (OQAM-FBMC). In both cases, the prototype filter design is a key to guarantee good performance, since it will be used to construct all the filters of the filter-bank. In this thesis, we address the problem of prototype filter design for OQAM-FBMC and QAM-FBMC systems, under the light of the optimization procedures. We proceed a careful choice of the objective function to be minimized for reducing the intrinsic interference while keeping the spectral confinement. We also investigate the performance of multicarrier systems through their bit error probability (BEP). To evaluate the performance of QAM-FBMC systems we propose a mathematical expression of its BEP. We investigate how the choice of the prototype filter affects the system interference and consequently the BEP. Although several prototype filters have been designed for QAM-FBMC systems, a residual interference is still observed and degrades system performance. Therefore, a more elaborated receiver is needed. Thus, we also conduct a research on receivers in order to reduce interference and we propose a receiver specifically designed for QAM-FBMC systems.

Keywords: Wireless communication, 5G, multicarrier systems, waveform design.